EE

GSI

GSI-Preprint-96-36
JULI 1996

THE PHYSICS OF HIGHLY-CHARGED HEAVY IONS REVEALED BY STORAGE / COOLER RINGS

P. H. MOKLER, TH. STÖHLKER

(To be published in : Advances in Atomic, Molecular, and Optical Physics)

Gesellschaft für Schwerionenforschung mbH
Postfach 110552 · D-64220 Darmstadt · Germany

The Physics of Highly-Charged Heavy Ions Revealed by Storage/Cooler Rings

P. H. Mokler[1] and Th. Stöhlker[2]

G S I - Darmstadt

Postfach 110552, 64220 Darmstadt, Germany

To be published in:

ADVANCES IN ATOMIC, MOLECULAR,

AND OPTICAL PHYSICS

[1] GSI-Darmstadt and University of Giessen

[2] Institut für Kernphysik, University of Frankfurt, and GSI-Darmstadt

1 Introduction

With the successful commissionning of storage and cooler rings for bright beams of really heavy ions near the threshold of the last decade of this century not only a prosperous development in heavy-ion accelerator technology (Möller, 1994; Pollock, 1991; Franzke, 1988) came to its present summit but also fundamental fields in heavy-ion physics had been opened widely for exciting explorations. Now, essential aspects in this area are accessible, aspects one dared to dream off another decade ago. In the meantime, already tremendous progress has been made concerning the fundamental physics in this field. (Schuch, 1993; Bosch, 1993; Müller, 1994; Lindgren *et al.*, 1995). This is particularly true also for the exciting achievements in the atomic physics of highly-charged heavy ions. In this article a review is presented on the current advances in this rapidly developing field.

There are two general aspects to be considered in the field of atomic physics with highly-charged heavy ions: the collision aspect and the atomic structure one. Both aspects have to be explored equally as they are strongly intercorrelated. One has to investigate the interaction processes in order to know, for instance, the population of excited states that may answer questions of the atomic structure; and vice versa, one has to know the structure in order to understand the interactions. In both the fields fundamental principles can be studied uniquely. This is in particular true for the heaviest ion species with only a few - or even none - electrons left.

In these very heavy few-electron ions extremely strong central fields are present which are probed by the residual inner electrons. For the highest nuclear charges or atomic numbers Z relativistic and even quantum-electro-dynamical effects (QED) may dominate the atomic structure of these ions as both effects increase roughly with Z^4 whereas the binding increases only with Z^2. For the heaviest species higher order QED contributions can be probed, which are not accessible to experiments for low-Z ions (cf. Lindgren *et al.*, 1995b; Mokler *et al.*, 1994; Indelicato, 1990; Johnson and Soff,1985). Moreover, due

to the shrinking of the electron wavefunctions with Z there is an appreciable overlap with the nucleus and strong hyperfine effects can be tested uniquely (Klaft *et al.*, 1994). These effects increase roughly with Z^3. The interaction of the atomic and nuclear parts may even be so large that new decay channels in the radioactive decay can be opened or closed. A typical example is the recently measured beta decay into bound atomic states (Jung *et al.*, 1992). However, also Rydberg states which are practically clean of nuclear influences provide deep insight into the atomic structure of high-Z few-electron ions (Borneis *et al.*, 1994; Schüssler *et al.*, 1995a; Schüssler, 1995b).

In collisions, especially at high velocities, β = v/c, subtle effects of the relativity may be probed (Grieser *et al.*, 1995). Here, in particular also, magnetic and spin-flip effects can be studied; and the interaction processes at high central fields may deviate considerably from those involving low-Z ions (Stöhlker *et al.*, 1995; Rymuza *et al.*, 1993). This is not only true for the typical excitation and ionization as well as for the different capture and recombination processes but also for the quasimolecular processes at lower collision velocities (Schuch *et al.*, 1988). By the study of superheavy collision systems with initial vacancies in inner shells quasiatoms in the superheavy nuclear charge region ($100 < Z_{eff} < 185$) can be tested (for a review see e.g. Mokler and Liesen, 1978). There, the strongest possible fields determine the atomic structure.

All these interesting and fundamental effects can be tested sensitively with the new tools, the heavy ion storage/cooler rings. Ions up to naked uranium (Z=92) can after acceleration and stripping be accumulated to high intensities in storage rings. By cooling - mainly by cold electrons - the phase space density can be increased, so that high luminosity beams of highly-charged heavy ions can be provided for experiments. (For a review on cooling techniques see e.g. Möhl, 1988). The extremely well-defined energy of the ions is precisely fixed by the cooling technique. On the other hand, the velocity of these projectiles can be changed actively to the requirements of the experiments; in particular

the highly-charged ions can be decelerated. With these tools, the interaction of the heavy ions with photons (Laser), with electrons and with atoms or even with ions can be studied selectively. Due to the long storage times for the heavy ions also lifetime measurements for both, atomic as well as nuclear states get accessible (Kluge, 1995; Andersen *et al.*, 1993; Irnich *et al.*, 1995; Schmidt *et al.*, 1994). And, last but not least, the storage rings can be tuned as high resolution mass spectrometers giving additional and important information on both, nuclear and atomic structure of these heavy ions. However, here only the first steps had been tried on the long way towards the extreme precision known from measurements in low-Z ion traps (cf. Kluge, 1995 and Thompson, 1990).

In the following we have first to explain the challenging physics of highly-charged heavy ions (Chapter 2) before we give an introduction to and a survey on storage rings with their cooling properties (Chapter 3). Then, the new results on the important charge changing processes - recombination and capture reactions - will be reviewed (Chapter 4), before the basic results on the atomic structure are discussed (Chapter 5). Here, the ground state transitions give direct insight into Lamb shift contributions. However, also the information from doubly-excited states, from Rydberg states and from the ground state hyperfine splitting elucidates the QED structure contributions. The radioactive decay gives another view into the interplay between atomic shell and nucleus. Finally, an outlook on future developments on the physics of highly-charged ions at storage/cooler rings is given (Chapter 6).

2 The Physics of Highly-Charged Heavy Ions

2.1 The structure of heavy few-electron ions

2.1.1 Isoelectronic sequences

The binding of electrons to nuclei gives the most direct access to the structure of ions or atoms and reveals most clearly the fundamental principles in physics. Hence, the precise spectroscopy of transitions mainly between two bound atomic levels was from the very earliest days in atomic physics the tool to study these principles. First, Bohr's atomic model discussed already in 1913, was roughly in agreement with the experimental findings. There at least for H-like atomic species the binding energy of the one electron increases with the square of the atomic number Z according to the Rydberg formula

$$E_{BIN} = -Ry \cdot Z^2/n^2 \tag{1}$$

where n is the main or shell quantum number. Later, the quantum mechanics (1926), both in the non-relativistic (Schrödinger) as well as in the relativistic (Dirac) regime was excellently confirmed by spectroscopic investigations. - For historical details the reader is referred to text books, see e.g. Bethe and Salpeter (1957) or more specifically, Labzowky *et al.* (1993) -. Finally, Lamb and Retherford (1947) discovered tiny deviations in their spectra from hydrogen atoms, the LAMB-shift, which is caused by quantum-electrodynamical effects. For light atomic species, like Hydrogen, the complete theory is now excellently confirmed by ultra-high precision spectroscopy experiments; see for instance the Doppler-free two-photon Laser experiment of Weitz *et al.* (1992). For heavy ions such a precision is not feasible. However, due to the increase in the central nuclear potential the effects on the atomic structure are dramatically increased and higher order effects can be studied there uniquely.

Within an isoelectronic sequence the electron-nucleus interaction is turned up in strength with increasing atomic number, changing considerably the atomic structure. Electron-electron interaction gets less and less important, while relativistic (REL) and quantum-electrodynamic (QED) influences get more and more important (see e.g. Mokler *et al.*, 1994). These influences are overlayed onto the general Z^2 dependence for the binding energies. Most clearly these effects can be studied for few-electrons, in particular for H- and He- like ions. This is demonstrated by Fig. 2.1; there the reduced binding energies E_{Li}/E_{GS} are plotted as a function of the atomic number for the various L-shell levels.

Fig. 2.1: Reduced L-shell binding energies, - E_{Li}/E_{GS}, normalized to the ground state binding energy in hydrogenic ions. The reduced energies are plotted as function of the atomic number Z for H- and He- like ions. The corresponding reduced K - L transition energies are given by 1 - E_{Li}/E_{GS}.

2.1.2 Hydrogen-like ions

For low Z hydrogenic ions the reduced L-shell binding energy is -1/4, in accordance with the Rydberg formula. In this reduced representation the (L - K) transition energy corresponds to 3/4. With increasing central atomic field (Z) the L shell splits up into the different j-states with $j = 1/2$ and 3/2. This fine structure splitting is caused by relativistic effects and increases with the 4^{th} power of the atomic number. In the reduced representation in Fig. 2.1 the fine structure splitting is proportional to Z^2. However, already in the shown representation, we find at high Z numbers a tiny splitting of the $^2S_{1/2}$ and $^2P_{1/2}$ levels, which cannot be described by the Dirac equation. This is the classical $LAMB$-shift lowering the absolute value for the binding of s states slightly. The total $LAMB$-shift is mainly caused by quantum electrodynamic effects and increases also

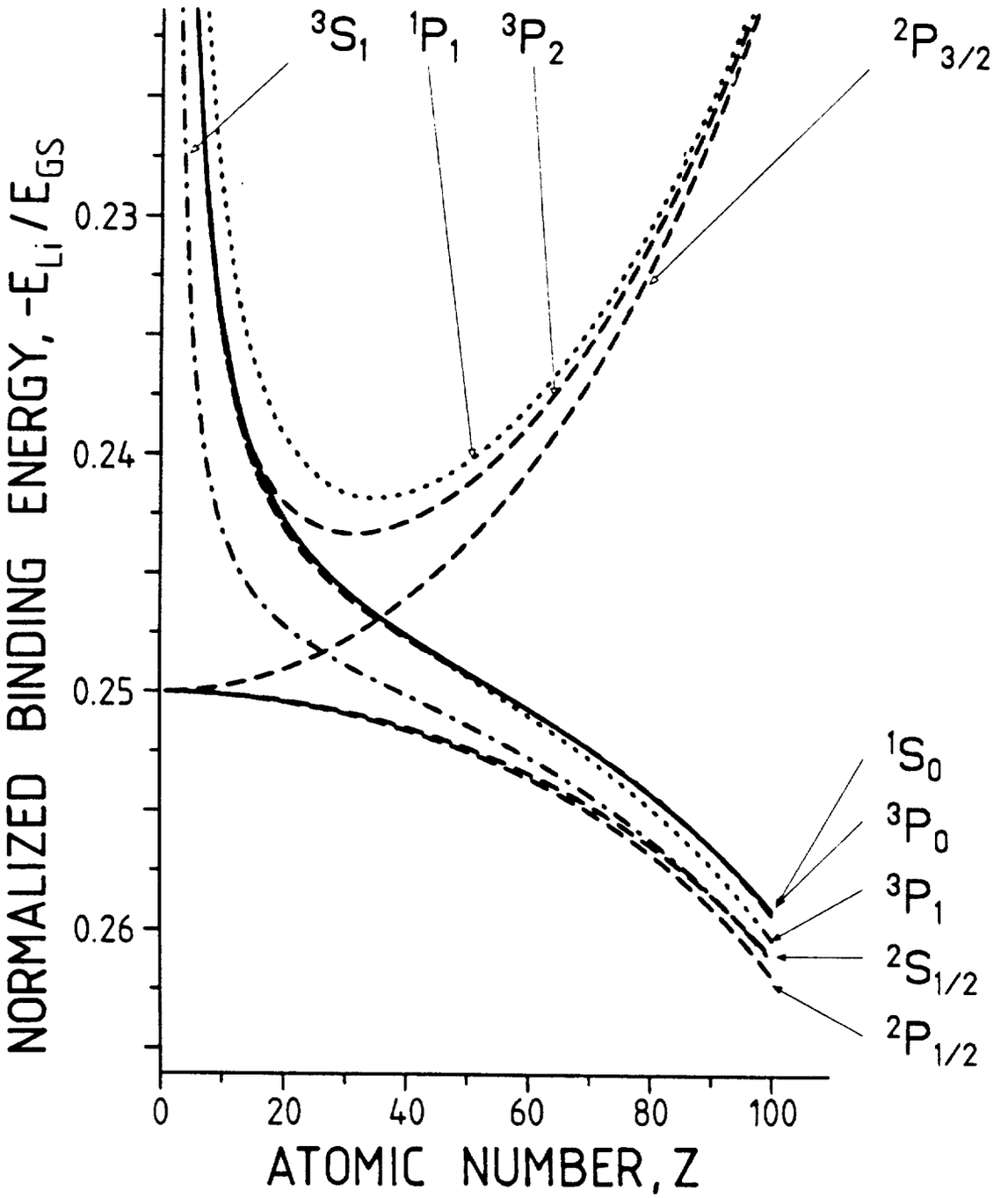
$^3S_1$
$^1P_1$
$^3P_2$
$^2P_{3/2}$
$^1S_0$
$^3P_0$
$^3P_1$
$^2S_{1/2}$
$^2P_{1/2}$
NORMALIZED BINDING ENERGY, $-E_{Li}/E_{GS}$
0.23
0.24
0.25
0.26
0
20
40
60
80
100
ATOMIC NUMBER, Z

with Z^4. The ground state, $1s\,^2S_{1/2}$, is naturally even more influenced by QED effects as the 1s electron probes more closely the strong part of the central potential than a 2s electron does (see also Fig. 2.6 below).

The main QED contribution to the $LAMB$–shift (Johnson and Soff, 1985) is at low Z the self energy (SE) of the bound electron, i.e. the emission and reabsorption of a virtual photon by the electron in the strong field. At higher Z values the vacuum polarization (VP) contributes more and more to the $LAMB$–shift. The vacuum polarization can be characterized in the lowest order as the coupling of the electron to a virtual electron-positron pair created in the strong central potential. For heavy Z, naturally, the finite size of the nucleus influences via the central potential the binding energy of the electron, see below. This effect is usually included in the $LAMB$–shift. Johnson and Soff (1985) did extended calculations on the $LAMB$–shift of H-like ions all over the periodic table. They explicitly calculated the mentioned first order (one loop) QED graphs, estimated the higher order terms and added also the nuclear size effects. In total, the $LAMB$–shift can be characterized by the formula:

$$L_{ns} = \alpha/\pi \cdot (Z\alpha)^4/n^3 \cdot F(Z\alpha) \cdot mc^2 \qquad (2)$$

where n is the shell quantum number, α the finestructure constant; and the function F can be written as a series expansion in $Z\alpha$. In Fig. 2.2 the ground state $LAMB$-shift for H-like systems is plotted in units reduced by Z^4; i.e., the dependence for the $F(Z\alpha)$ function is given. The separate contributions from self energy, vacuum polarization, and from the finite nuclear size are also shown in Fig. 2.2.

Fig. 2.2: Relative contributions $\Delta J/Z^4$ to the ground state $LAMB$–shift in H-like ions according to Johnson and Soff (1985). The graphs for the first order QED contributions, self energy (SE, left) and vacuum polarization (VP,

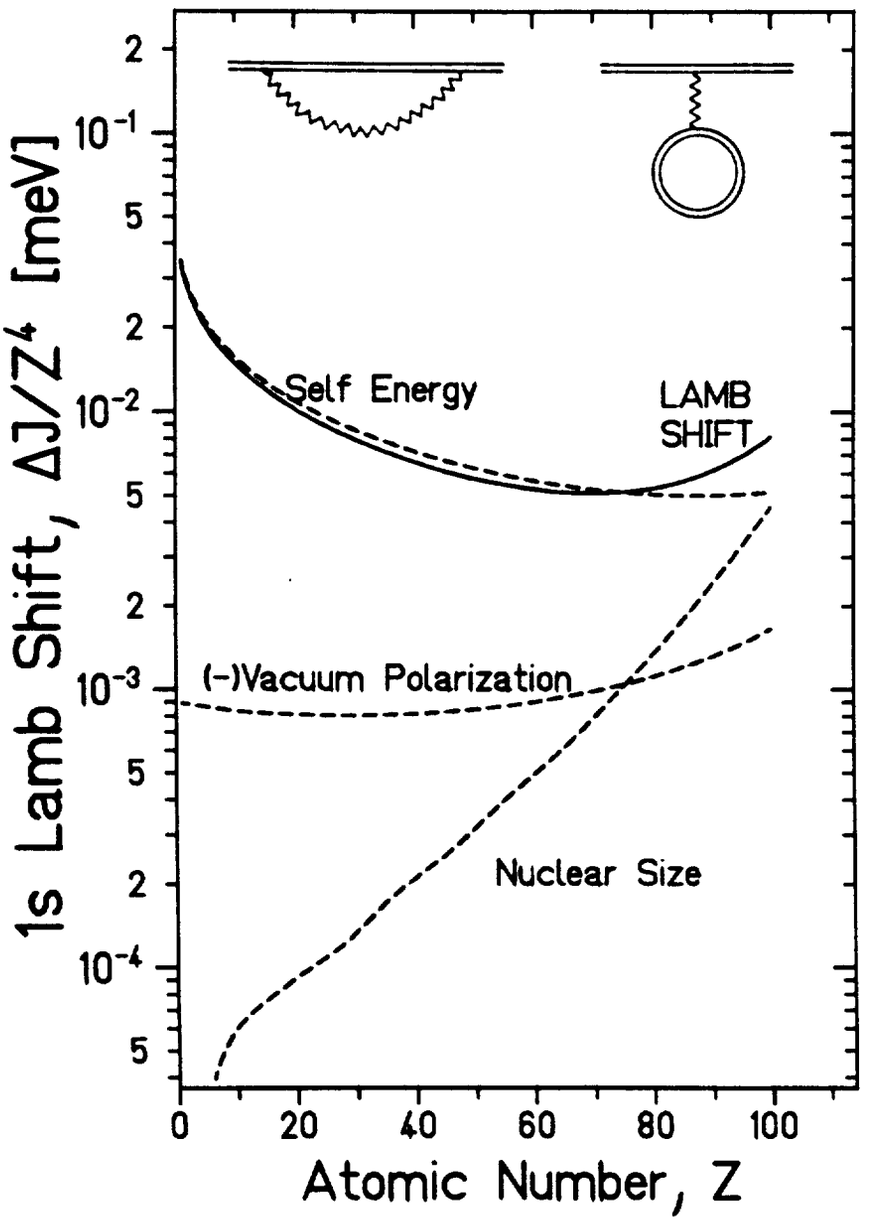
1s Lamb Shift, ΔJ/Z⁴ [meV]
2
10⁻¹
5
2
10⁻²
5
2
10⁻³
5
2
10⁻⁴
5
Self Energy
LAMB
SHIFT
(-)Vacuum Polarization
Nuclear Size
0
20
40
60
80
100
Atomic Number, Z

right) are inserted at the top of the Figure. SE, VP and nuclear size (NS) contributions are separately shown in addition.

In order to have a feeling for the absolute energy range covered by Fig. 2.2, we give rough energies for a Hydrogen atom and for a H-like U^{92+} ion in comparison: The $Lyman-\alpha$ transition energies are about 10 eV and 100 keV, respectively; the L shell fine structure splitting corresponds to 45 μeV and 4.56 keV, the $2s-2p_{1/2}$ $LAMB-$shift to 4.4 μeV and 75 eV, and the ground state $LAMB-$shift to 35 μeV and 458 eV, respectively (Johnson and Soff, 1985).

We like to point out that beyond about Z = 40 higher order terms in the $Z\alpha$ expansion start to dominate the self energy (see e.g. Indelicato, 1990). The higher order aspects can only be tested by highly-charged, very heavy atoms. Actually, second order (two loop) graphs are now accessible to calculations (*cf.* Mohr, 1994) and will give a real deep insight into the QED physics in strong fields. This will particularly be true when corresponding experimental high-precision data will be available in future.

2.1.3 Helium-like ions

He-like ions are the simplest multielectron systems. They represent an ideal testing ground for our understanding of relativistic and quantum electrodynamic effects in many body systems. Unlike to hydrogenic species there is no exact solution for the structure of heliumlike ions and the theory of two-electron ions has to consider beside the dominant Coulomb term effects from electron-electron correlations such as the Breit interaction, screening of the Lamb shift and higher order radiative corrections. Due to the electron-electron interaction the binding energies are lowered with respect to the H-like systems (i.e. the normalized ground state transition energies in Fig. 2.1 are increased) and the triplet levels are more tightly bound than the corresponding singulet levels. As the electron-electron interaction decreases with $1/Z$ relative to the electron-nucleus interaction with

increasing nuclear charge, the He-like level structure approaches for high-Z ions a H-like character. Consequently, the LS coupling scheme, valid for low-Z ions, gets meaningless and one has to consider a pure jj-coupling.

Very recently, substantial progress in the theory of two-electron systems has been achieved, in particular for the ground state of these ions (Lindgren *et al.*, 1995a). On the basis of many-body Lamb-shift calculations the two-photon QED contributions to the electron-electron interaction (non-radiative QED, screened vacuum polarization and self-energy) can now be calculated without any approximation and the theoretical precision for the ground state energies in He-like ions is now as precise as the one for one-electron systems (Persson *et al.*, 1995).

Fig. 2.3: Relative contributions $\Delta J/Z^4$ to the ground state ionization potential in He-like ions are plotted as a function of atomic number Z according to Drake (1988). For the different contributions see text.

In Fig. 2.3 the various contributions to the ground state binding energies in He-like ions are plotted using the tabulated values from Drake (1988). Although these data were evaluated by means of the $Z\alpha$ expansion, which is known to be incomplete at the level of $(Z\alpha)^4$, the figure depicts the general scaling of the most important effects which contribute to the binding energies, i.e. relativistic effects (REL) including the full Breit interaction, the mass polarization (MP), the nuclear size effect (NS), as well as the various QED effects. Note, that the latter is essentially dominated by one-electron QED terms.

2.1.4 Forbidden transitions

Beside the ground state and the transition energies, the lifetimes of the excited levels are of particular interest for atomic structure investigations. In low-Z hydrogenic systems, the $2\ ^2S_{1/2}$ level is metastable and decays by the non-relativistically allowed 2E1 decay.

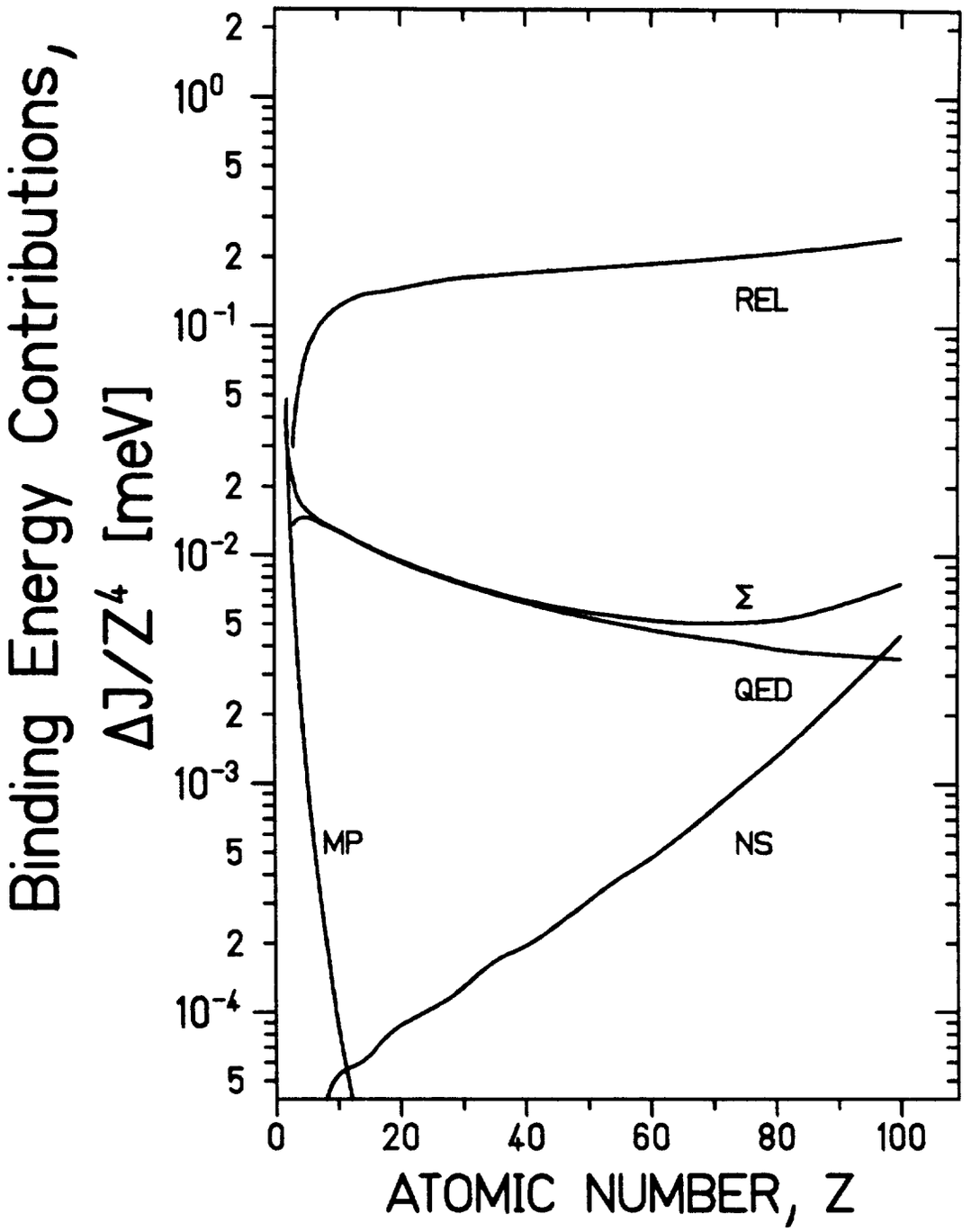

'AP08.SHEME1.DATA(HELIKE1)'

For very high-Z ions, however, the M1 spin-flip transition is about an order of magnitude faster than the 2E1 decay mode leading to a prompt decay of the the $2\,^2S_{1/2}$ level. The general scaling of the transition modes for hydrogenic systems along with the level scheme is given in Fig. 2.4.

Fig. 2.4: The level scheme of the excited L-shell levels in H-like ions (top) along with their transition rates which are plotted as a function of Z (bottom). There, the spectroscopic ranges typically accessible for fast beams (FB), storage rings (SR), and ion traps (IT) are also given.

For H-like heavy ions as U^{91+} all ground state transitions can be considered in the experiment as prompt. The Lyman α_2 transition ($2\,^2P_{1/2} \rightarrow 1\,^1S_{1/2}$) is here blended by the M1 decay ($2\,^2S_{1/2} \rightarrow 1\,^1S_{1/2}$). For convenience we marked in the figure the lifetime regions typically accessible to fast beam spectroscopy ($FB \sim ns$), to long lifetime measurements in storage rings ($SR \sim \mu s$ to ms) and those in ion traps ($IT \sim s$). Depending on the experimental goals, these regions can be extended considerably e.g. in ion traps down to the ns-domaine and in storage rings up to the years time scale.

Fig. 2.5: Level diagrams of the excited L-shell levels in He-like ions given for both Ar^{16+} and U^{90+} (top). The corresponding transition rates are given in addition as a function of atomic number Z (bottom).

For He-like ions the level scheme is more complex; see Fig. 2.5. Going along the isoelectronic sequence the atomic structure changes drastically as it is illustrated for the two cases of Ar^{16+} (LS coupling) and U^{90+} (jj-coupling). Also given in the figure are the decay rates of the non-relativistically forbidden transitions modes as well as of the 2E1 decay. As seen from the figure, the increase of the nuclear charge and therefore of

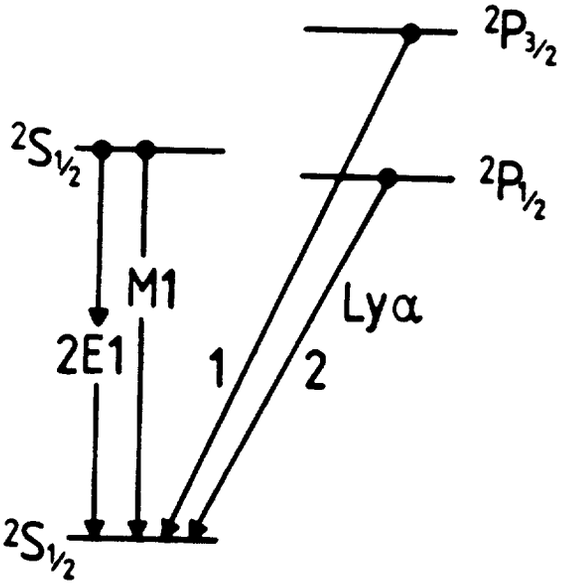
$^2P_{3/2}$
$^2S_{1/2}$
$^2P_{1/2}$
M1
2E1
Lyα
1
2
$^2S_{1/2}$

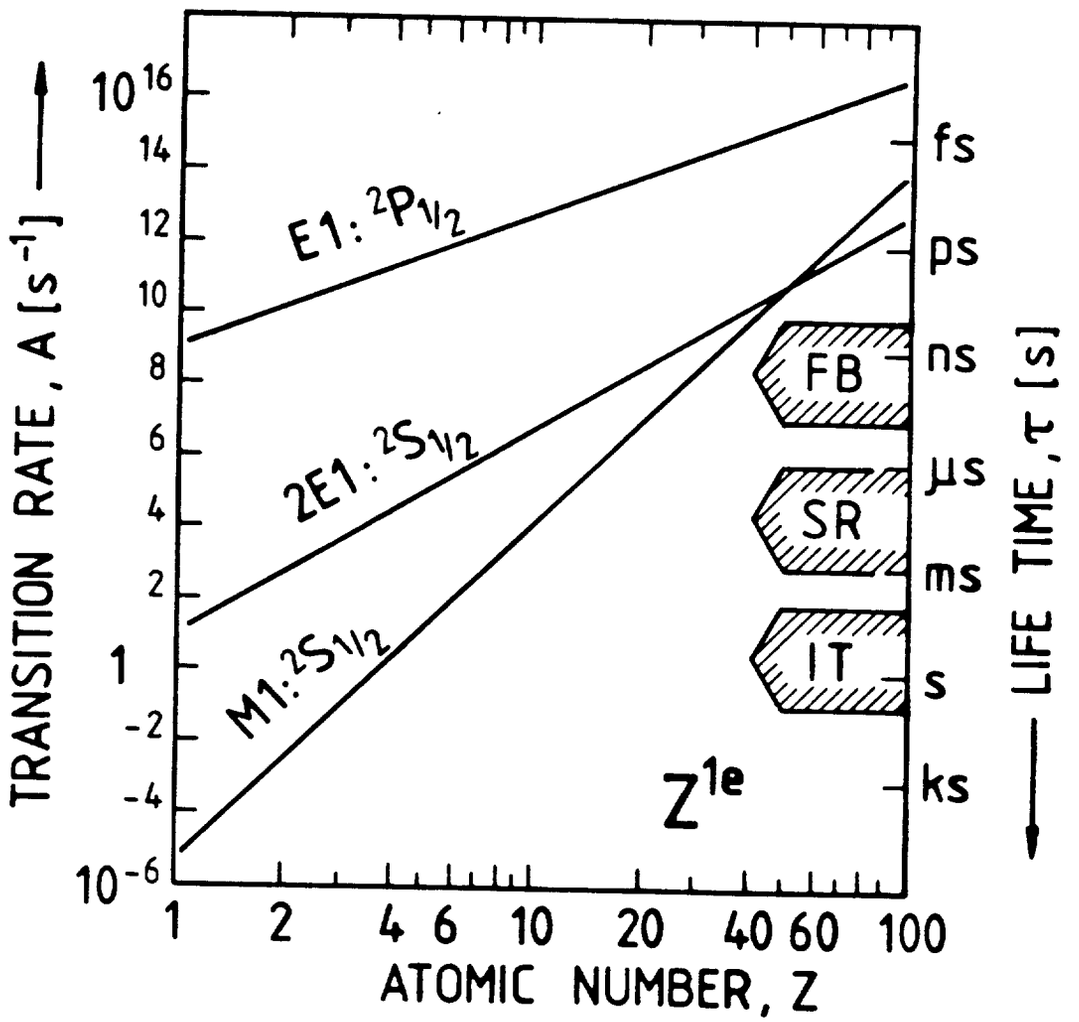
TRANSITION RATE, A [s^{-1}]
LIFE TIME, τ [s]
ATOMIC NUMBER, Z
E1: $^2P_{1/2}$
2E1: $^2S_{1/2}$
M1: $^2S_{1/2}$
FB
SR
IT
fs
ps
ns
μs
ms
s
ks
Z^{1e}
10^{16}
14
12
10
8
6
4
2
1
-2
-4
10^{-6}
1
2
4
6
10
20
40
60
100

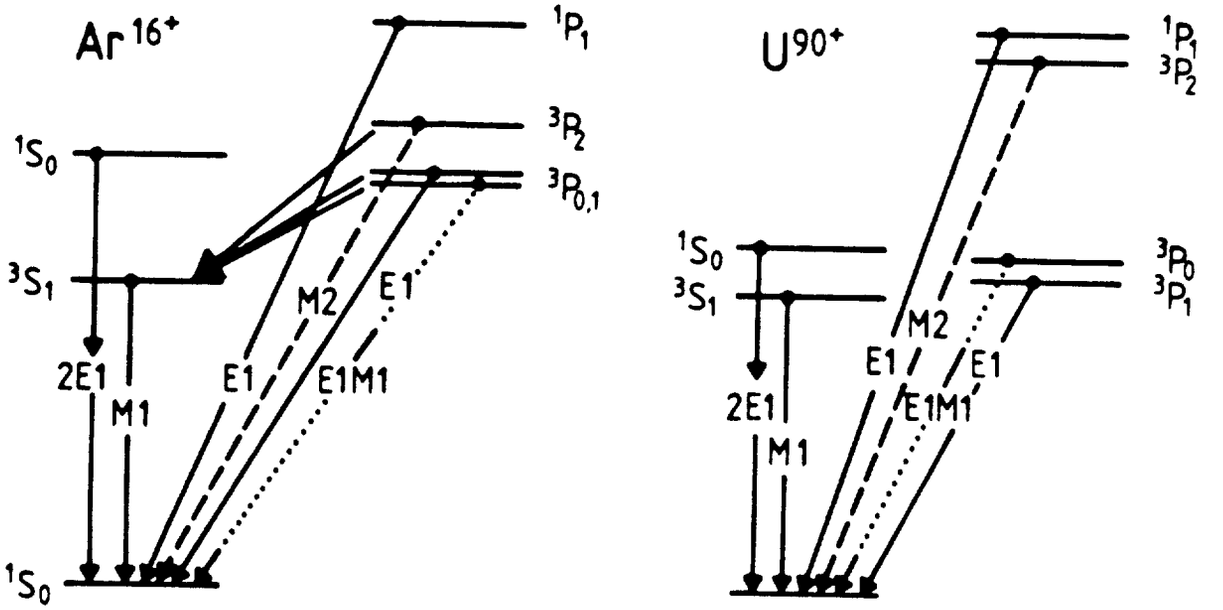
Ar 16+
1P1
3P2
3P0,1
1S0
3S1
2E1
M1
E1
M2
E1
E1M1
1S0
U90+
1P1
3P2
1S0
3S1
3P0
3P1
M2
E1
E1
2E1
E1M1
M1

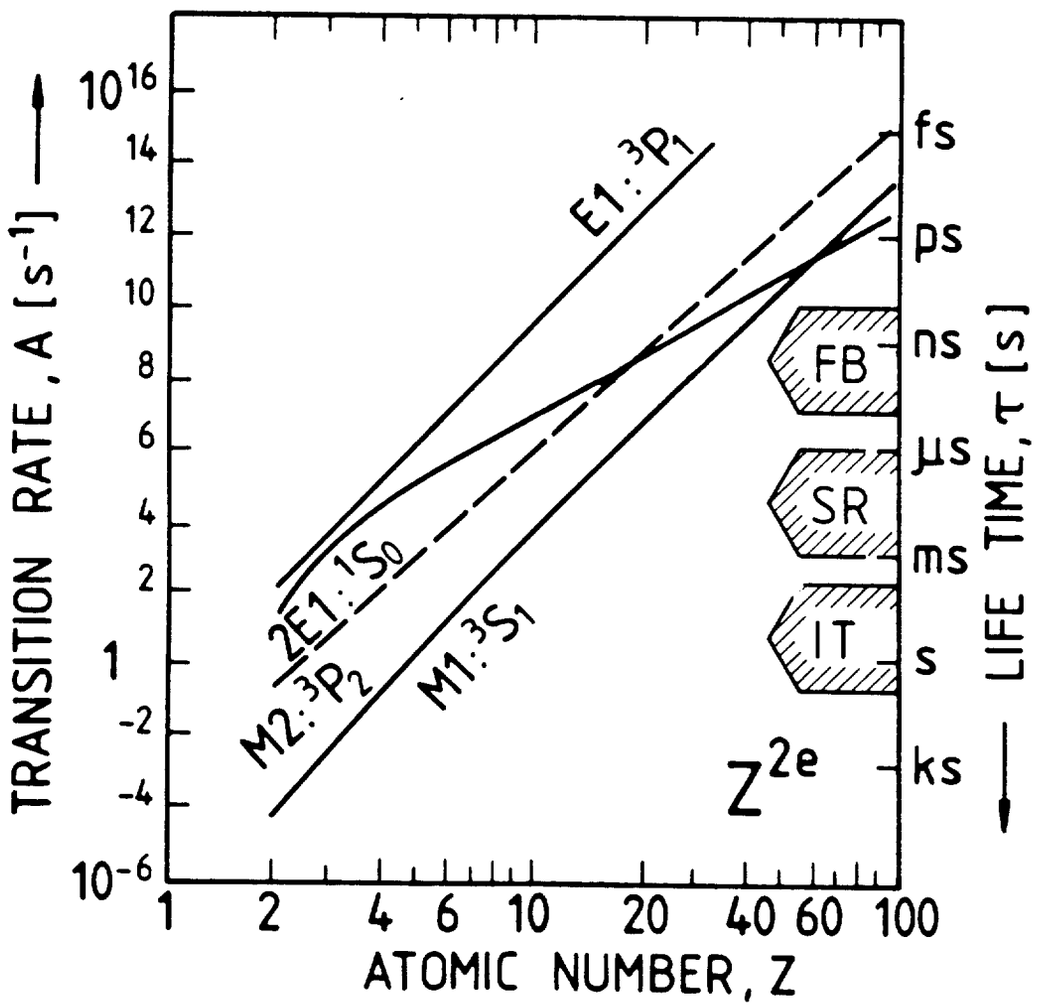
TRANSITION RATE, A [s-1]
LIFE TIME, τ [s]
ATOMIC NUMBER, Z
E1: 3P1
2E1: 1S0
M2: 3P2
M1: 3S1
FB
SR
IT
Z2e
fs
ps
ns
μs
ms
s
ks
10^16
14
12
10
8
6
4
2
1
-2
-4
10^-6
1
2
4
6
10
20
40
60
100

relativistic effects propagates a drastic increase in the decay rates of all forbidden transitions ($^3P_1 : Z^{10}(E1)$, $^3S_1 : Z^{10}(M1)$, $^3P_2 : Z^8(M2)$, $^1S_0 : Z^6(2E1)$, $^3P_0 : Z^6(E1M1)$ (cf. Marrus and Mohr, 1978)). Consequently, for U^{90+} all exited L-shell levels decay predominately to the ground state by direct transitions. Only in the case of the $^3P_2$ and $^3P_0$ levels Δn=0 transitions must also be considered (decay to the $^3S_1$ state). Moreover, for a fast beam spectroscopy we emphasize that all ground state transitions from the L shell can be considered as prompt except for the $^3P_0$ decay. This is true for all heavy He-like species, such as U^{90+}.

2.1.5 Interaction with the nucleus

As already mentioned above the structure of the nucleus may cause important corrections for the binding energies mainly of the s electrons. Due to the radial shrinking of the wavefunctions with Z and the increase of the nuclear radius, an appreciable overlap of the innermost electrons with the nucleus is present for heavy ions. In figure 2.6 the radial part $(r\Psi)^2$ of the 1s (solid line), 2s (dashed-dotted line), $2p_{1/2}$ (dashed line), and $2p_{3/2}$ (dotted line) wave functions of hydrogenic Bi^{82+} (Soff, 1995) is depicted where the radius of ^{209}Bi (r = 7.125 fm) is marked in addition.

Fig. 2.6: In the radial part $(r\Psi)^2$ of the 1s (solid line), 2s (dashed-dotted line), $2p_{1/2}$ (dashed line) and $2p_{3/2}$ (dotted line) wave functions of hydrogenic Bi^{82+} given as function of the distance from the center of the nucleus. The mean square radius of ^{209}Bi of r = 7.125 fm is marked in addition (Soff, 1995).

Due to the finite overlap of the s electron wavefunctions with the nucleus, the nuclear charge distribution does not only influence the Dirac eigenvalue; it leads also to important corrections for the QED contributions itself. This is in particular true for the 1s level of high-Z ions where the total finite nuclear size correction is larger than the vacuum

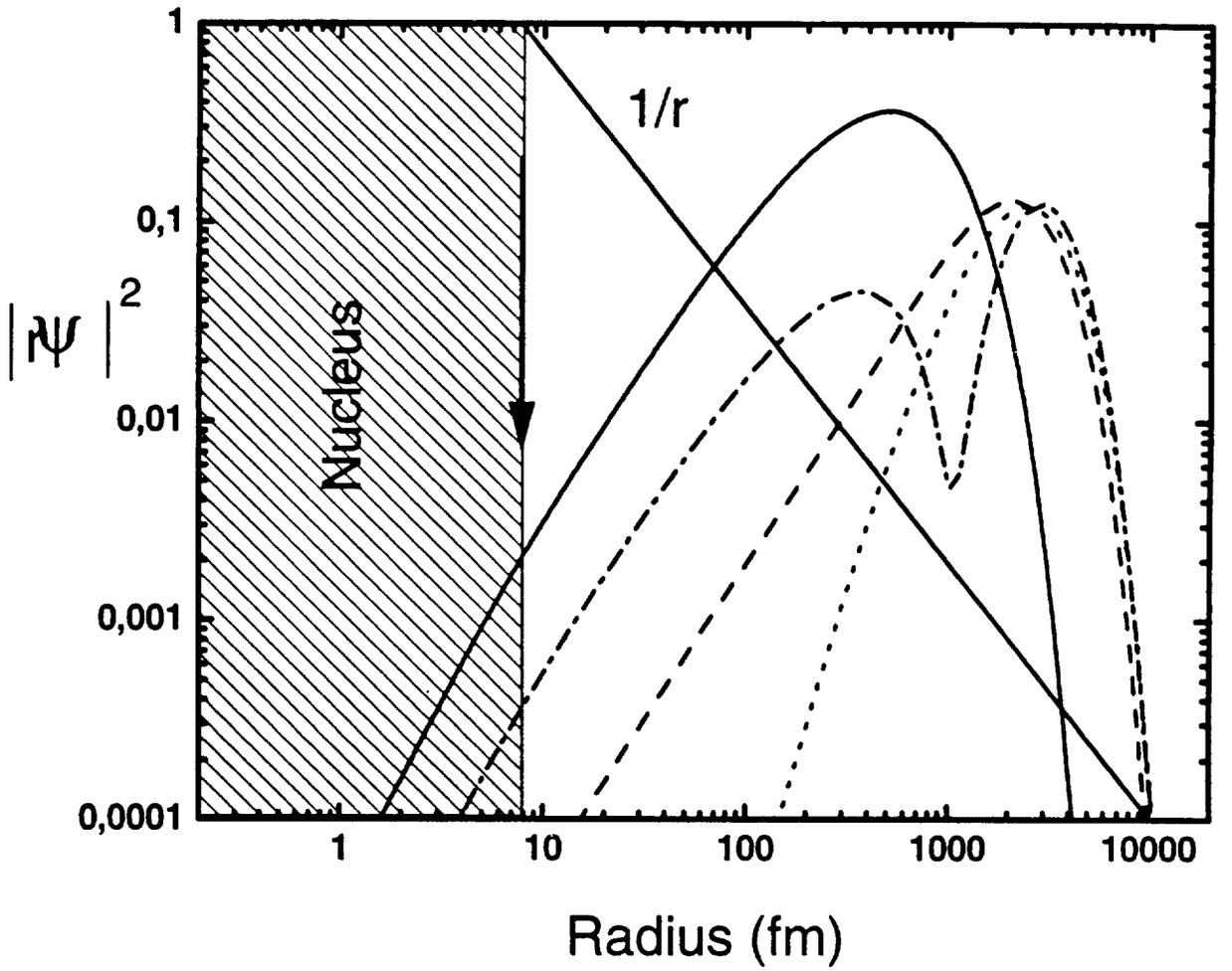
1
0,1
0,01
0,001
0,0001
$|\psi|^2$
Nucleus
1/r
1
10
100
1000
10000
Radius (fm)

2.6

polarization and approaches already the size of the self energy contribution (see Fig. 2.1). Therefore, an ultimate test of QED corrections in high-Z systems requires a detailed understanding of the nuclear structure, i.e. of the nuclear charge distribution.

Moreover, the magnetic moment distribution of the nucleus (Bohr-Weisskopf effect, (Bohr and Weisskopf, 1950)) may have a considerable impact on the atomic structure. For the case of nuclei with an unpaired number of neutrons or protons (e.g. ^{209}Bi) the nuclear spin I couples together with the angular momentum of the atomic core J. The resulting total angular momentum F causes the, in general small, hyperfine structure splitting which is approximately given by

$$\Delta E_{HFS} \sim const \cdot \frac{Z^3}{n^3} g_I \tag{3}$$

where g_I denotes the g-factor of the nucleus. As depicted in Fig. 2.7, the ground state splitting approaches for H-like ions beyond Z=50 the eV region which is accessible for Laser spectroscopy. A precise measurement of this splitting gives not only access to the nuclear magnetic moment but probes also higher-order QED effects in particular, the magnetic part of the radiation field.

Fig. 2.7: The hyperfine structure transition energy in H-like ions plotted for some nuclei as a function of atomic number Z. The shaded area depicts the regime which is accessible by Laser spectroscopy (Kühl et al., 1995).

2.2 Interaction processes for highly-charged heavy ions

2.2.1 Capture and recombination

Interaction with the photon field

QED experiments dealing with few-electron systems require a detailed understanding of the interaction processes of highly-charged ions with matter. More general, the precise

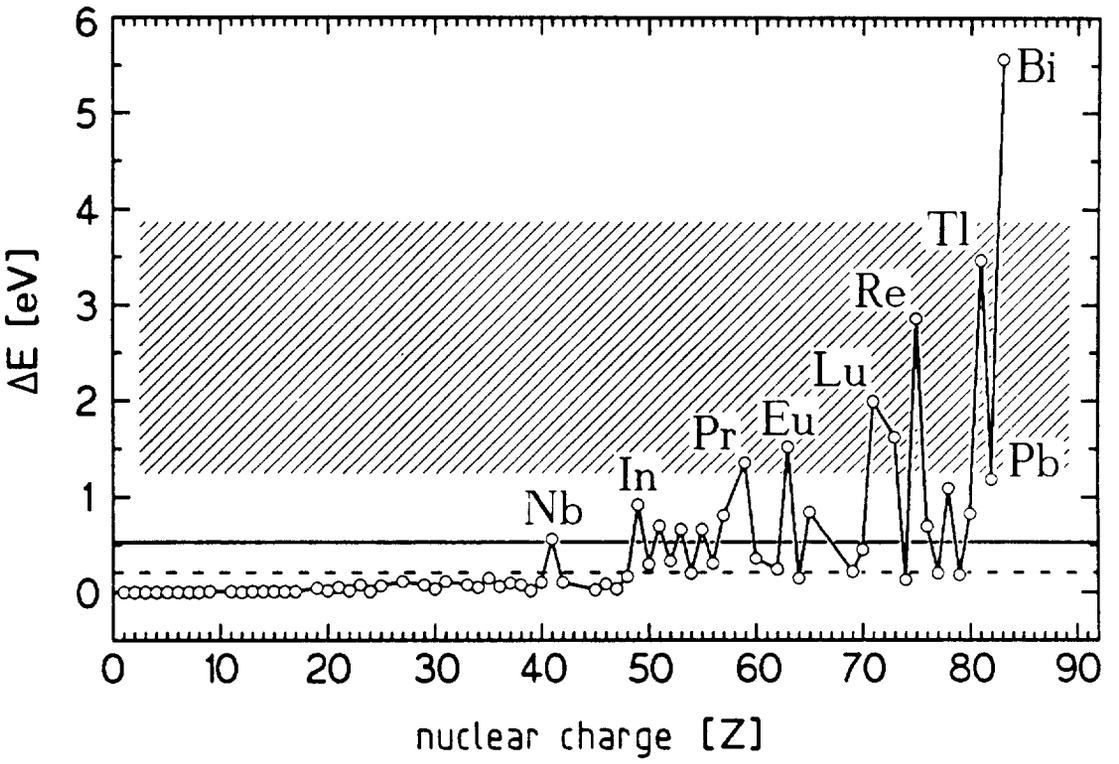
ΔE [eV]
nuclear charge [Z]
Nb
In
Pr
Eu
Lu
Re
Tl
Bi
Pb

knowledge of all possible atomic projectile charge-exchange-processes constitutes the basis for accelerator-storage-ring based research as well as for the operation of electron-beam-ion sources/traps (EBIS/EBIT). In the following, we discuss briefly the most important electron capture mechanisms for bare, H- and He-like heavy ions colliding with atoms or electrons, i.e.: Radiative Electron Capture (REC) or Radiative Recombination (RR), Resonant Transfer and Excitation (RTE) or Dielectronic Recombination (RR), Non-Radiative Capture (NRC) or Three-body Recombination (TR). Here we treat first the radiative processes mediated by the coupling of the electron with the photon field of the nucleus.

Fig. 2.8: Right side: Recombination processes which take place in collisions of free electrons with highly charged ions (RR: Radiative Recombination, DR: Dielectronic Recombination, TR: Three-body Recombination). On the left side of the figure, the corresponding processes for collisions between highly charged ions and bound electrons are given (REC: Radiative Electron Capture, RTE: Resonant Transfer and Excitation, NRC: Non-Radiative Electron Capture).

In collisions of highly charged ions with free electrons an electron may undergo a direct transition into a bound state of the ion via simultaneous emission of a photon with the energy $\hbar\omega = E_{kin} + E_B$, where E_{kin} denotes the kinetic electron energy and E_B the electron binding energy in its final bound state (see Fig. 2.8). This process is the inverse of the fundamental photoelectric effect (Stobbe, 1930). Due to the requirements of momentum and energy conservation this Radiative Recombination (RR) process constitutes the only possible recombination process between bare ions and free electrons in an isolated environment, for instance in low dense plasmas. Similar to the RR process, also target electrons can be captured radiatively into a bound state of the projectile. If the kinetic energy of the electron greatly exceeds the initial binding energy of the target electron

CAPTURE

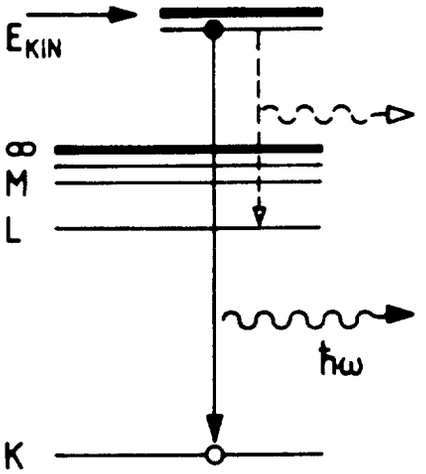

REC

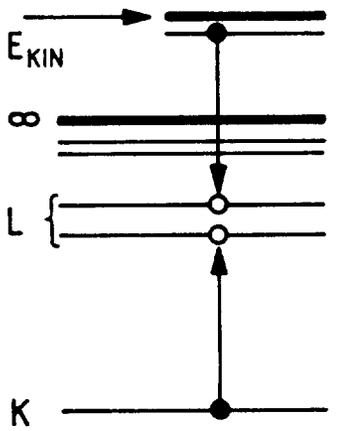

RTE

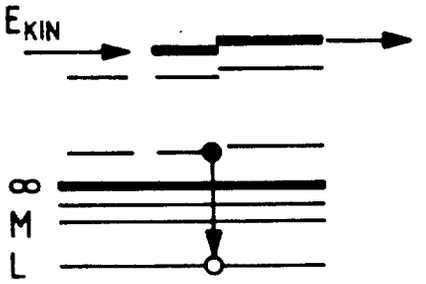

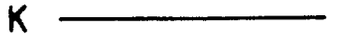

NRC

RECOMBINATION

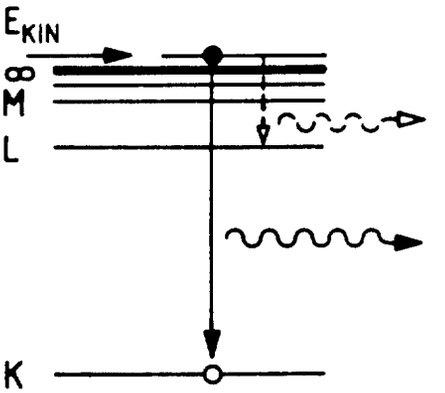

RR

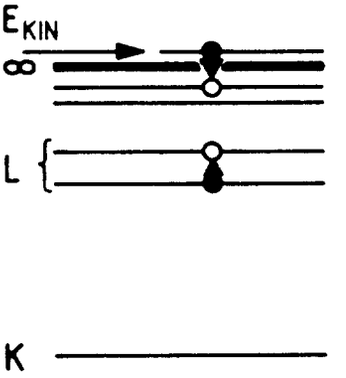

DR

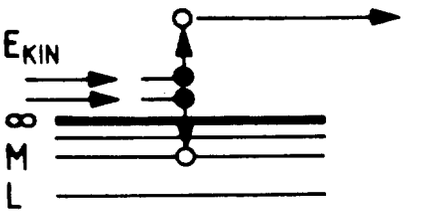

TR

(impulse approximation) one may disregard the latter, so that this Radiative Electron Capture process (REC) is equivalent to the RR mechanism. In addition, one has to take into account the initial momentum distribution by folding in the Compton profile of the target electron into the cross section for radiative recombination.

As early as 1930 Stobbe (1930) derived within the framework of the non-relativistic dipole approximation a general result for RR into an arbitrary (n,l) state of a bare ion. The result of Stobbe is of the form

$$\sigma_{nl}^{\text{Stobbe}} = \frac{\pi^2}{3}\alpha^3 a_0^2 \left(\frac{\nu^3}{1+\nu^2}\right)^2 \left((l+1)\,[C_{nl}^{l+1}(\nu)]^2 + l\,[C_{nl}^{l-1}]^2\right), \tag{4}$$

where $\nu = \alpha Z/n\beta$ is the Sommerfeld parameter, $\beta = v/c$ and a_0 the Bohr radius. The quantities $C_{nl}^{l\pm1}$ are the dipole matrix elements for transitions between bound states (n,l) and continuum states with angular momenta $l \pm 1$. An estimate for REC cross sections for light target atoms can be obtained from the equation given above by multiplying σ^{Stobbe} with the number Z_{T} of quasi-free electrons in the target (Kleber and Jakubassa, 1974). If only capture into the projectile K-shell is considered, the equation given above simplifies to the well-known expression (Bethe and Salpeter, 1957)

$$\sigma_{1s}^{\text{Stobbe}} = 9.165 \times \left(\frac{\nu^3}{1+\nu^2}\right)^2 \frac{e^{-4\nu\,\arctan(1/\nu)}}{1-e^{-2\pi\nu}} \times 10^{-21}\text{cm}^2 \tag{5}$$

We emphasize that the projectile charge number Z and the velocity v enter the Stobbe cross sections not separately, but only in the combination Z/v occurring in the Sommerfeld parameter ν. The Sommerfeld parameter is simply related (non-relativistically) to the "adiabaticity parameter η" regularly used to describe collision processes by (Madison and Merzbacher, 1975)

$$\eta = \frac{1}{\nu^2} = E_{kin}/E_B. \tag{6}$$

This means, that the Stobbe formula provides an universal cross section scaling law, valid for all non-relativistic ion-atom collision systems. It is interesting to note, that

exact relativistic RR (REC) calculations, performed very recently (Ichihara *et al.*, 1994) demonstrate that this simple dipole-approximation is even applicable for high projectile charges (e.g. uranium) and relativistic beam energies up to a few hundred MeV/u.

RR is the dominant loss process in storage rings equipped with electron cooler devices and is hence of great practical importance. In a cooler the relative kinetic energy of the free electrons with respect to the ions is extremely small, characterized by the electron temperature, see Fig. 2.8. REC into heavy projectiles opens via the time reversal the relativistic regime of the photoeffect which is not accessible even at the third generation synchrotron facilities. Here, the relative energy of the quasifree electrons is normally close to the size of the K-shell binding energy ($\eta > 1$, cf. Fig. 2.8).

Electron-electron interaction processes

Beside the interaction of a free or quasifree electron with the radiation field of a fast moving projectile also the electron-electron interaction may give rise to capture of a free electron into a bound projectile state. In this Dielectronic Recombination process (DR) (Burgess, 1964) the energy gain by electron capture into the projectile is used to excite radiationless an initial projectile electron, forming in general a doubly excited projectile state (which in the end stabilizes radiatively). Consequently, DR requires the presence of at least one projectile electron in the intial state and it represents the time reversal of the important Auger effect. Due to energy conservation this process can occur only at certain resonance energies E_{res} which correspond precisely to the energy transfer needed for projectile excitation (ΔE), i.e. $E_{RES} + E_d = \Delta E$, where E_d denotes the intermediate state populated by the recombination process (cf. Fig. 2.8). Applying the adiabaticity parameter definition used above, we find e.g. for the case of a KLL resonance (Auger notation: excitation from the K to the L shell via resonant capture into the L shell) the

general non-relativistically correct resonance condition (Mokler and Reusch, 1988)

$$E_{RES}^{KLL} = \frac{1}{2} \cdot \eta. \tag{7}$$

In a given resonance the DR cross section may drastically enhance the total recombination cross-sections and a measurement of the cross section strength, in particular of subshell resonances, provides a unique tool for the investigation of electron-electron interaction effects such as the Breit interaction (Zimmerer *et al.*, 1990). Also the spectroscopy of the resonance energies can be applied for detailed atomic structure studies, for instance for QED investigations in few-electron systems (Spies *et al.*, 1995).

Resonant Transfer and Excitation (RTE), which occurs in ion atom collisions, can be treated within the impulse approximation as DR process and it refers to initially quasifree instead of free electrons. In this process, which has been studied systematically for low as well as for high-Z ions up to uranium (Graham *et al.*, 1990, Kandler *et al.*, 1995a), the resonance profiles are broadened by the Compton profiles of the quasifree target electrons. However, unlike to DR, this broadening does in general not allow, except for high-Z ions, to resolve experimentally the fine structure splitting of the ions. We like to add that with RTE high lying resonance states such as KLL resonances ($\Delta n = 1$) can be probed whereas with cooler devices normally low lying resonances ($\Delta n = 0$) are accessible (cf. Fig. 2.8).

Three body interaction

Three body recombination (TR), which may take place in electron-ion collisions, is caused by transfer of the "recombination energy" onto a second electron present during the collision (see Fig. 2.8). Consequently this process requires extremely high electron densities and it can only contribute significantly to the total recombination cross-section at low collision velocities (Stevefelt *et al.*, 1975). With respect to the present experimental conditions at electron cooler devices, electron targets and electron beam-ion sources, this

process can in general be neglected. This is completely in contrast to the electron capture process mediated by three body interaction in ion-atom collisions, the non-radiative or Coulomb electron capture (NRC) (Eichler, 1990). Here, the third particle involved in the collision is the target atom and the electron is transferred radiationless from a bound target state into a bound state of the projectile where the target recoil takes the access momentum. At medium and high collision energies ($\eta \geq 1$) only the most tightly bound target electrons determine the total NRC reaction cross section. In general, a precise theoretical description is difficult to perform as the Coulomb field of the projectile leads to distortions of the atomic wave functions in the target even at infinite distances. However, already the simple first order OBK approximation gives the rough cross-section scaling dependence,

$$\sigma_{NRC} \sim \frac{Z^5 Z_T^5}{E_{kin}^5}. \tag{8}$$

It is important to note that for relativistic collision conditions the above energy dependence has to be modified which approaches asymptotically a E_{kin}^{-1} form. The strong scaling of the NRC cross section with the nuclear charge of the target implies that at not too high energies this capture process is by far the dominant one in collisions of high-Z projectiles with medium or high-Z target atoms (Eichler *et al.*, 1990).

2.2.2 Excitation and ionization

Electron loss

Beside the non-resonant electron capture processes REC and NRC, projectile ionization is the most important charge-exchange channel in collisions between few-electron projectiles and neutral target atoms. In the relativistic energy domain and for high-Z projectiles the K-shell ionization is of particular importance as the interplay between electron capture and K-shell ionization processes crucially determines the production yield for bare ions.

Within the non-relativistic first order perturbation theory (Plane Wave Born Approximation, PWBA (Rice *et al.*, 1977) or the Semi-Classical Approximation, SCA (Rösel *et al.*, 1982)) the K-shell ionization cross sections follow the simple scaling law (cf. Madison and Merzbacher, 1975 and Refs. cited there).

$$\sigma_{ion} \sim const \cdot \frac{Z_T^2}{Z_P^4} \cdot f(v/v_k). \tag{9}$$

Here $f(v/v_k)$ is a slowly varying function with η which has its maximum close to collision velocities v equal to the velocity of the active K-shell electron v_k, i.e. at an adiabaticity parameter $\eta \approx 1$. For K-shell target ionization by fast moving ions the same equation is valid and one has simply to consider the reversed collision system. Taking into account correct relativistic bound and continuum wave functions this simple scaling law is abolished. However, for collision velocities around $\eta = 1$ these corrections are of minor importance.

It is important to note, that within the framework of the first order perturbation theory the ionization cross section is independent of the sign of the charge of the ionizing particle, and hence, the cross sections for electron and proton impact are the same. This is true for high-energies where the collision velocity greatly exceeds the velocity v_k. However, at velocities close to $v \sim v_k$ one has a threshold behavior for electron impact, i.e. only at energies $v \geq v_k$ the momentum transfer by electron impact is sufficient to promote the bound K-shell electron into the continuum.

Fig. 2.9: Ionization cross sections for H-like uranium projectiles colliding with protons (full lines) and electrons (dashed lines) plotted versus the adiabaticity parameter η (see text).

In Fig. 2.9 the calculated K-shell ionization cross sections for H-like uranium projectiles colliding with protons (full lines) and electrons (dashed lines) are given versus the

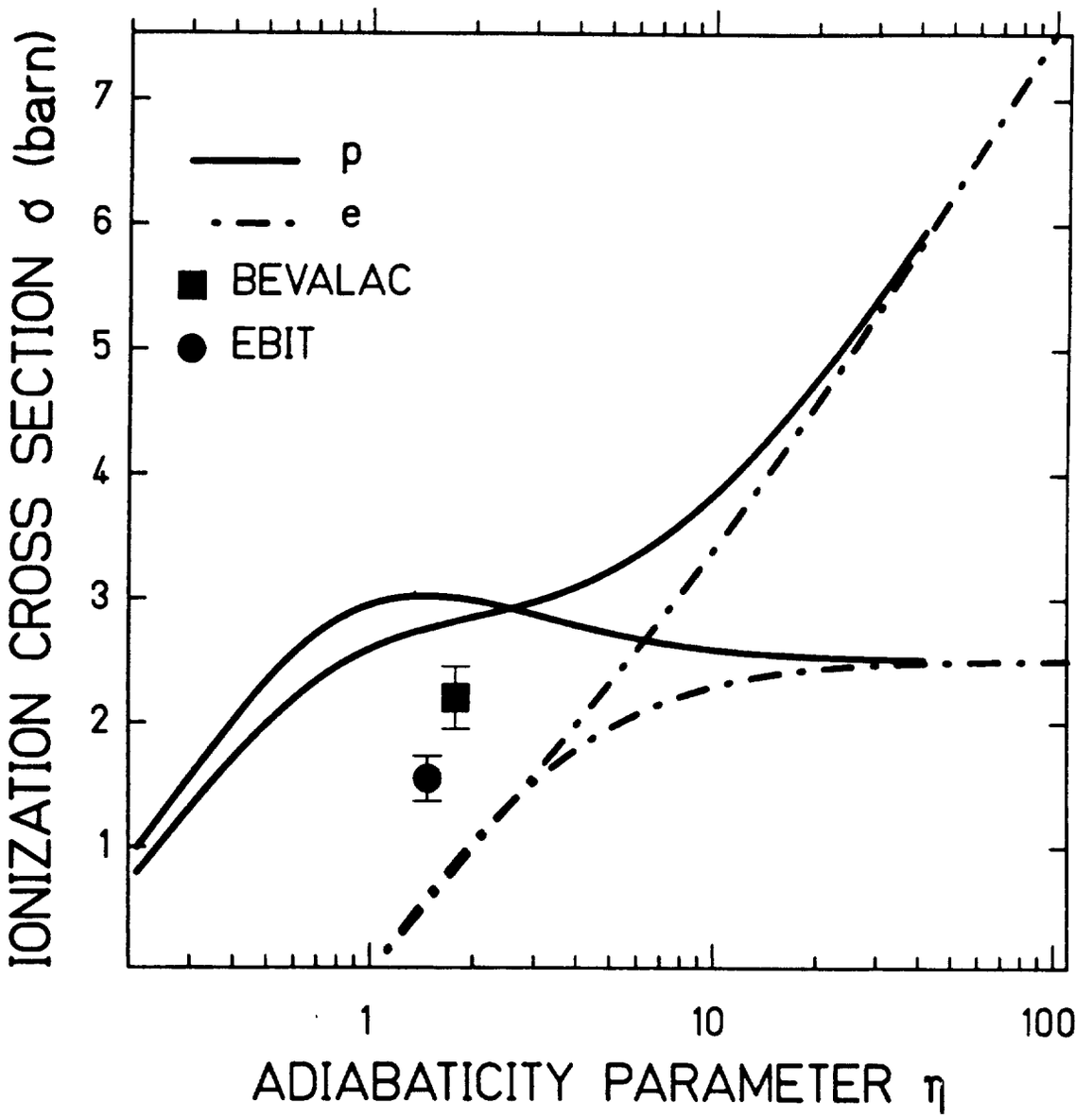
IONIZATION CROSS SECTION σ (barn)
7
6
5
4
3
2
1
p
e
BEVALAC
EBIT
1
10
100
ADIABATICITY PARAMETER η

adiabaticity parameter η. For the calculation of the electron impact ionization cross sections the Lotz formula was used (Lotz, 1968), and the proton impact cross sections were calculated by applying the PWBA formalism (Anholt, 1979). For both cases two curves are plotted in the figure. The curves which approach an almost constant cross section value represent the pure non-relativistic predictions. The second ones, which show an increasing cross section with increasing η value, consider also the transverse ionization term (Anholt, 1979). Here, for the case of the PWBA calculation, corrections due to the relativistic bound state wavefunctions are taken also into account. The experimental data given in addition were measured at the Super-EBIT for electron impact (Marrs *et al.*, 1994a) and at the BEVALAC for U^{91+} onto Mylar foils (Meyerhof *et al.*, 1985a). For the latter case the simple Z_T^2 scaling law for ionization was applied in order to compare the measured value with the predictions for proton impact. We have to emphasize, that for electron impact, precise fully relativistic ab initio calculations are available which are in excellent agreement with the experimental value (Fontes *et al.*, 1995).

Excitation mechanisms

Ionization is mediated by the time variation of the distortion from the collision partner seen by the electron of concern. The same interaction can also yield instead to an ionization to an excitation for instance of a projectile electron of a highly charged ion by a target electron. The same difference in the cross section behaviour between electron and proton impact is present at small "η" whereas at high scaled velocities both cross sections approach each other asymptotically. At small "η" we have for electron impact excitation a specific threshold behaviour and for ion impact a smooth increase with "η" (cf. Fig. 2.9).

In the adiabatic collision domain ($\eta < 1$) mainly the monopole part of the perturbation dominates excitation (and ionization). In contrast, in the high velocity region ($\eta \geq 1$) the

dipole contribution is dominant. In the relativistic region additionally higher multipole contributions, in particular magnetic induced transitions, have to be considered. More clearly, at low energies $s \rightarrow s$ transitions and at high energies $s \rightarrow p$ transitions dominate.

Beyond the various capture and recombination processes discussed previously in this chapter which are the main processes for populating excited states in highly-charged heavy ions, we have also to consider Laser induced population processes. However, as can be read from Figs. 2.4 and 2.5 not only the transition energies increase with Z; also the transition rates increase dramatically. As powerful Laser light is only available in a very limited energy region (< 10 V) Laser induced transitions can only bridge gaps between very adjacent levels, i.e. inter shell transitions in light ions, transitions in high Rydberg states of medium heavy ions, or transitions in hyperfine ground state levels of very heavy ion species. Moreover, the radiative recombination which is a free-bound transition can also be stimulated by a Laser field. Additionally, Laser induced transitions provide extremely narrow resonances giving an ideal probe to test the qualities of ion beams such as e.g. their absolute velocities. Also Laser cooling of the lighter heavy ions is a very powerful tool where it is applicable (Schröder *et al.*, 1990, Hangst *et al.*, 1991). Here, we should also mention that at high velocities even the theory of special relativity can be tested by laser resonance excitation of fast light ions in the ring. In Fig. 2.10 the various Laser stimulated population possibilities for particular excited levels are summarized. The radiation emitted during deexcitation gives an additional spectroscopic information on the levels of interest.

Fig. 2.10: Laser stimulated processes:

- excitation for light ions (left side)
- stimulated recombination in medium heavy ions (center part)
- induced ground state hyperfine transitions in very heavy ions (right side)

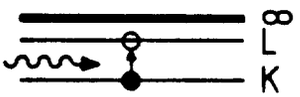

EXCITATION

RECOMBINATION

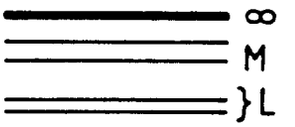

HYPERFINE EXC.

LASER - STIMULATED PROCESSES

3 Storage and Cooler Rings for Heavy Ions

3.1 The production of highly-charged heavy ions

Atoms can be ionized by photon interaction, by electron impact or by bombardment of heavy particles like ions or atoms. In order to ionize inner shell electrons in heavy atoms correspondingly high energy or momentum transfers are involved. As for photons the necessary high fluxes at high energies are presently not available for an efficient ionization of large atom quantities only heavy particle or electron impact techniques can provide sufficient numbers of highly charged heavy ions for experiments. In the previous section it was shown that at equivalent collision velocities with $\eta \geq 1$ the cross sections for ionisation of the last inner shell electron are comparable for electron or heavy particle impact. In particular around $\eta \approx 1$ and due to the Z^2 dependence of the inner shell ionisation heavy ion impact is superior to electron impact. For both cases, experimental cross sections reduced to the same charge for distortion (electrons and protons) are given in Fig. 2.9 for one typical example in uranium. In the case of heavy particle bombardment the classical role of projectile and target atom is interchanged: *Fast* heavy projectiles are ionised by bombardment through target atoms in a stripper (inverted collision system).

Both ionisation methods, direct electron impact and heavy particle impact by stripping, have been applied very successfully to produce ultimately charged, very heavy ions. The electron impact ionization is exploited by the EBIT (Electron Beam Ion Trap) technique, where trapped ions are progressively ionized to higher charges by continuous electron bombardment (Levine *et al.*, 1989; Knapp *et al.*, 1993; Marrs *et al.*, 1994b). In contrast, ionization by heavy particle impact is utilized in the cooler ring technique; here, in an injector, heavy ions are accelerated to high energies and then stripped before they are accumulated in a storage ring, see e.g. Pollock (1991). Both methods are schematically shown in Fig. 3.1.

Fig. 3.1: The two methods to produce highly-charged heavy ions:
TOP - The storage ring technique, where ions are accelerated to high energies and then stripped to high charge states before they are stored and cooled in a huge ring and
BOTTOM (within the magnifying glass) - the EBIT technique, where ions which are confined in a small trap are continuously ionized by a high energy electron beam to high ionization stages.

In the EBIT device the ions are confined by magnetic and electric fields in the trap and the ions are continuously bombarded by an intense beam of electrons. If the electron energy is sufficiently high the trapped ions will successively be ionized until they have lost even their last electron - provided recombination and loss processes are not too fast. In the SUPER-EBIT device in Livermore the electron beam energy can be turned up to about 200 keV which is even in uranium well above the ionization energy for the last K shell electron (Marrs *et al.*, 1994a). A small number of bare U^{92+} ions have already been produced in the trap. The advantage of having the ions almost at rest in the trap is counterbalanced by the drawback of the environment of ions in different ionisation stages.

In storage rings which can also be considered as traps for ions at high energies this drawback of charge state mixing is clearly avoided; however, the high ion velocities may cause via the Doppler effect restrictions for precision experiments (see below). On the other hand, really high intensities of the heaviest and ultimately charged ions can be provided by this acceleration/stripping/storing technique. In the storage ring at the heavy ion accelerator facility at GSI in Darmstadt up to 10^8 bare U^{92+} ions have been stored already for experiments in the ESR (Experimental Storage Ring) (Franzke, 1995). In order to strip the heavy ions to the necessary high charge states before injection into the ring they have to be accelerated to velocities corresponding about to the orbital velocities of the most strongly bound electrons of concern. As can be read from Fig.

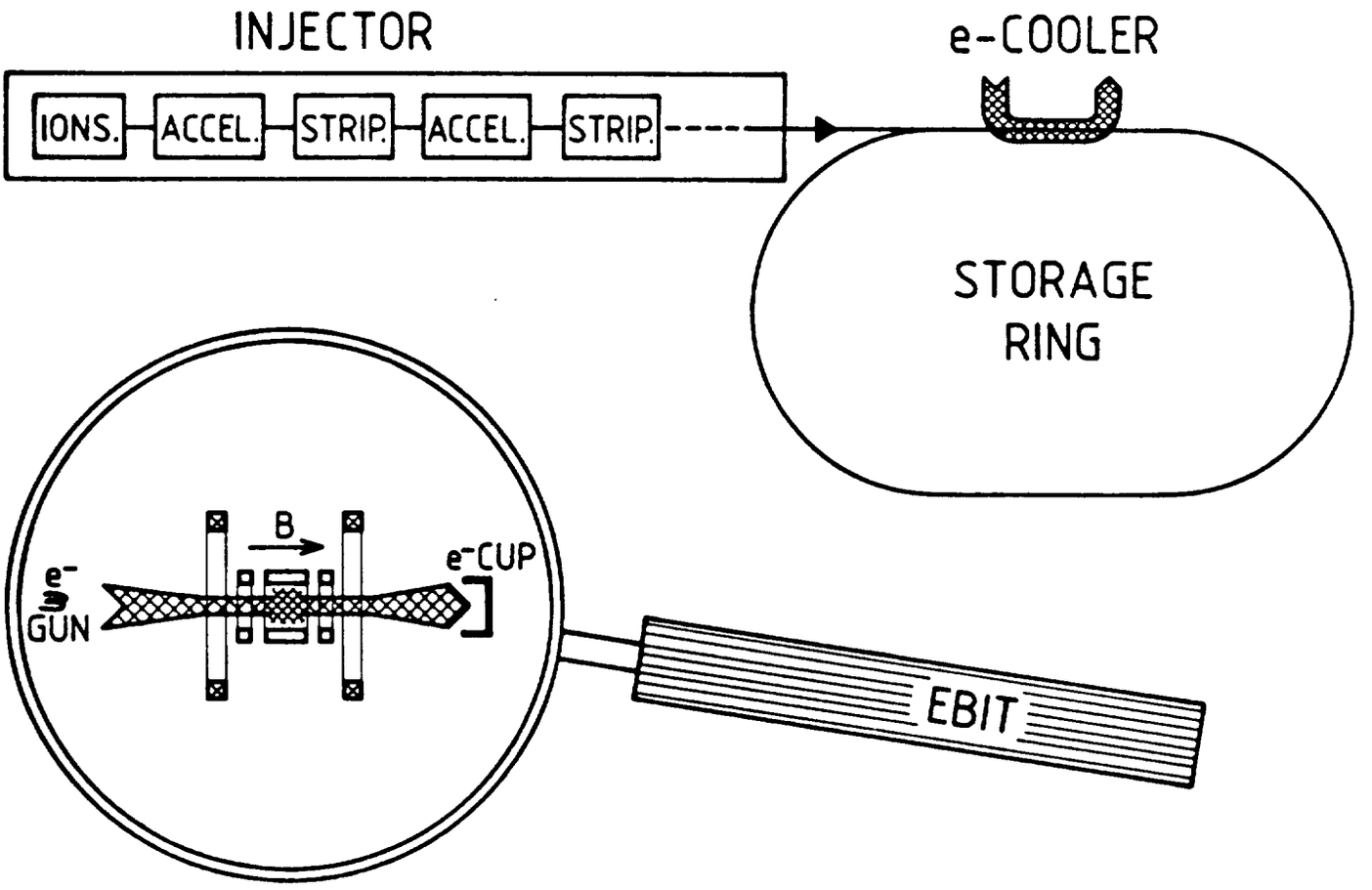
INJECTOR
e-COOLER
IONS.
ACCEL.
STRIP.
ACCEL.
STRIP.
STORAGE
RING
B
e⁻
GUN
e⁻CUP
EBIT

3.1

2.9 this is about equal to the electron beam velocity for electron impact ionization at the threshold of concern. For fast U ions energies between 250 and 500 MeV/u are needed to produce sufficiently high fractions of completely stripped ions. In this case, the acceleration/stripping technique has to be applied in several stages, as is indicated in Fig. 3.1.

The stripping technique will certainly increase the emittance of the ion beam; it will become more divergent, i.e. slightly hotter. Such a stored beam will further heat up by intrabeam scattering and distant collisions with the remnant gas molecules in the ring. Hence, the advent of efficient beam cooling techniques was extremely crucial for the prosperous development of heavy ion storage rings (Möhl, 1988). By various beam cooling techniques - mainly by electron cooling - stored heavy ion beams can be cooled down to low emittances. That means, even for high intensity beams all highly charged ions have almost exactly the same velocity vector and the ions are confined to a small beam diameter. The cooling techniques fix the ion velocity extremely stable over long time periods counterbalancing also the energy loss of the ions colliding with remnant gas particles. Cooling is the prerequisit for heavy ion storage rings providing high luminosity beams of ultimately charged heavy ions even for precision spectroscopy experiments. Moreover, in a ring the charge states of the ions are well-defined and accessible to experiments before and after any reaction.

Both the methods to produce highly-charged heavy ions have advantages and have drawbacks. It is evident that for acceleration of heavy ions to the high velocities and confining them by magnets in a ring a large scale facility is compulsory, whereas for the electron impact technique a relatively small arrangement is sufficient. However, as stripping is more efficient than electron impact ionization mainly due to the higher particle densities in the stripper foils quite large quantities of ultimately charged heavy ions can be provided in a well defined charge state in a storage ring. Due to continuous cooling

the Doppler effect can accurately be taken into account. The drawback of the charge state distribution in EBIT will be overcome by extracting the ions and retrapping charge state pure ions, see the RETRAP-project (Schneider, 1994). The disadvantage of the high velocities in storage rings may be overcome by actively decelerating the ions in the ring; finally these decelerated ions can be extracted and after some further steps stored in a smaller ring or maybe even in a trap, see the HITRAP-proposal initiated by Poth (Beyer *et al.*, 1990). In the following we restrict the discussion only to the results from storage rings for very heavy ions.

3.2 Survey on heavy ion storage rings

After the tremendous success with the initial cooling experiments at CERN (Bell *et al.*, 1981) numerous particle storage rings have been designed and built for various applications. For a complete survey we have to refer to the literature (see e.g.: Pollock, 1991; Franzke, 1988; Bosch, 1993; Schuch, 1993; Müller, 1994; Larsson, 1995). Here, we concentrate only on storage and cooler rings for really heavy ions. These are the facilities at GSI in Darmstadt, at MPI (Max-Planck-Institut für Kernphysik) in Heidelberg, at the MSI (Manne Siegbahn Institute) in Stockholm, and at ISA (Institute for Synchrotron radiation Aarhus) in Aarhus. These storage rings are called ESR = Experimental Storage Ring (Franzke, 1987), TSR = Test Storage Ring (Jaeschke *et al.*, 1990), $CRYRING$ = CRYogenic ion source / injector / RING (Herlander, 1991), and $ASTRID$ = Aarhus Storage RIng Denmark (Möller, 1990), respectively. The corresponding beam guidance magnets can bent beams to closed orbits up to magnetic rigidities for the swift ions of 11, 1.5, 1.4, and 2 Tm, which determine in the end the size of the rings. In Fig. 3.2.a sizes and arrangements for these four heavy ion storage rings are compared. They have circumferences of 108.4, 55.4, 51.6, and 40.0 m, respectively.

Fig. 3.2: A survey on storage rings for very heavy ions.

a – Sizes and general configurations for the presently running heavy ion storage rings in comparison.

b – The layout of the ESR storage and cooler ring is displayed. The beam guidance system, i.e. bending magnets, quadrupoles and hexapoles, are indicated; the systems for beam handling, kicker, RF-cavities as well as the electron cooler are assigned; the Schottky noise pickup detector and the supersonic gas jet target are also shown.

The ion injectors used are for ESR the heavy ion synchrotron facility SIS, for TSR the MP-tandem postaccelerator facility, for $CRYRING$ a cryogenic ion source in connection with an RFQ accelerator, and for $ASTRID$ an isotope separator. For $ASTRID$ also an injection from the available Tandem accelerator is planned; $ASTRID$ is additionally used as an electron storage ring at ISA (Institute for Synchrotron radiation Aarhus university). From these facilities the $SIS - ESR$ arrangement is the only one which can store the heaviest ions as e.g. bare U^{92+}. Therefore, in Fig. 3.2.b the configuration of the ESR is displayed in more detail. The main components are assigned in the figure caption.

In order to strip U ions down to the K shell one needs extremely high energies between 250 and 500 MeV/u, cf. Fig. 2.9; that means, adiabaticity parameters η between 1 and 2. After a stripper we find a charge state distribution for the ions which depends critically on η and via the interplay between ionisation and capture also on the Z number of the stripper material. For very heavy ions at these energies a Cu stripper may be best. Nevertheless, for comparison we display in Fig. 3.3 , the equilibrium charge state fractions for bare, H-, He- and Li-like U ions for a C stripper as a function of the general adiabaticity parameter. The calculations were performed using the code of Stöhlker (Stöhlker *et al.*, 1991). In general, around $\eta = 1$ the K shell is opened, and the bare ion fraction starts to evolve. At about $\eta = 2$, that means for U at about 500 MeV/u, the H-like ion fraction is already

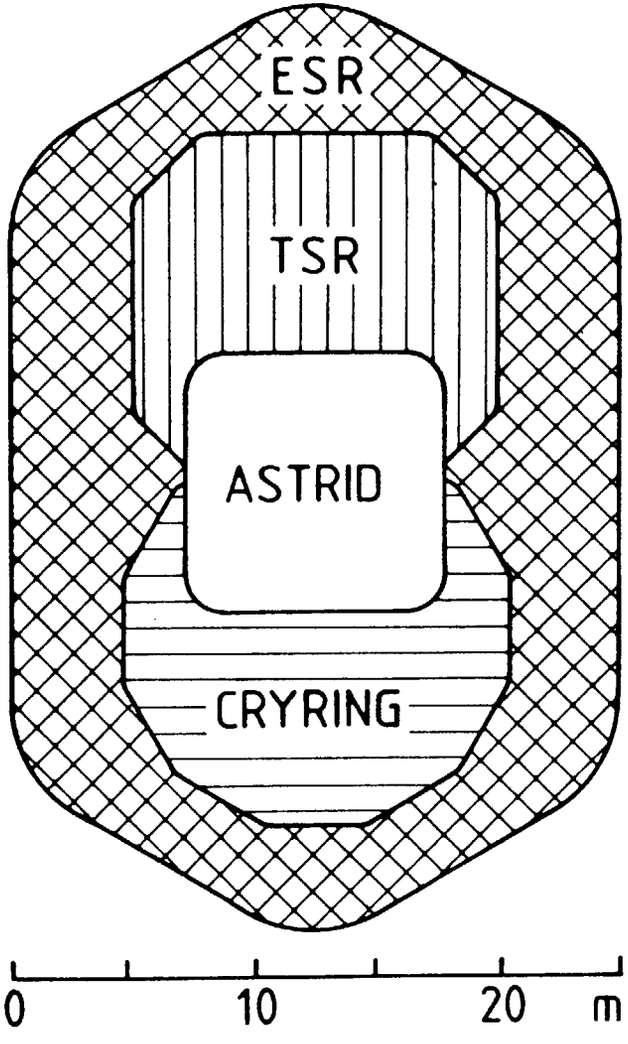
ESR
TSR
ASTRID
CRYRING
0
10
20
m

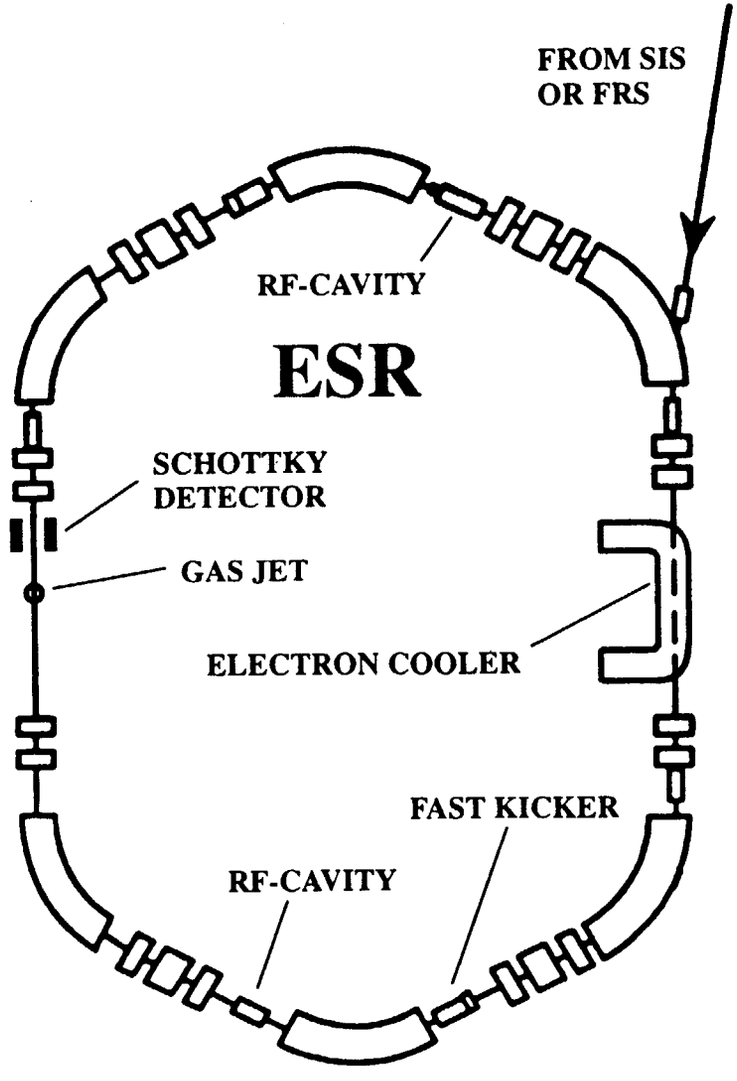
FROM SIS
OR FRS
RF-CAVITY
ESR
SCHOTTKY
DETECTOR
GAS JET
ELECTRON COOLER
FAST KICKER
RF-CAVITY

more abundant than the one for He-like ions.

Fig. 3.3: Equilibrium charge state fractions for U ions behind a C-stripper as a function of the scaled kinetic energy, the adiabaticity parameter η. For calculations see the code given by Stöhlker *et al.* (1991).

The η representation chosen in Fig. 3.3 is in general approximately valid for all ions over the whole periodic table, giving only minor variations with the atomic numbers for ion species and stripper material. Therefore, we can use such a representation to show the ranges of operation for the various rings more generally. In Fig. 3.4 these ranges are plotted in the coordinate system η and Z, i.e. adiabaticity parameter and atomic number of the stored ions. As in a non-relativistic consideration the orbital velocities for the K-shell electrons of concern are proportional to Z and η is proportional to $1/Z^2$, the specific ion energies "MeV/u" follow straight lines in a double logarithmic plot.

Fig. 3.4: Ranges of operation for the presently running heavy ion storage rings in the parameter field atomic number Z of the ion and scaled ion energy η. Specific ion energies "MeV/u" are indicated for several "diagonals". The years when the storage rings came into operation are given in brackets.

Fig. 3.4 demonstrates once more, that the ESR is the only storage ring which can store all heavy ions up to bare U^{92+} ($\eta > 1$). The typical range of operation (dark hatched area) is between 100 and 350 MeV/u. From the η range it is clear that predominantly bare and few-electron ions starting from Ne upwards to U can be stored. Moreover, after injection the stored ions can be actively decelerated in the ESR so that its final range will cover in the end specific energies down to about 10 MeV/u. Presently, bare U^{92+} ions have already been decelerated in a first experiment from about 360 MeV/u down to 50

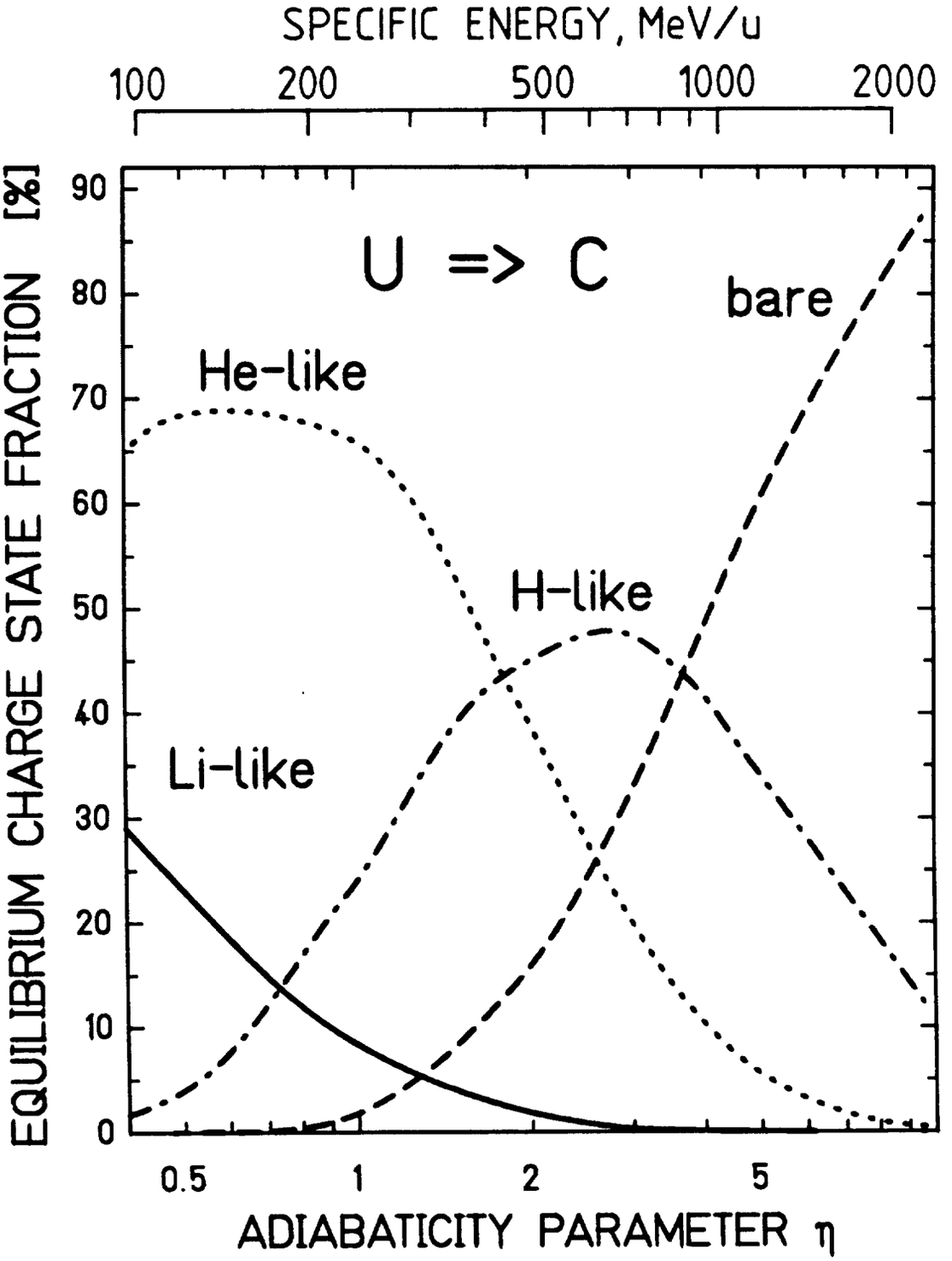

'APOB.PAP94#.DATA(MEYER)'

2.3

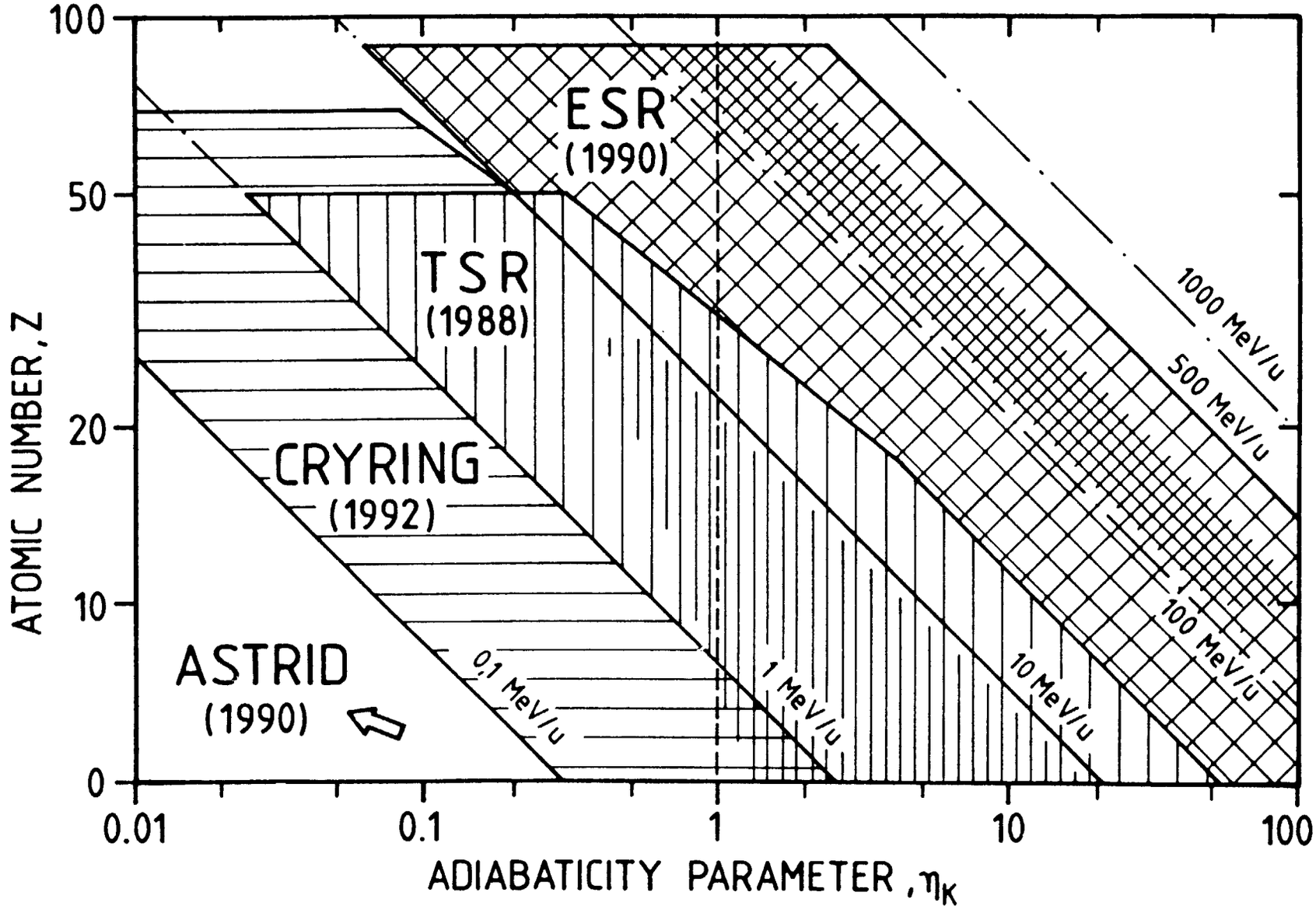
ESR
(1990)
TSR
(1988)
CRYRING
(1992)
ASTRID
(1990)
1000 MeV/u
500 MeV/u
100 MeV/u
10 MeV/u
1 MeV/u
0,1 MeV/u
ATOMIC NUMBER, Z
ADIABATICITY PARAMETER, η_K
100
50
20
10
0
0.01
0.1
1
10
100

3, 4

MeV/u with an efficiency of 90 %, where at the lowest energy the cooling was switched on again (Stöhlker, 1995 and Mokler *et al.*, 1995b).

The TSR operates typically below about 10 MeV/u, see dark hatched area. For high-Z ions ($Z \geq 25$) η gets smaller than 1 and it is difficult to produce few-electron ions for injection. The TSR is the first heavy ion ring which came into operation, already in the year 1988. The $CRYRING$ started with its operation only in 1992; until recently light heavy ions have mostly been used there. As for $ASTRID$ the injection from the tandem accelerator is not yet finished, only moderately charged or light ions from the mass separator have been injected at very low η. On the other hand $ASTRID$ is designed also for high rigidity ions; and indeed extremely heavy species, as charged C_{60} clusters have successfully been stored there (Andersen *et al.*, 1995a). Also the structure and collision dynamics of negative ions and molecules were studied there intensively (Andersen *et al.*, 1993 and Andersen *et al.*, 1995b). Despite the results for light heavy ions or for heavy clusters as well as for negative ions and molecules are also very exciting, we concentrate in this review only on the challenging physics of the very heavy, ultimately charged ions. Therefore, we report mainly on the results from the ESR and include partially also those from the other heavy ion storage rings, especially from the TSR.

3.3 Cooling and experimental facilities at the ESR

3.3.1 Ion beam cooling techniques

For all ion storage rings beam cooling is *the* crucial issue. In general there are three different beam cooling techniques (for a review see e.g. Möhl, 1988):

(i) stochastic cooling,

(ii) electron cooling,

(iii) Laser cooling.

The principle of these techniques will briefly be described below; for details we have to refer to the literature.

In stochastic cooling the mean position of a small bunch of particles in the phase space is measured and then this bunch is transferred by active kickers to the correct spot, i.e. to the center of the emittance ellipse. The stochastic cooling is in particular appropriate for hot beams, i.e. beams with large emittances. This is for instance important if reaction products from nuclear reactions or exotic particles are accumulated in a ring (Van der Meer, 1972). At the ESR stochastic cooling will be installed in 1996 in order to cool efficiently hot fragments injected from the fragment separator FRS placed between SIS and ESR.

In electron cooling the ions dive in the cooler into a bath of cold co-moving electrons (*cf.* Poth, 1990a). The electron beam is merged by magnetic guidance fields with the ion beam, where both beams have the same mean logitudinal velocity. Due to the variance in the velocities (temperature) the ions transfer the excess in their temperature via elastic scattering onto the cold electrons. The cooling works best if the initial ion temperature is not too hot compared to the electron beam temperature. Electron cooling is ideal for accelerator beams injected after stripping into a storage ring. The electron coolers are the working horses for all the ion storage rings giving low emittance beams with high luminosities. (Wolf, 1988; Poth, 1990b).

Ions can also interact efficiently with photons from Laser beams as long as a proper excited state in the ion is available. By photon absorption a certain uni-directional momentum is transfered to the ion, whereas the re-emission is isotropic. Therefore, a Laser can transfer on the average momentum to ions of a certain velocity class. This effect can be used also in combination with other techniques to squeeze the ions almost into one

velocity class. Ultra cold ion beams have been produced by Laser cooling (Schröder *et al.*, 1990; Hangst *et al.*, 1991). However, as the energy range for Laser is very limited only low-Z ions have been cooled until now. Laser cooling seems not to be a general cooling technique for highly-charged very heavy ions, despite it is extremely efficient - if applicable.

For stored beams of heavy, highly-charged ions electron cooling is *the* cooling technique. In the ESR the electron gun can accelerate electrons up to 270 keV corresponding to a specific ion energy of about 500 MeV/u. The electron beam with a total current up to 5 A is merged at the bottom of the U-shaped magnetic guidance field with the circulating beam over a length of 2 m, corresponding to about 2 % of the ring circumference (Spädtke *et al.*, 1991). The ions traverse the cooling section about 10^6 times per second.

3.3.2 The ESR facility

The ESR facility with its devices is shown once more in Fig. 3.5. After injection (1) the ions are cooled in the electron cooler (2) (Spädtke *et al.*, 1991). The intensity of the stored beam is measured by a current transformer and the beam position can be probed by different pick-up devices (both devices are not shown in the figure). From the frequency analysis of the Schottky noise, picked up by the electrode of the $SCHOTTKY-detector$ (see also Fig. 3.2.b), one can deduce the longitudinal momentum distribution of the circulating particles. A corresponding frequency spectrum is shown in the insert in Fig. 3.5 for the case of bare U^{92+} injected at 295 MeV/u into the ring. The non-cooled beam has a longitudinal momentum spread $\Delta P/P$ of about $1 \cdot 10^{-3}$ (FWHM), whereas a continuous cooling with 250 mA electrons reduces this spread to $1 \cdot 10^{-5}$ (Eickhoff *et al.*, 1991). This inserted plot shows most drastically the necessity and efficiency of electron cooling.

Fig. 3.5: The main devices of the ESR relevant for experiments are shown:
(1) ion beam injection

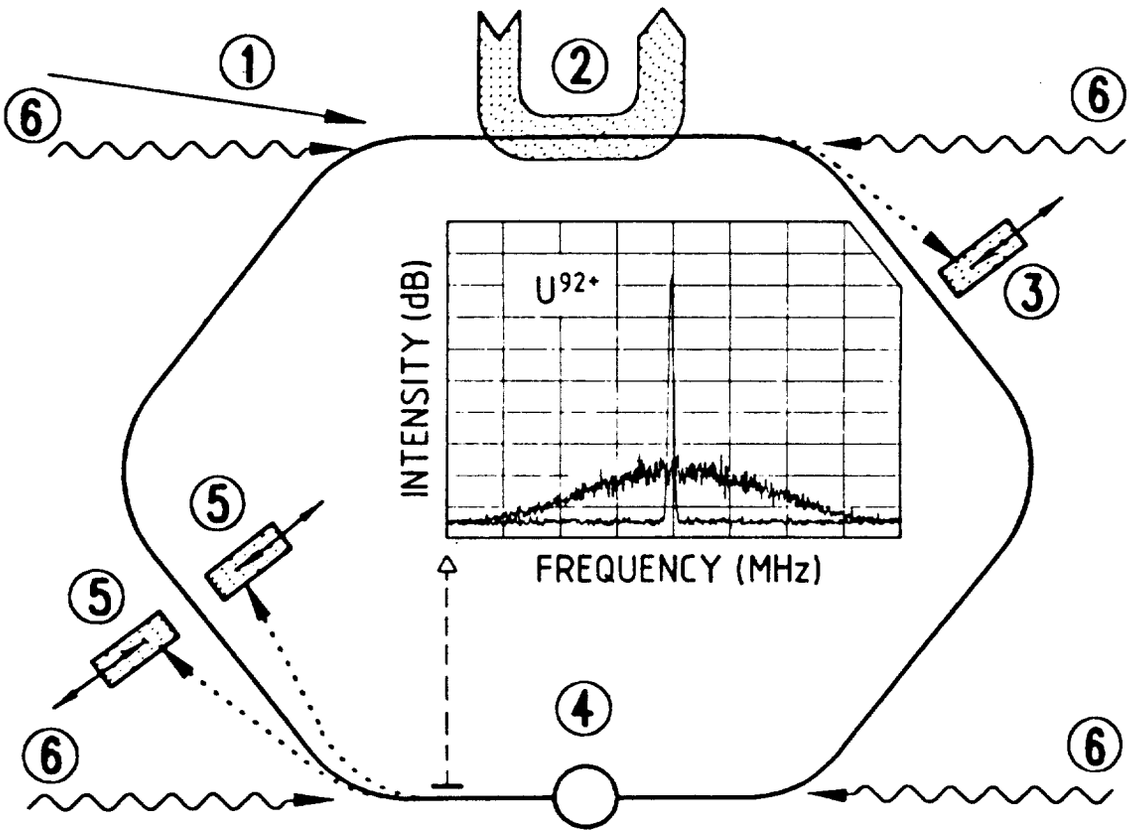

3.5

(2) electron cooler

(3) particle detector for ions recombined in the cooler section

(4) gas-jet target

(5) particle detectors for charge changed (ionization/capture) ions

(6) Laser beams to merge the ion beam at the cooler or gas target

The insert shows the *SCHOTTKY* frequency spectrum for the circulating ions (relative units "*dB*"). For the case of 295 MeV/u U^{92+} the longitudinal momentum distribution is displayed for a non-cooled and continuously cooled beam (expanded spectra with zero point supressed).

In the cooler electrons may recombine with ions changing their charge state. These ions will be separated from the original ion beam in the next down-stream magnet and can then be detected in a position sensitive detector mounted behind a thin window in a movable pocket (3) (Klepper *et al.*, 1992). The size of the beam spot for the recombined ions in this detector reflects the transverse momentum spread of the circulating beam. In Fig. 3.6 an example is given for a He-like U^{90+} beam circulating in the ring at 250 MeV/u. Unfolding the detector resolution of 1.2 mm, we can deduce for this case an emittance of 0.05 $\pi \cdot mm \cdot mrad$ (Bosch, 1993; Bosch, 1989). Within the logarithmic representation of Fig. 3.6, we see also some electron capture events from collisions with the remnant gas particles in the dipole and, additionally, some rare events where finally two electrons are captured in the total straight section around the cooler of the *ESR*.

Fig. 3.6: Position and charge spectrum of ions having changed their charge in the cooler by recombination for the case of He-like U^{90+} ions circulating at 250 MeV/u in the *ESR* (Bosch, 1993).

In the long straight section opposite to the cooler, see Fig. 3.5, we have the experimental area of the *ESR* with a supersonic gas-jet target (4) (Gruber *et al.*, 1989). Gas

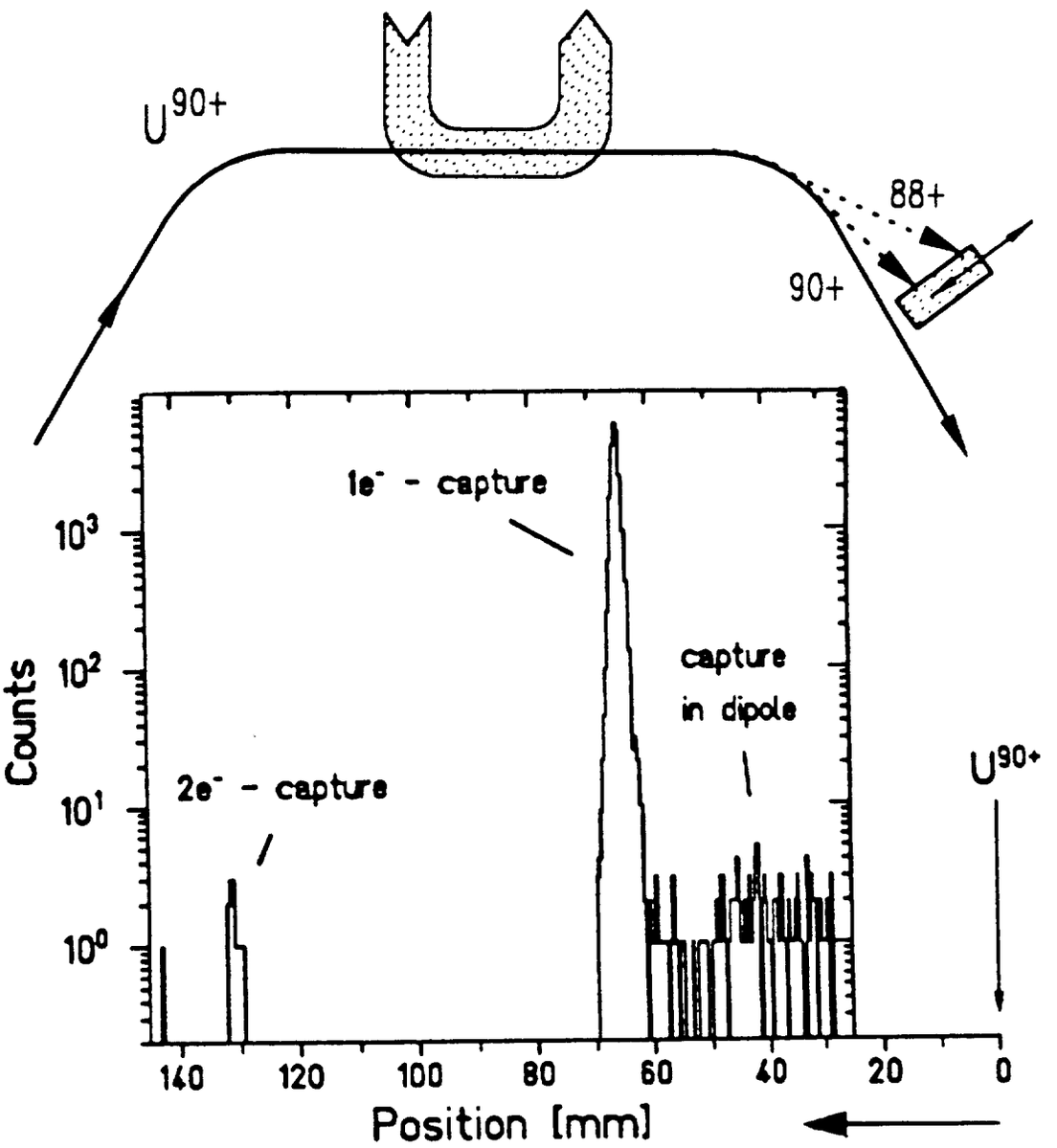
U90+
88+
90+
1e⁻ - capture
capture
in dipole
2e⁻ - capture
U90+
Counts
10³
10²
10¹
10⁰
140
120
100
80
60
40
20
0
Position [mm]

3.6

jets of e.g. H_2, CH_4, N_2, Ar a.s.o. with particle densities of 10^{11} to 10^{13} cm^{-2} can be provided for experiments. Behind the next bending magnet the ions which have changed their charge either by ionization or by capture can be monitored by position sensitive detectors mounted in movable pockets (5) (Klepper *et al.*, 1992). The gas target itself is easily accessible for detectors, in particular for photon and x-ray detectors.

In both straight sections of the *ESR*, the cooler section and the gas target section, colinear and/or counter-propagating Laser beams (6) can additionally be merged with the ion beam and in the cooler section additionally with the electron beam, see Fig. 3.5. So excitation or recombination can be induced by Laser beams.

3.3.3 Storage of heavy ions

For a stable and long term storage of swift heavy ions in a ring a continuous cooling of the ion beam is indispensible. By intra-beam scattering, i.e. ion-ion interaction, the beam will spread out in phase space incessantly. By interaction with remnant gas atoms in the vacuum the ions will loose energy by small angle scattering which additionally increases the beam divergence. Both the effects will in the end destroy the stored beam if it is not cooled continuously. The SCHOTTKY spectra shown in Fig. 3.7. demonstrate clearly what happens to a beam if the cooling is switched off for the case of a stored bare Ar^{18+} beam: The beam becomes hotter and hotter and looses permanently energy (Spädtke *et al.*, 1991). At the used high ion energy of 250 MeV/u energy loss and scattering cross sections for collisions with the remnant gas atoms are tiny for the Ar ions (the mean vacuum in the ring was at that time 10^{-10} *mbar*, a factor of 10 worse than present).

Fig. 3.7: Propagation of the SCHOTTKY signal for a stored 250 MeV/u Ar^{18+} beam after switching off the electron cooling. Three elapse times are displayed: t = 0, 30, and 63 *min* after switching off (Spädtke *et al.*, 1991).

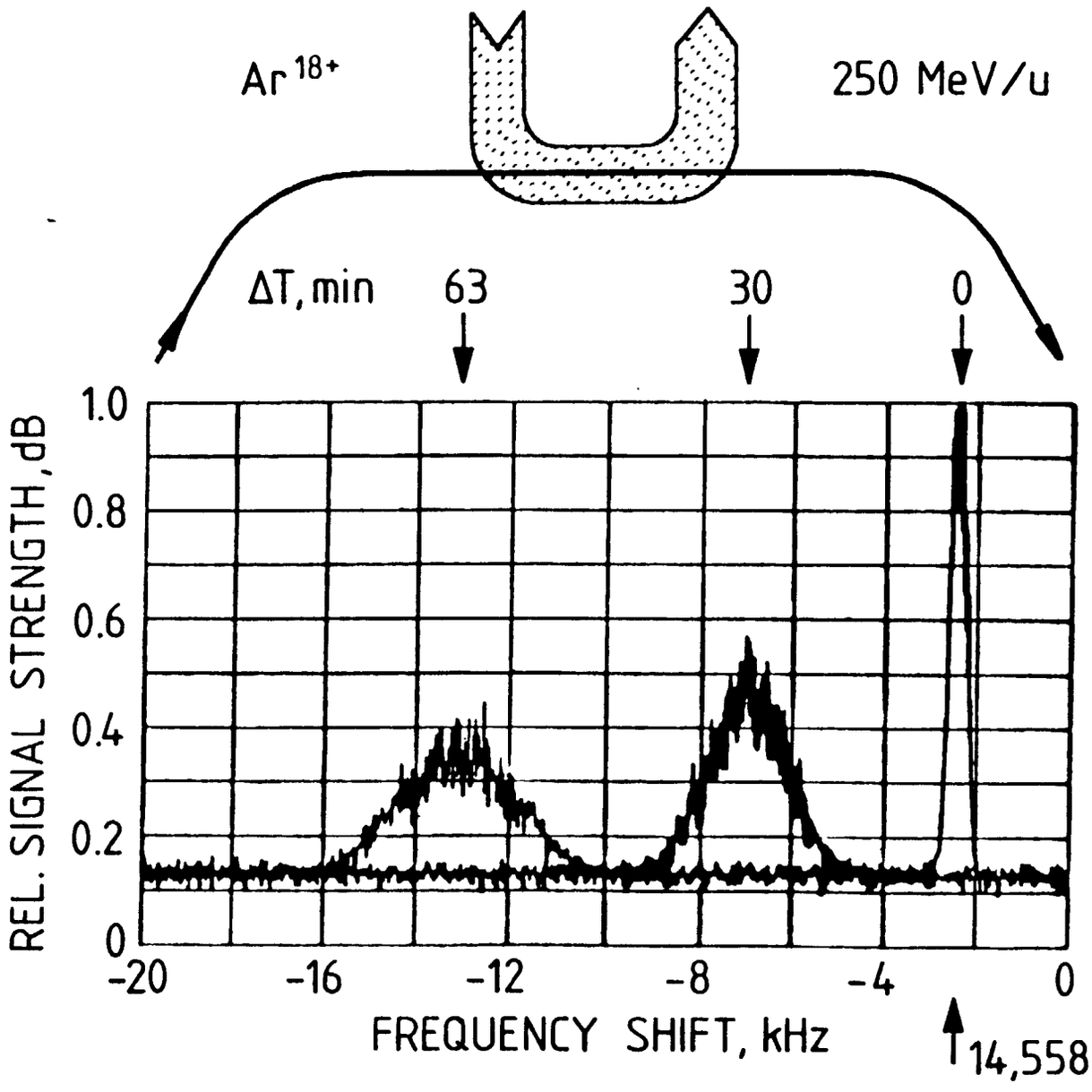
Ar 18+
250 MeV/u
ΔT, min
63
30
0
1.0
0.8
0.6
0.4
0.2
0
REL. SIGNAL STRENGTH, dB
-20
-16
-12
-8
-4
0
FREQUENCY SHIFT, kHz
14,558

3.7.

As nuclear cross sections are small compared to atomic scattering or charge exchange cross sections, nuclear reactions do normally not influence the lifetime of a stored ion beam. Also at high ion velocities, characterized by $\eta > 1$, the beam losses by charge exchange with the remnant gas atoms (10^{-11} $mbar$) are not dominant, despite they are already large. The most important loss channel there is the electron-ion recombination in the cooler. These recombined ions will be separated in the next down-stream magnet behind the cooler and can be monitored by the corresponding particle detector (cf. Fig. 3.5.).

For recombination we have normally to consider only the radiative recombination. These cross sections, σ_{RR}, are proportional to Z^2 and to the phase-space overlap of electron and ion beams $< \sigma \cdot v_e >$ (Bosch, 1993). For the rate of recombined atoms we have :

$$\lambda_{RR} = \quad < \sigma \cdot v_e > \cdot n_e \quad \sim \quad Z^2 \cdot n_e \tilde{n}^{-1} \cdot (kT_e)^{-1/2} \tag{10}$$

where v_e, n_e, and T_e are the electron velocity, density, and transverse temperature; $\tilde{n}$ is the the mean ionic shell into which the recombination occurs. The measured recombination rates for bare and H-like heavy ions agree roughly with the predictions. From these rates one can deduce the lifetimes for the corresponding ion beams. The measured lifetimes of stored heavy ion beams are indeed mainly determined by radiative recombination.

In Fig. 3.8. the measured half lifes of heavy bare ion beams stored in the ESR are plotted as a function of Z. The Z^{-2} dependence predicted for radiative recombination is evident. At a current of 100 mA for the cooling electrons and specific ion energies between 250 and 300 MeV/u we find lifetimes in the order of a day for light ions and around an hour for the heaviest species like U^{92+}.

Fig. 3.8: Half lifetime of bare heavy ion beams stored in the ESR as a function of the atomic number Z of the ions. The data are normalized to an electron current of 100 mA (Bosch, 1993).

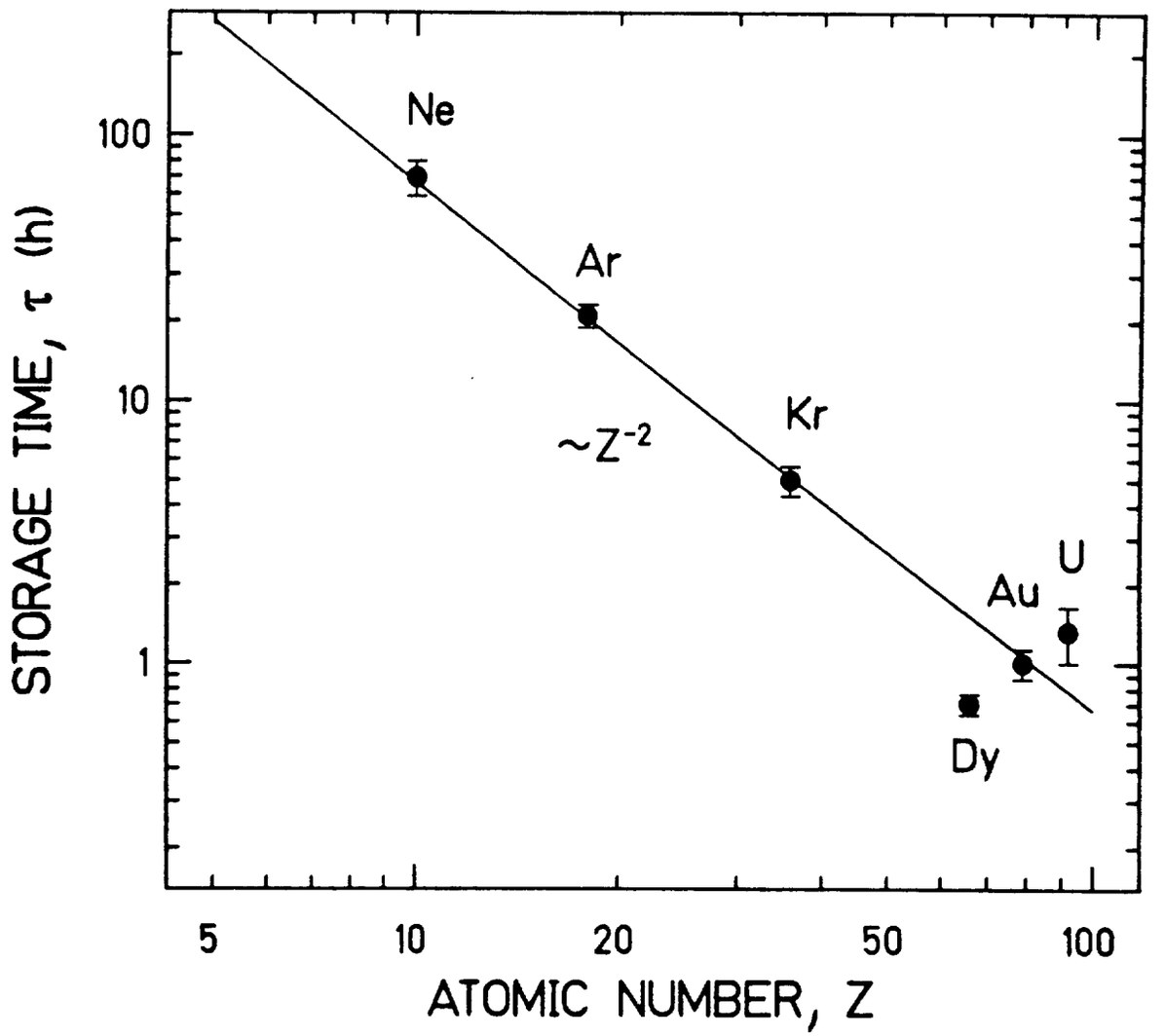
STORAGE TIME, τ (h)
100
10
1
Ne
Ar
Kr
Au
U
Dy
~Z^-2
5
10
20
50
100
ATOMIC NUMBER, Z

3.8

At the end of this paragraph the characteristics for stored ion beams which at present can routinely be expected at the ESR are summarized. Assuming the typical specific ion energies mentioned (200 to 300 MeV/u) and a low electron current of 100 mA for cooling we have approximately the following relations:

Number of stored ions: $N(Z) \approx 5 \cdot 10^{11} \cdot Z^{-2}$

Momentum spread: $\Delta P/P \approx (N \cdot 10^{-20})^{1/3}$

Storage times: $\tau_{1/2} \approx Z^{-2} \cdot 10^4$ in hours

It has to be pointed out that these rough equations give only typical numbers. In particular the number of stored ions will be improved in future. Also the given storage times can only give guidelines. If one decelerates the ions in the ring also the capture in the remnant gas of the vacuum has to be taken into account. For instance, for a bare U^{92+} beam decelerated to 50 MeV/u the lifetime was reduced to the order of 10 min at 50 mA cooling current (Stöhlker, 1995). Still the radiative recombination was the dominant loss channel at the used conditions. The momentum spread given is mainly determined by the counterbalance between cooling force and intra-beam scattering.

3.3.4 Special applications

The recombination in the cooler can also be utilized to transfer the stored ion beam into a beam with ions down-charged by one unit, provided the recombination particle detector (device (3) in Fig. 3.5) is pulled out of the way. The momentum acceptance of the ESR is about 3.6 % so that for the heaviest ions up to three beams of adjacent charge states can circulate in the ring at the same time. All the beams may match in the electron cooler and will be cooled simultaneously to the same velocity. The slow transfer by recombination into a beam with ions down-charged by one unit can be used to extract continuously a cooled beam to an external experimental area (Mokler *et al.*, 1989). However, it can also be used to breed internally an adjacent charge state for a particular experiment. This was

done, for instance, for the measurements of dielectronic recombination in Li-like ions like Au^{76+} or U^{89+}, where at high energies He-like ions have originally been injected and the Li-like fraction was bred in the ring (Müller *et al.*, 1992). This technique, where the ions had been injected at a high energy, provided a more intense beam of Li-like ions than the direct method.

What is true for the electron target should also be valid for the gas-jet target. In the gas target we may have both, ionization and capture, and we can transfer the ions to both the neighbouring charge states. Measuring, for instance, capture cross sections in the gas target with the down-stream capture detector, it may be reasonable to transfer the fraction of further ionized ions in the cooler back to the wanted charge state by recombination and use these ions again. For the method see the example given in Fig. 3.9 using initially injected bare Pb^{82+} ions at 277 MeV/u (Kandler *et al.*, 1995b). The bare ion beam is confined to a narrower orbit which does not see the gas target; by recombination it is gradually transferred into H-like ions hitting the gas target; the down-charged ions are monitored in the corresponding particle detector, whereas the ionized fraction feeds again the original bare fraction. Naturally, also the recombination of H-like into He-like ions in the cooler can be detected by the recombination monitor. The whole evolution of the various beam intensities is governed by differential rate equations, where the appropriate cross sections have to be plugged in. This is done in Fig. 3.9 by the full lines. These calculations are compared with the measured total circulating current (Pb^{82+} + Pb^{81+}) and the He-like rate measured by the capture detector which is proportional to the intensity of the circulating H-like beam. In the figure the data have been normalized to the calculations in absolute height. An almost perfect agreement results for the evolution of charge fractions with time.

Fig. 3.9: Charge state breeding of charge state neighbouring ion beams. Bare 277 MeV/u Pb^{82+} ions are injected and H-like ions are bred; behind

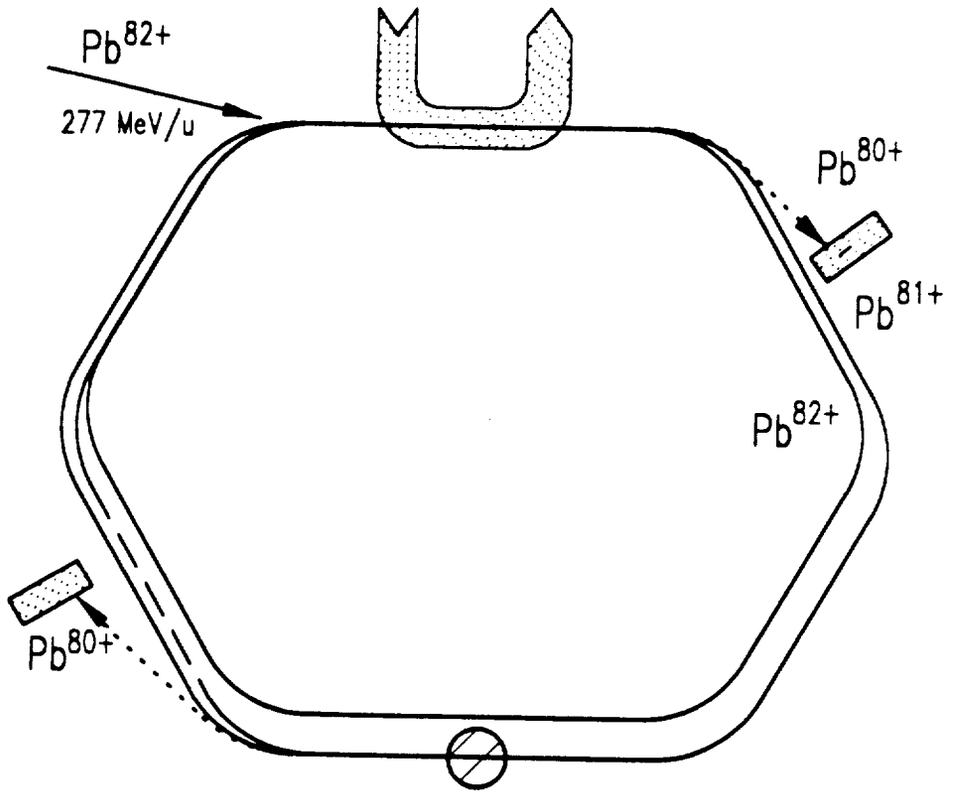
Pb82+
277 MeV/u
Pb80+
Pb81+
Pb82+
Pb80+

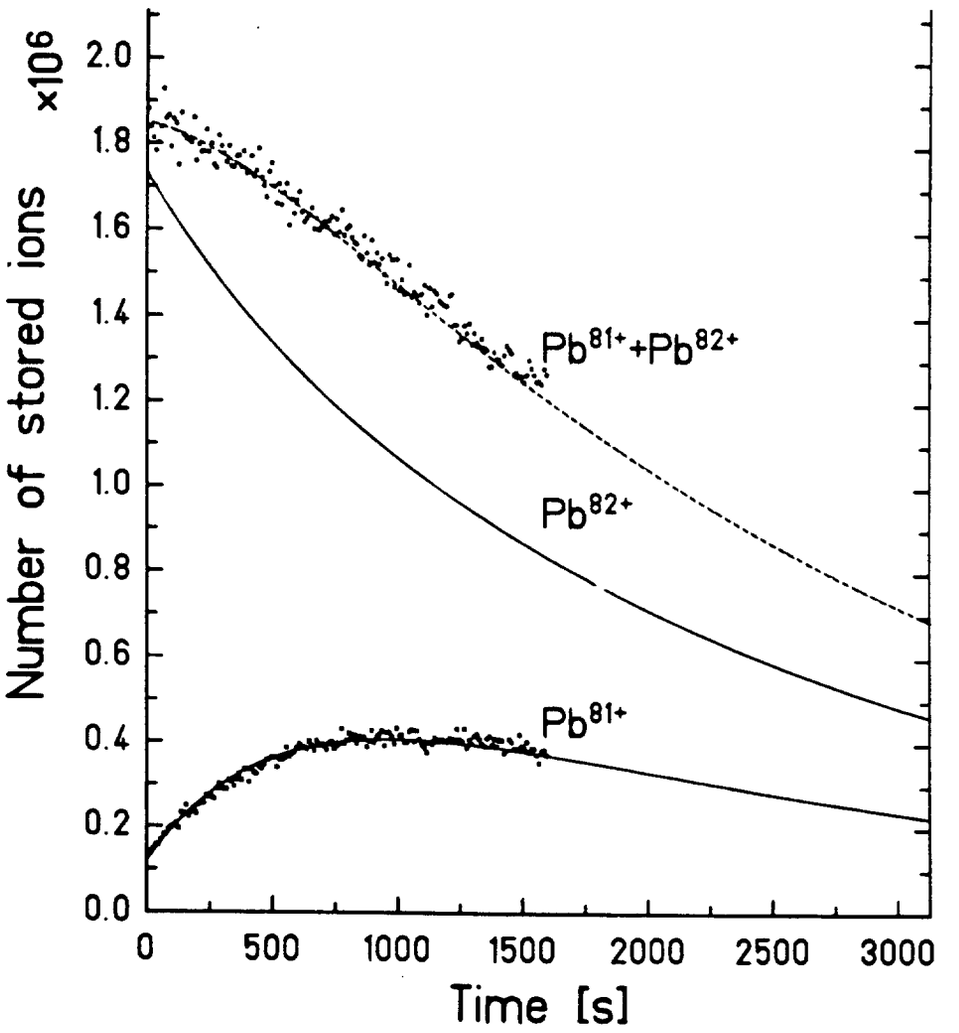
Number of stored ions
×10⁶
2.0
1.8
1.6
1.4
1.2
1.0
0.8
0.6
0.4
0.2
0.0
0
500
1000
1500
2000
2500
3000
Time [s]
Pb81+ + Pb82+
Pb82+
Pb81+

3.9

the gas target and behind the cooler the He-like ion fractions are monitored. The intensity of the circulating ion current and the capture rate behind the gas target are compared with theoretical predictions for the evolution of the various ion fractions (Kandler *et al.*, 1995b).

As the different ion beams are confined according to their charges to different tracks in the storage ring, i.e. to slightly different long circumferences, and as all beams have due to cooling exactly the same velocity, the revolution frequency is different for the differently charged ions. Therefore, the evolution of the various fractions in the ring can also be read from the SCHOTTKY-frequency spectrum, showing isolated lines for the different charge states.

From this it is also clear, that storage rings can not only be considered as traps for high velocity ions at a very specific charge state, they can also be used as extremely sensitive filters for their momentum. As the velocity of the ions is accurately fixed by cooling, storage rings can also be utilized as precise mass spectrometers distinguishing for instance between isotopes or even isomeric states (Bosch, 1993). In Fig. 3.10 an example is given: The SCHOTTKY-noise spectrum shows a stored beam of bare $^{163}Dy^{66+}$ ions together with neighbouring nuclei produced by nuclear reactions in the N_2 gas target. H-like $^{163}Ho^{66+}$ions are created by bound-state β-decay from bare Dy ions; these ions are then stripped off in the gas target to the bare ions seen (Jung *et al.*, 1992). From the evolution of the intensities for the various peaks with time reaction cross sections or lifetimes can be deduced. The SCHOTTKY noise diagnosis is extremely sensitive so that even a single circulating highly charged ion may be probed. As the reaction products have tiny differences in their masses, and hence in their momenta, the reaction products do not feel the same intra beam scattering as the original ions do in the high intensity beam. Therefore, the SCHOTTKY signals for the reaction products show extremely narrow lines. At the ESR, the mass resolution of this method is tested to $\Delta M/M \approx 10^{-6}$

(Kluge, 1995).

Fig. 3.10 Frequency spectrum of the SCHOTTKY noise picked up for a stored and cooled beam of bare $^{163}Dy^{66+}$ ions (broad line). After switching on the gas target narrow lines show up which are signals from neighbouring nuclei made by nuclear reactions. The $^{163}Ho^{67+}$ line results from bound state β-decay of the bare Dy ions into H-like Ho ions which are then stripped in the gas target into the circulating bare ions observed (Bosch, 1993).

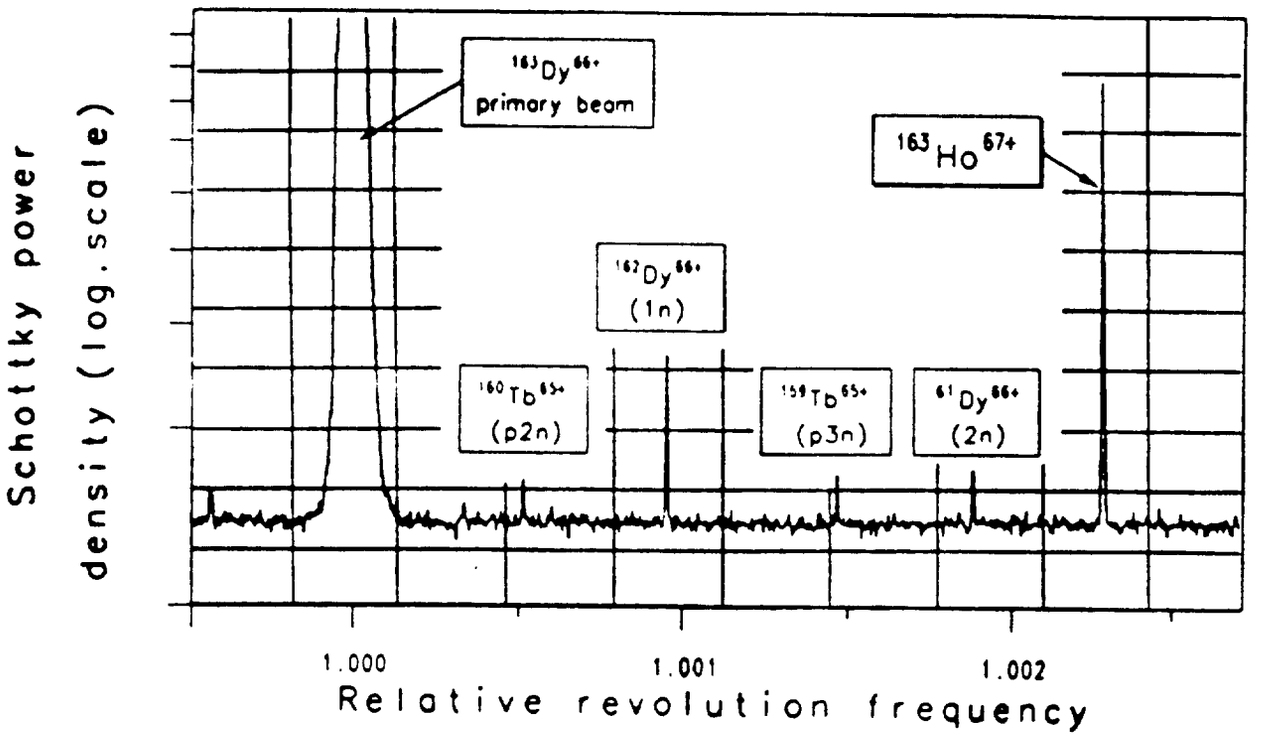
Schottky power density (log.scale)
$^{163}Dy^{66+}$ primary beam
$^{163}Ho^{67+}$
$^{162}Dy^{66+}$ (1n)
$^{160}Tb^{65+}$ (p2n)
$^{159}Tb^{65+}$ (p3n)
$^{61}Dy^{66+}$ (2n)
1.000
1.001
1.002
Relative revolution frequency

Fig 3.1

4 Charge changing processes

4.1 Recombination processes in the cooler

As was emphazised in the previous section cooling of ions by electrons is the pre-requisite for a successful operation of heavy ion storage rings. The question on recombination losses in an electron cooler was one of the most fundamental issues during the design phases of the heavy ion storage rings. Therefore, we show in Fig. 4.1. the estimated cross section ratio for radiative recombination and for cooling (*cf.* Kienle, 1985). For bare ions this ratio is plotted as a function of the atomic number assuming different equivalent electron energies T(rel) relative to the ions, corresponding to different temperatures. For ion beams injected from the accelerator, we have to assume for T(rel) typically a value of a few eV, for reaction fragments a value of more than 10 eV and for a cooled ion beam we have to assume T(rel) around 0.1 eV. From the figure it is evident, that even for the heaviest ions the recombination losses are small compared to the cooling effect; this is in particular true for an already cooled ion beam.

Fig. 4.1: Calculated cross section ratios for radiative recombination and electron cooling as a function of the atomic number Z for bare ions at different equivalent electron temperature T(rel) relative to the ions (cf. Kienle 1985).

In general, the half-lifetimes of stored beams can reliably be estimated by using theoretical cross sections for radiative recombination, compare Fig. 3.8. However, for an exact comparison of measured recombination rates with theory one has to convolute the cross sections with the actual velocity distributions for electron and ion beams. Here, not only the velocity distributions have to be known exactly, but also all possible field inhomogenities in the magnetic solenoid field of the cooler, small mis-alignments between both the beams, reionization of electrons in high n states in the next down-stream dipole

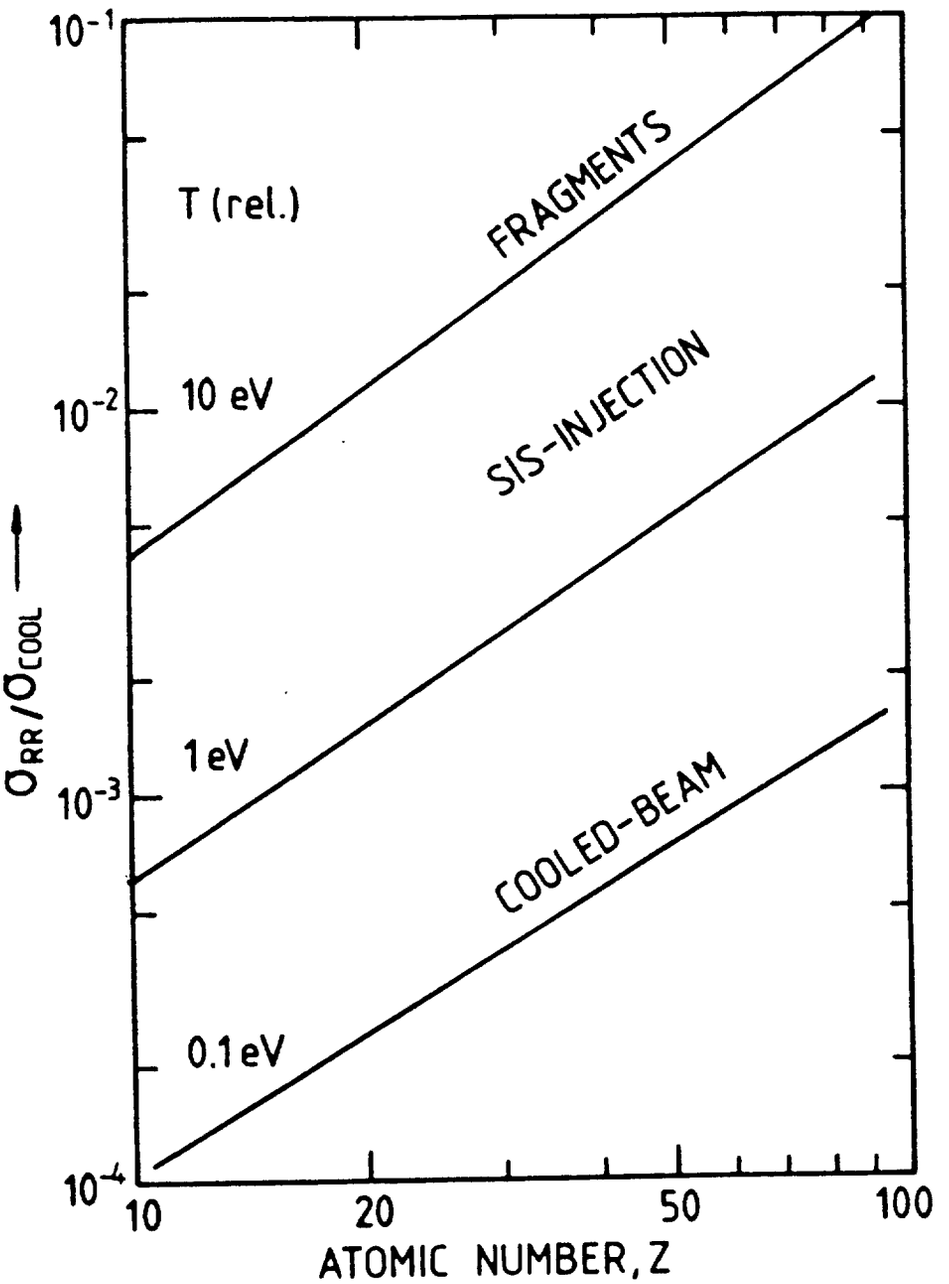
10^{-1}
10^{-2}
10^{-3}
10^{-4}
T (rel.)
10 eV
1 eV
0.1 eV
FRAGMENTS
SIS-INJECTION
COOLED-BEAM
$\sigma_{RR}/\sigma_{COOL}$
10
20
50
100
ATOMIC NUMBER, Z

magnet by the motional electric field seen by the ions, and other subtle effects have to be included into the calculations. Under cooling conditions often slightly too large recombination rates are found in particular for heavy ions. Beyond Z = 5 enhancement factors between 1.5 and 2 have been reported from the *TSR*. (Wolf *et al.*, 1993) Large enhancement factors up to at least 40 have been found for very heavy ions like U^{28+} also in single pass experiments, see below (Uwira *et al.*, 1995). More detailed studies are needed for this important issue.

As the cooling forces are strong, it is difficult to measure in a storage ring the recombination rate as a function of the relative velocities between both the beams. For slightly detuned velocities the beam velocity is almost instantaneously pulled towards the electron velocity. Hence, near matching velocities single pass experiments will be more accurate. Using the ASTRID cooler target off-line at the Aarhus tandem van-de-Graaff accelerator Andersen and Bolko (1990a) found an excellent agreement in the dependence of the radiative recombination rate on the detuning energy with predictions according to Bethe and Salpeter (1957) or to Stobbe (1930) for bare ions up to F^{9+}. In Fig. 4.2 this energy dependence is shown. The radiative recombination strongly decreases with increasing relative energy between electrons and ions.

Fig. 4.2: Radiative recombination rates for bare C^{6+} and F^{9+} as function of the relative energy between ion and electron beam according to Andersen and Bolko (1990a). (For the flattened velocity distributions in the electron target we have temperatures of $kT_\perp = 150\ meV$ and $kT_\parallel = 2\ meV$.) The rate predictions according to Bethe and Salpeter (1957) and Stobbe (1930) are shown as dashed and full lines, respectively.

Also for heavier ions the radiative recombination rates agree fairly well with predictions especially at non vanishing relative velocities. For matching velocities a considerable

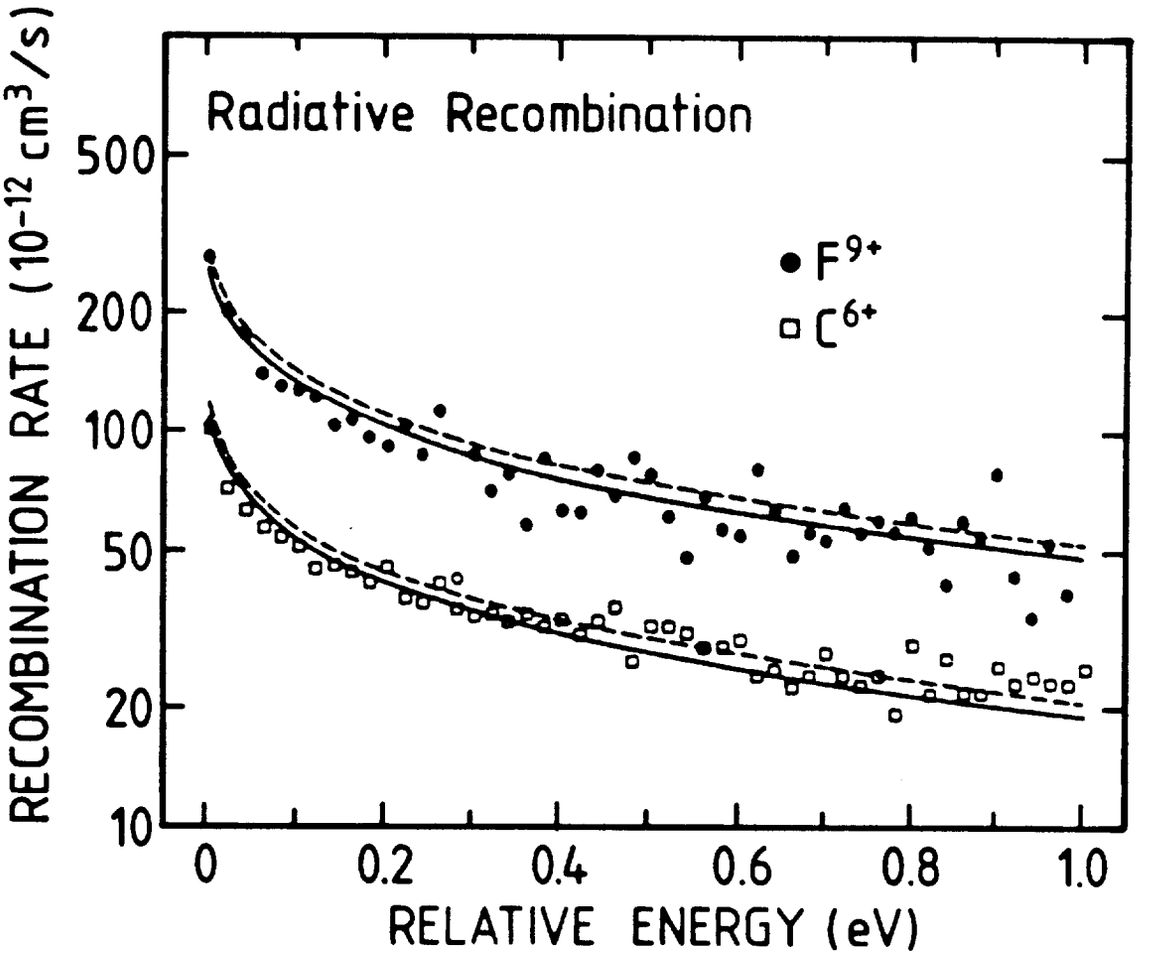
Radiative Recombination
RECOMBINATION RATE (10^{-12} cm^3/s)
500
200
100
50
20
10
F^{9+}
C^{6+}
0
0.2
0.4
0.6
0.8
1.0
RELATIVE ENERGY (eV)

4.2

enhancement over the predictions is found for heavy species. This is in particular true for dressed heavy ions as e.g. U^{28+} (Schennach *et al.*, 1991 and Uwira *et al.*, 1995). For illustration we show in Fig. 4.3 the recombination rate for Li-like Ar^{15+} ions measured with a very dense electron target at a single pass experiment at the UNILAC, GSI-Darmstadt (Schennach *et al.*, 1994). In the enlarged spectrum at the top the expected radiative recombination is shown as dashed line. At cooling, i.e. at zero relative energy, the recombination rate is found to be a factor of 4 larger than predicted.

On top of the radiative recombination we find strong resonance contributions from dielectronic recombination (DR), see bottom figure. There are two DR-resonance series, an excitation of the $2s_{1/2}$ electron into the $2p_{1/2}$ and the $2p_{3/2}$ level, respectively, and a resonant capture to the nl level series (or vica versa). Using an isolated-resonance approximation an overall good agreement is found for the rates and the position of the dielectronic resonances on top of the radiative recombination continuum.

Fig. 4.3: Recombination rate for Li-like Ar^{15+} ions ($1s^2 2s_{1/2}$) measured in a single pass experiment through a dense electron target (with temperatures $kT_{||}$ = 2.4m eV and $kT_{\perp}$ = 260 meV). The dielectronic recombination resonances $1s^2 2p_{1/2} nl$ and $1s^2 2p_{3/2} nl$ are seen on top of the radiative recombination continuum. In the spectrum at the top part of the figure the energy region up to about a relative energy of 1.5 eV is enlarged. There the DR resonance is fitted by convoluting the resonance with the actual temperatures of the electron target. Correspondingly the radiative radiation continuum is calculated (dashed curve). The insert at the very top shows the arrangement of the electron target used; for details see Schennach *et al.* (1994).

As the natural widths of the DR resonances are small compared to the involved temperatures of the electron beam the shapes of the resonances are mainly determined

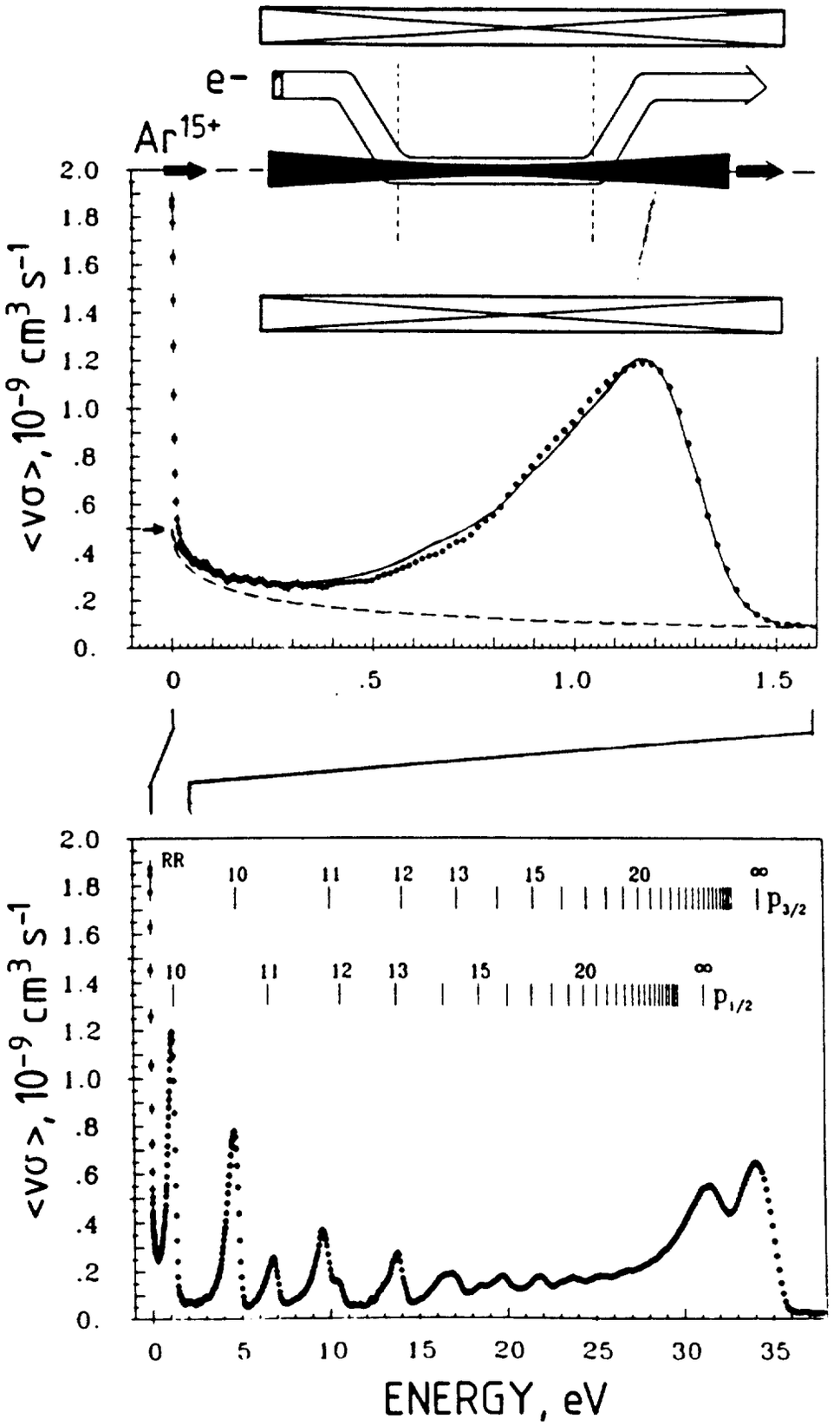
e-
Ar15+
<vσ>, 10-9 cm3 s-1
2.0
1.8
1.6
1.4
1.2
1.0
.8
.6
.4
.2
0.
0
.5
1.0
1.5
RR
10
11
12
13
15
20
∞
p3/2
p1/2
0
5
10
15
20
25
30
35
ENERGY, eV

4.3

by the actual velocity distributions. The resonances are asymmetric, where the low-energy side is mainly determined by the transverse temperature and the high-energy side reflects more the longitudinal temperature of the electron beam (Andersen *et al.*, 1989 and 1990b). Due to the acceleration of the electrons in the gun a so-called flattened velocity distribution is seen for the target electrons (Poth, 1990a). The resonance at about 1.2 eV can be fitted best with electron temperatures of $kT_{\|} = 2.4\ meV$ and $kT_{\perp} = 260\ meV$ (full curve). For calculating the radiative recombination contribution these temperatures have been used, see dashed curve in the top spectrum of Fig. 4.3. At truely matching velocities an appreciable excess in the recombination rate is found. Three body recombination seems not to be responsible for this enhancement. On the other hand, the strong central potential of the highly charged ions may increase locally the electron density in the target. Moreover, a stimulated radiative recombination caused by the electromagnetic radiation of the neighbouring electrons from their cyclotron motion and by the black body radiation may also contribute to this enhancement.

In order to measure the recombination at small relative energies in a cooler at an in-ring experiment one has to switch continuously the relative energy between both the beams from zero (cooling) to the measuring value (detuning) and back again. The switching has to be fast enough so that on the one side the ion beam stays cooled and on the other side the ion energy is not changed by the dragging force of the electron beam towards the measuring energy. The cycle is typically in the 20 *ms* region. This method gives a perfect normalization of the recombination to the rate at cooling. The first in-ring measurements have been performed in this way at the TSR for highly charged heavy ions (Kilgus *et al.*, 1990). In Fig. 4.4 a measurement from the TSR is shown for Li-like Cu^{26+} ions (Kilgus *et al.*, 1992). Once more, on top of the radiative recombination continuum decreasing with the relative energy between both the beams we see the resonances for the $\Delta n = 0$ series with $1s^2 2s_{1/2} + e \rightarrow 1s^2 2p_{1/2} nl$ and $1s^2 2p_{3/2} nl$. Up to the series limit good agreement is

found both for the resonance energies as well as for the cross sections. The same is true for $\Delta n = 1$ transitions, i.e. for the $1s^2 3lnl'$ resonances (Kilgus *et al.*, 1992 and 1993).

Fig. 4.4: Recombination rate measured for Li-like Cu^{26+} ions at the TSR. On top of the radiative recombination continuum resonances from dielectronic recombination appear for $\Delta n = 0$ transitions, $1s^2 2s_{1/2} + e \rightarrow 1s^2 2p_{1/2} nl$ and $1s^2 2p_{3/2} nl$) (Kilgus *et al.*, 1992).

For the $\Delta n = 0$ resonances in Li-like ions it is evident, that for heavier ions more resonances are resolved and that the two series limits split rapidly with increasing atomic number Z. This splitting gives in the limit ($n \rightarrow \infty$) the fine structure splitting between the $p_{1/2}$ and the $p_{3/2}$ levels in Li-like ions, while the absolute energy positions of the series limits give additionally the splitting to the $2s_{1/2}$ level. An appreciable part of the last splitting is caused for heavy species by QED contributions. As will be shown in the next chapter, the positions of the resonances within these series can be utilized for a precise spectroscopy in particular of very heavy ions. At the ESR dielectronic resonances have been studied for Li-like Au^{76+} ions, see below (Spies *et al.*, 1992). Also for these heavy ions good agreement was found between experiment and theories applying fully relativistic codes including Breit term, QED corrections, and nuclear size effects.

As was pointed out already, good agreement between resonance strengths and experimental rates have been found for $\Delta n = 0$ transitions in Li-like ions even for the heaviest species. This indicates that the electron-electron interaction is reasonably well understood - within the available accuracies - if one includes all relativistic and all the other effects. On the other hand, the electrons involved for Li like ions do not probe sensitively the innermost part of the strong central potential of the atomic nucleus (cf. Fig. 2.6). For such a test one has to measure $\Delta n = 1$ resonances involving a K-shell electron, as was already done at the TSR for lighter ions (Kilgus *et al.*, 1990). For heavy ions where the

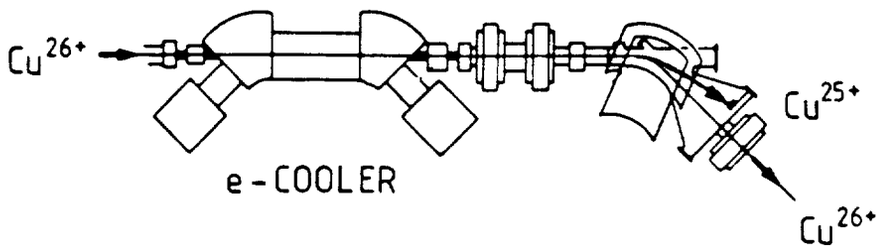
Cu26+
e-COOLER
Cu25+
Cu26+

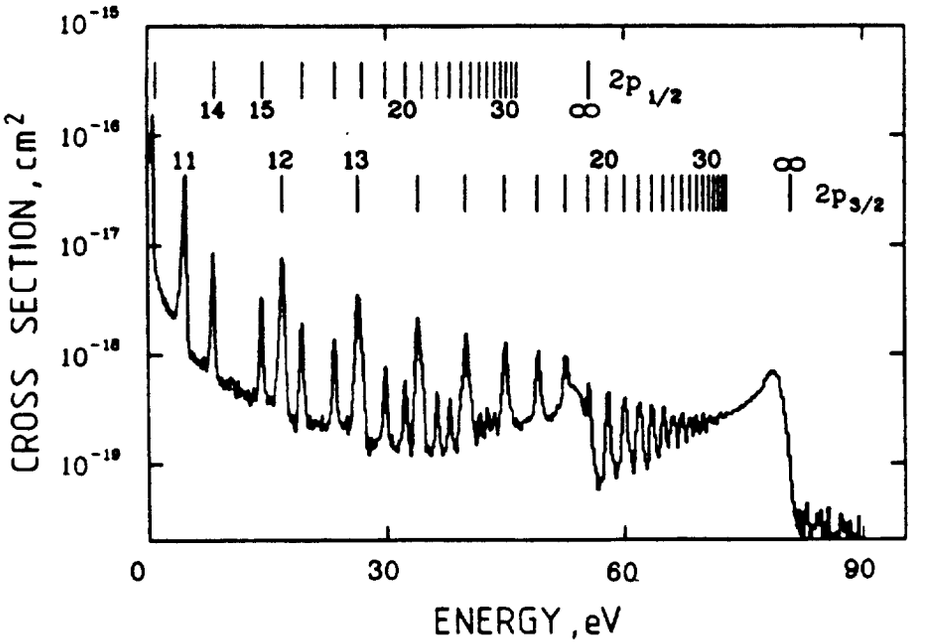
CROSS SECTION, cm2
10-15
10-16
10-17
10-18
10-19
14
15
20
30
∞
2p1/2
11
12
13
20
30
∞
2p3/2
0
30
60
90
ENERGY, eV

4.4

relativistic influence can be probed best the resonance energies are so high that the cooler can technically not be detuned fast enough. For those measurements an independent second electron target has probably to be installed in a heavy ion storage ring. Such a second electron target is currently being projected for the *ESR*. Then the current-current interaction can be measured under truely relativistic conditions (Zimmerer *et al.*, 1990; Chen, 1991).

In order to demonstrate the drastic influence of the relativistic and the Breit interaction on the dielectronic recombination we show in Fig. 4.5 the dependence of the involved KLL-Auger rates as a function of the atomic number Z for the case of final He-like ions (Zimmerer, 1992; Zimmerer *et al.*, 1991). In the non-relativistic approach (NRW) or in a 1/Z expansion the Auger rate is independent on Z. Using relativistic wavefunctions the Auger rate increases beyond about Xe considerably, yielding for U on the average an enhancement factor of about 1.5. On top of this, the Breit interaction gives an additional increase of the same order of magnitude. For selected resonances the enhancement can increase up to an order of magnitude compared to the non-relativistic approach. This is shown for the $2s_{1/2}2p_{1/2}\,^3P_0$ resonance for final two-electron systems.

Fig. 4.5: KLL-Auger rates for final He-like ions as a function of the atomic number Z according to Zimmerer (1992):
top) mean Auger rates and
bottom) Auger rate for the $2s_{1/2}2p_{1/2}\,^3P_0$ doubly excited state.
NRW, 1/Z, RW, and GBI means non-relativistic approach, 1/Z expansion, relativistic calculation, and Breit interaction, respectively.

At present these interesting questions can only be studied by applying quasi-free electron targets, i.e. electrons confined to bound states by target atoms (Graham *et al.*, 1990; Kandler *et al.*, 1995c and 1995b). Unfortunately, the bound electrons have a certain intrinsic velocity distribution (Compton profile) so that no isolated resonances can

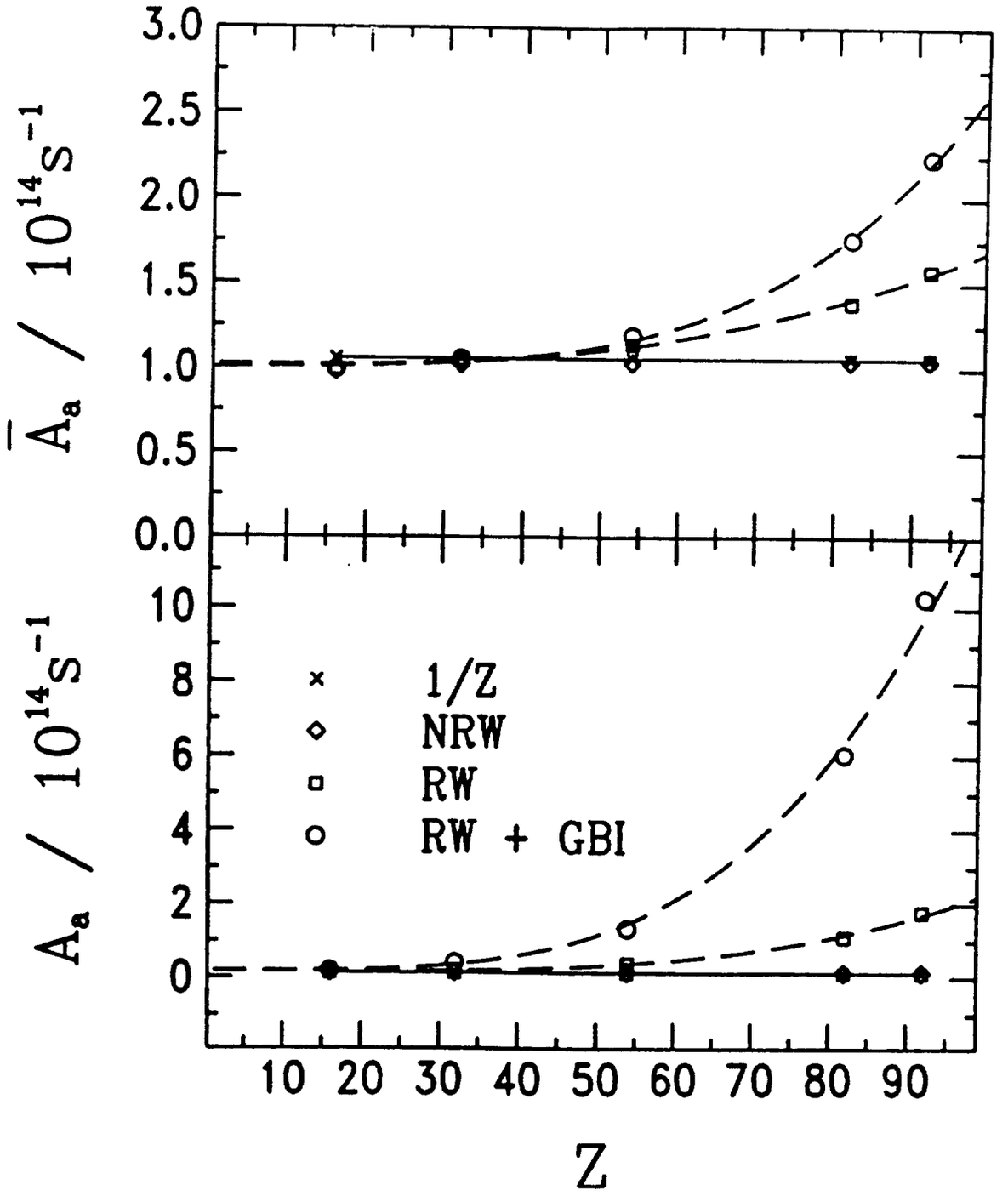
3.0
2.5
2.0
1.5
1.0
0.5
0.0
$\bar{A}_a$ / $10^{14}s^{-1}$
10
8
6
4
2
0
A_a / $10^{14}s^{-1}$
1/Z
NRW
RW
RW + GBI
10 20 30 40 50 60 70 80 90
Z

4.5

be resolved by those measurements. Nevertheless, a reasonable agreement is found with predicted cross sections in an experiment for He-like U^{90+} projectiles. At the *SIS* facility for this resonant transfer and excitation process coincidences between the "recombined" Li-like U^{89+} projectiles and the stabilizing x rays have been measured (Kandler *et al.*, 1995a and 1995c). In Fig. 4.6 the $K\alpha_1$ and $K\alpha_2$ excitation function for KLL RTE are shown for this case. Three resonance groups for the various jj' doubly excited L states (1/2 1/2, 1/2 3/2, 3/2 3/2) are resolved. Due to the Breit interaction the reaction strength for jj'=1/2 1/2 is enhanced by a factor of two over the non-relativistic approach. Moreover, the experimental value for this resonance group overshoots even the relativistic calculations, whereas the other two groups are in accordance with theory.

Fig. 4.6: Measured differential $K\alpha_1$, $K\alpha_2$ excitation function for KLL-RTE observed in U^{90+} →C collisions. In addition the total $K\alpha$=$K\alpha_1$+$K\alpha_2$ yield is given in the figure (Kandler *et al.*, 1995a). (The shown curves are eye guides)

4.2 Electron capture processes in the gas-jet target

The investigation of projectile charge-exchange processes in encounters of high-Z ions with neutral target atoms provides not only a test of the theory of atomic collision dynamics, but is also of general importance for the operation of heavy ion accelerators and storage rings. The ESR is the only storage ring equipped with a gas-jet target. Due to the high luminosity of the ESR, the gas-jet target provides the unique possibility to study projectile charge-exchange in encounters of high-Z ions with low dense matter. This is in particular true for the relativistic collision velocity regime and for low-Z targets. At such collision conditions, where the charge-exchange cross-sections are comparably low, one has to rely in standard single pass experiments on the application of solid targets with typical densities of 10^{23} particles/cm^3. The latter has to be compared with the densities

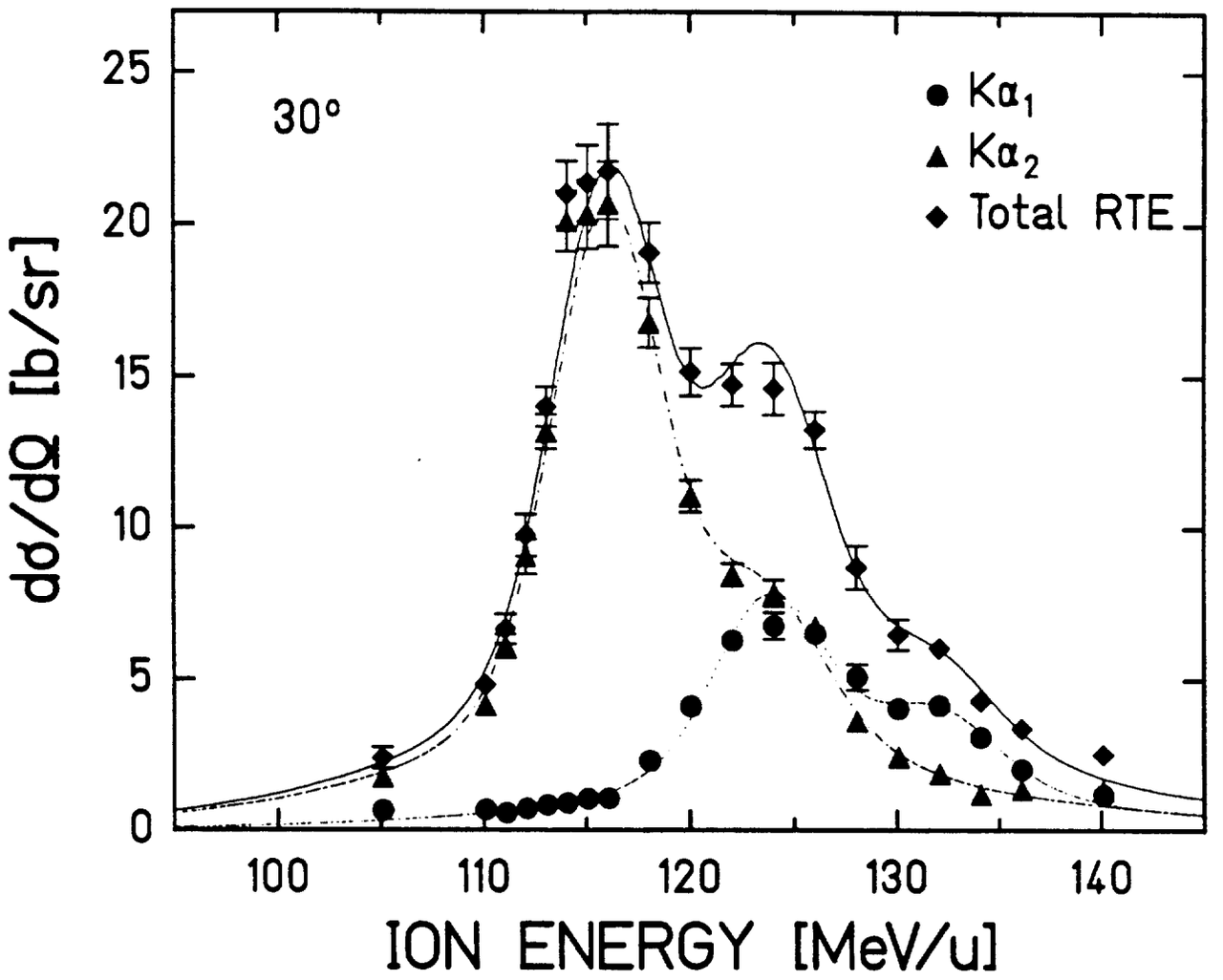
30°
Kα1
Kα2
Total RTE
dσ/dΩ [b/sr]
ION ENERGY [MeV/u]
0
5
10
15
20
25
100
110
120
130
140

4.6

of the gaseous targets at the ESR of about 10^{13} particles/cm^3 which exclude the possible influence of multi-step processes (solid targets effects) on the charge-exchange processes to be studied. In the following we will concentrate on the discussion of the electron capture processes and particularly of the radiative capture process.

Fig. 4.7: Total electron-capture cross-sections for bare U^{92+} ions at 295 MeV/u colliding with gaseous targets (see ■ for $U^{92+} \rightarrow N_2$, Ar) and with solid targets (see ● for $U^{92+} \rightarrow$Be, C) (Stöhlker *et al.*, 1995). For both cases the cross sections per target atom are given. The results are compared with the theoretical cross-section predictions for the NRC and the REC processes (dashed and dotted line). The sum of both cross sections is given by the full line.

In fast collisions of bare high-Z projectiles with low-Z target atoms, REC is the only relevant charge-changing process. This is illustrated in Fig. 4.7 where the total one-electron projectile pickup cross sections are plotted versus target atomic number Z_T for 295 MeV/u bare uranium ions (Stöhlker *et al.*, 1994). The measured data are compared with theoretical predictions for the two competing electron capture-processes, i.e. for REC and NRC. For NRC the relativistic eikonal approximation (Eichler, 1985) was applied whereas for REC the Stobbe theory (Stobbe, 1930) was used. As seen in the figure, a very good agreement between the predicted Z_T cross-section dependence and the experimental data is observed ($\sigma_{NRC} \sim Z_T^5, \sigma_{REC} \sim Z_T$; compare also Chap. 2). In particular, the experimental data confirm the prediction that for $Z_T < 13$ the NRC contribution can be neglected. It is emphasized that the presentation in Fig. 4.7 includes data from solid as well as from gaseous targets. Obviously, for such bare, high-Z projectiles target density effects do not influence the electron capture probability. This observation can be explained on the basis of the electron capture cross-section dependence on the final projectile main

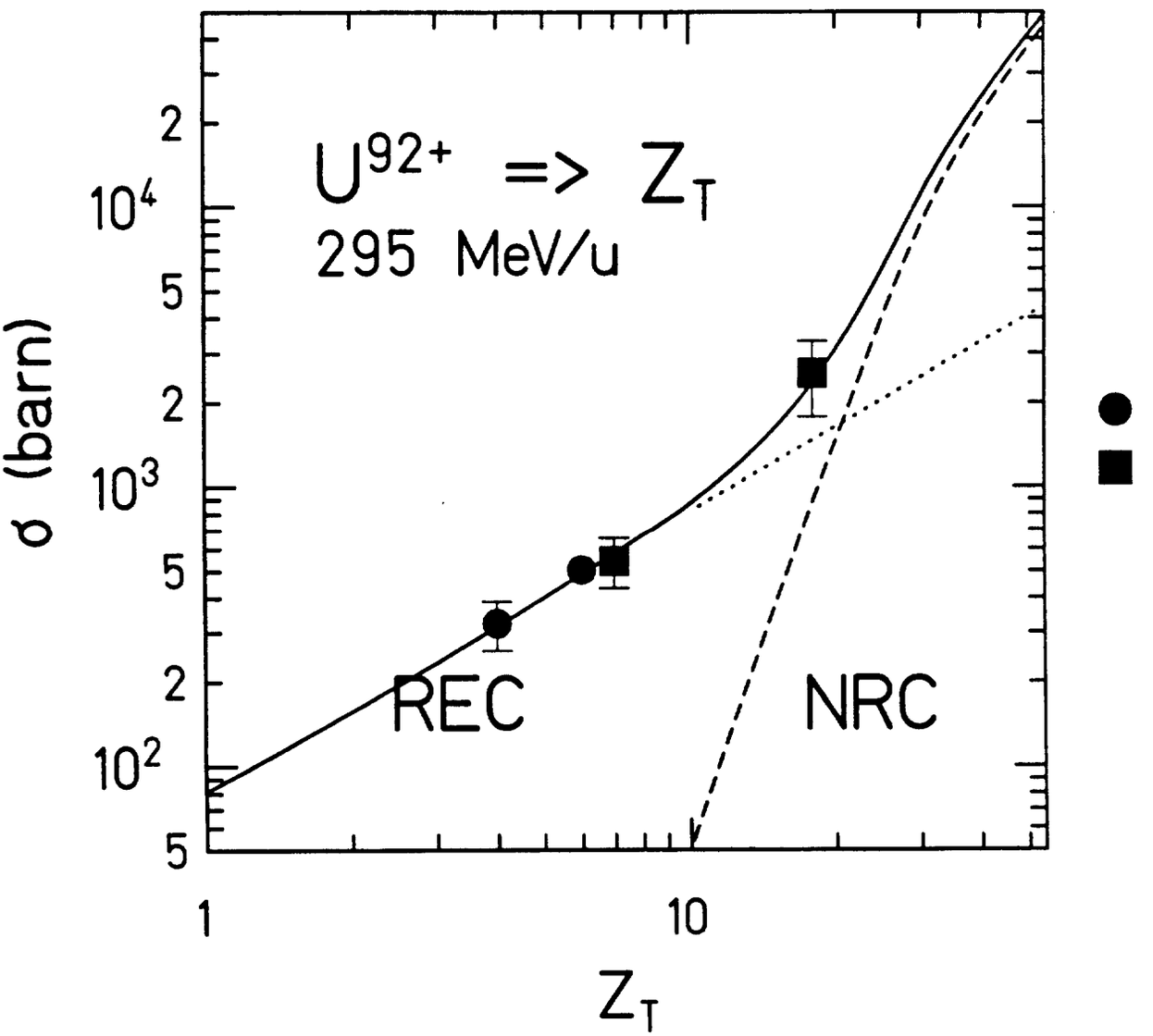

4.7.

quantum number n_f. At high beam energies the cross sections for both capture processes, REC and NR, scales with $1/n_f^3$. Moreover, the fast decay rates of the excited levels in such high-Z systems contribute significantly to the vanishing of solid states effects.

As it has been discussed already in chapter 2, the Stobbe cross section for REC depends only on the adiabaticity parameter η of the collision. It provides a convenient way for a systematic comparison of cross sections gained for different projectile target combinations and collision energies. In order to show this for a large number of collision systems, it is useful to define an "adiabaticity parameter" η by connecting it to the Sommerfeld parameter ν through the non-relativistic relation (cf. Equ. (6) in chapter 2)

$$\eta = 1/\nu^2 \simeq 40.31 \times \frac{E_{\mathrm{kin}}(\mathrm{MeV/u})}{Z^2}. \tag{11}$$

In Fig. 4.8 all available total charge-exchange cross-sections related to REC, normalized to the number of quasifree target electrons are plotted versus the η-parameter (for references see Stöhlker *et al.*, 1995). In addition, the upper x-axis of the figure shows the energy scale for the particular case of Z=80. The predictions of the non-relativistic dipole-approximation are given in the figure by the full line whereas the dashed line depicts the results of the rigorous relativistic calculations performed for Z=80 (Ichihara *et al.*, 1994). The error bars displayed account for both the statistical and the systematic uncertainties of the individual measurement. The bunch of data cover a projectile Z regime from $Z = 54$ to $Z = 92$ and beam energies ranging from 80 to 1000 MeV/u. They were gained in solid target experiments performed at the BEVALAC (Meyerhof *et al.*, 1985b; Meyerhof, 1994) and SIS accelerator (Stöhlker *et al.*, 1995) as well as in experiments utilizing gaseous targets at the ESR. The latter are given also separately in the inset of the figure.

Fig. 4.8: Total electron-capture cross-sections per target electron measured for bare high-Z ions ($Z \geq 54$) in collisions with light target atoms (the data from the ESR gas-jet are depicted separately by the inset). The results are

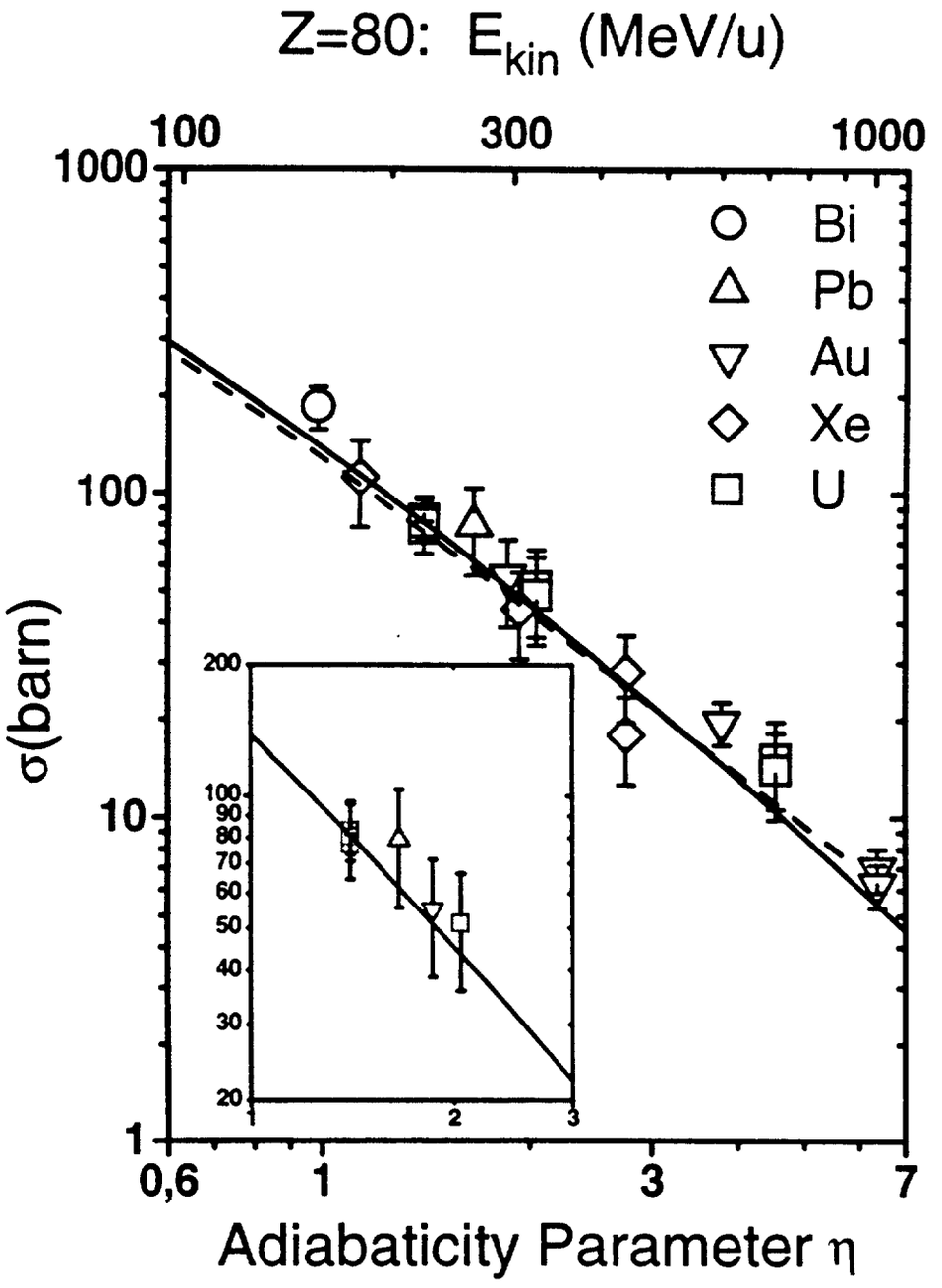
Z=80: E_kin (MeV/u)
100
300
1000
1000
100
10
1
σ(barn)
Bi
Pb
Au
Xe
U
200
100
90
80
70
60
50
40
30
20
1
2
3
0,6
1
3
7
Adiabaticity Parameter η

plotted as a function of the η-parameter (lower x-axis) and are compared with the result of a relativistic exact calculation for $Z = 80$ (dashed line) as well as with the prediction of the non-relativistic dipole-approximation (full line). For the particular case of Z=80 the cross section values are given in addition as a function of beam energy (upper x-axis).

In general an excellent agreement between experiment and theory is found for the total cross sections, see Fig. 4.8. The experimental data are, within the error bars, not sensitive to the slight cross-section variation predicted by the relativistic theory for different Z systems using one common non-relativistic η parameter, especially for $\eta \leq 3$. Based on these findings, it is evident that the simple dipole-approximation can be applied in order to get reliable cross-section estimations even for high-Z projectiles but not too high collision energies. In the high-energy regime (e.g. 500 MeV/u for Z=80 projectiles) the application of the exact relativistic theory is certainly more appropriate. Here the results of the latter theory performed for Z=80 already deviate from the predictions of the non-relativistic approach. In fact, the result of the latter approach seems to underestimate the measured cross-sections at higher-η values. We have to emphasize that a non-relativistic velocity description was used for the η definition given above. Applying a correct relativistic velocity description the dipole approximation would already fail completely for high-Z ions at intermediate η parameters. Obviously, by using the non-relativistic scaling law several relativistic effects cancel arbitrarily.

Fig. 4.9: X-ray spectra measured at 132° and corrected for the energy dependent detector efficiency for incident U^{91+}, U^{92+} ions on N_2 at 295 MeV/u. The spectra were accumulated at the ESR gas-target in coincidence with the down-charged ions.

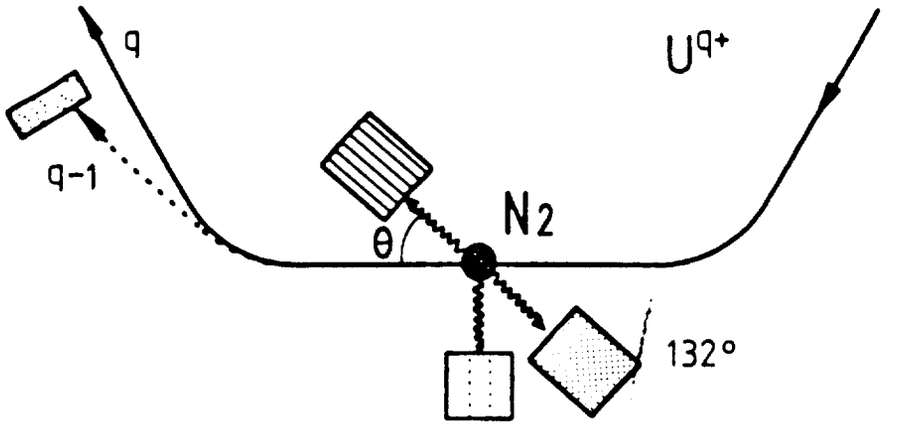
q
U^{q+}
q-1
N_2
θ
132°

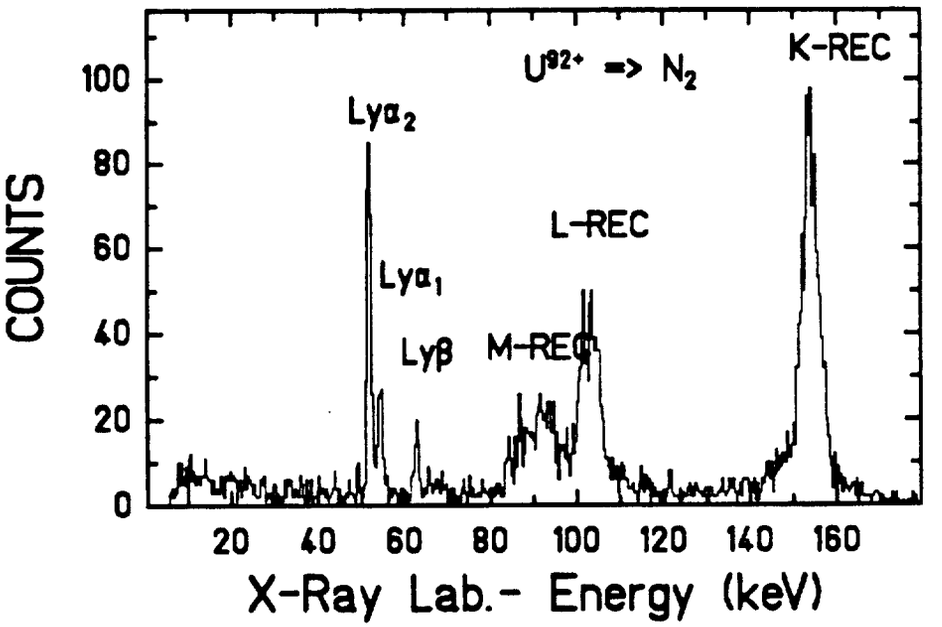
U^{92+} => N_2
K-REC
$Ly\alpha_2$
L-REC
$Ly\alpha_1$
Lyβ
M-REC
COUNTS
100
80
60
40
20
0
20 40 60 80 100 120 140 160
X-Ray Lab.- Energy (keV)

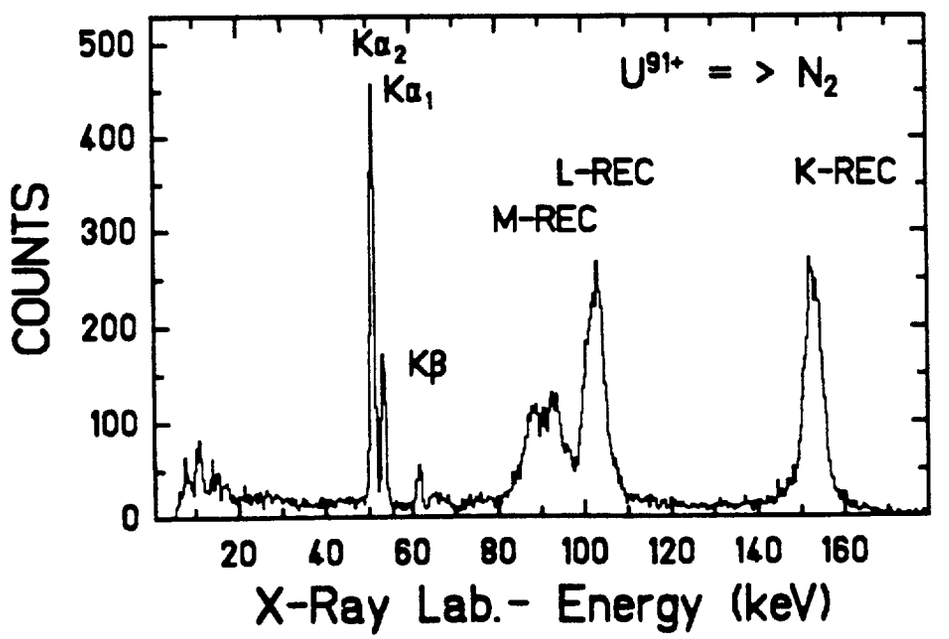
$K\alpha_2$
$K\alpha_1$
U^{91+} = > N_2
L-REC
K-REC
M-REC
Kβ
COUNTS
500
400
300
200
100
0
20 40 60 80 100 120 140 160
X-Ray Lab.- Energy (keV)

Analysing the projectile photon emission associated with electron capture, shell differential cross sections can be obtained. In Fig. 4.9 we present the efficiency-corrected x-ray spectra, taken in coincidence with the down-charged ions at the internal gas-target of the ESR. The two spectra (lab. system) correspond to capture from N_2 molecules into bare U^{92+} and H-like U^{91+} ions which were taken at a collision energy of 295 MeV/u and a detection angle of 132^o (Stöhlker *et al.*, 1993; and 1995). The energy range displayed in the figure covers the x-ray energy regime relevant for REC transitions into the ground state and into exited states as well as for the characteristic projectile transitions, i.e. the Lyα and Kα emission. All the REC contributions appear well resolved in the figure. A comparison of the spectra in Fig. 4.9a and in Fig. 4.9b manifests a reduction by a factor of two for the K-REC intensity for the H-like projectiles due to the partially blocked K-shell. In contrast, REC into excited projectile states is equivalent for both cases. From these x-ray spectra one can deduce shell differential as well as angular differential REC cross sections.

Fig. 4.10: K-REC angular distribution for 295 MeV/u U^{92+} $\rightarrow$N collisions. The dotted line gives a $\sin^2\theta_{lab}$ distribution; the solid line represents relativistic correct calculations and the shaded area depicts the spin-flip contribution (Stöhlker *et al.*, 1996).

Also the total K-REC cross sections, determined by the K x-ray emission follows closely the non-relativistic prediction over an extremely wide η range, $0.1 < \eta < 10$ and for projectiles from Z=8 to Z=92. In Fig. 4.10 one angular differential K-REC cross section value measured for bare uranium in collisions with N_2 target molecules is compared with result of exact relativistic calculations (Ichihara *et al.*, 1994; Eichler *et al.*, 1995) as well as with the non-relativistic $\sin^2\theta_{lab}$ distribution. According to the relativistic description, the differential cross sections for K-REC show a pronounced deviation from

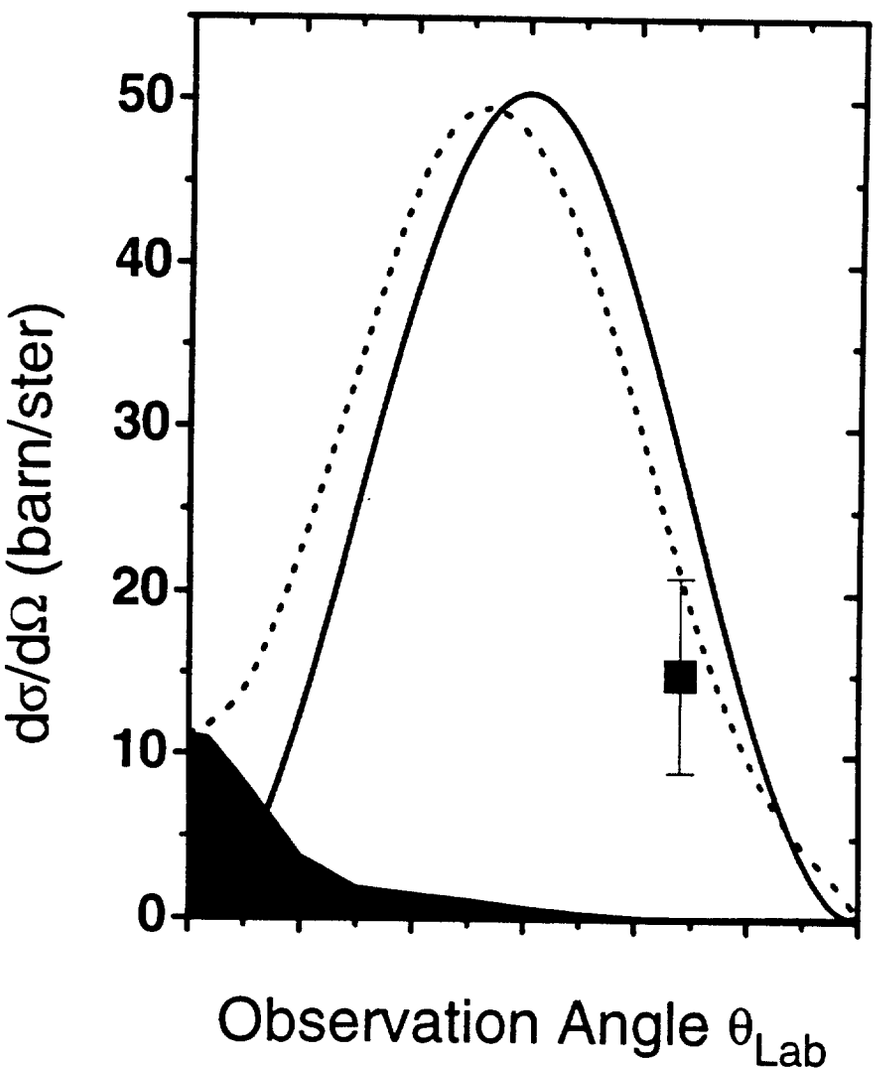
50
40
30
20
10
0
dσ/dΩ (barn/ster)
Observation Angle θLab

symmetry around $\theta_{lab} = 90^o$ and the maximum is shifted slightly towards the forward direction. This behavior is essentially associated with the occurrence of magnetic (spin-flip) transitions which are not considered by a non-relativistic approach. This spin-flip contribution to the angular-distribution is depicted separately in Fig. 10 by the hatched area. For the particular case of radiative capture into a projectile s-state only spin-flip transitions can produce non-vanishing cross sections at 0^o and 180^o. The latter follows directly from angular-momentum conservation laws for electric multipole transition (Eichler *et al.*, 1995). It is important to note, that there is no other case up to now, in which spin-flip effects in relativistic atomic collisions have such an unambiguous finger print. Within the total experimental uncertainty, a fair agreement between experiment and relativistic theory is found for the absolute values. Here, the prediction of the dipole-approximation (dotted line in Fig. 4.10) overestimates considerably the experimental value at 132^o.

Angular differential REC cross-sections are extremely sensitive to details of the atomic wave functions and provide therefore detailed insight into the atomic structure of one- and few-electron systems. For such studies high-Z ions are of particular interest. Here, the large fine structure splitting provides direct experimental access even for the investigation of the angular distributions associated with REC into the different j-sublevels of the L-shell. The potential of such challenging studies, was demonstrated for the first time experimentally in an experiment conducted at the GSI Fragment Separator for 89 MeV/u $U^{90+} \rightarrow C$ collisions (Stöhlker *et al.*, 1994). At this low projectile energy the L-REC lines split already into the two j-components. The results obtained within this experiment are depicted in Fig. 4.11. There, the measured angular distributions for REC into the j=1/2 and j=3/2 levels of the L-shell of He-like uranium, normalized to the sum of both contributions are plotted in comparison with the predictions of the exact relativistic theory.

Fig. 4.11: Experimental angular distribution - 89 MeV/u $U^{90+} \rightarrow C$ collisions - for REC into the $2s_{1/2}$ and $2p_{1/2}$ states (solid circles) and for REC into the $2p_{3/2}$ level (solid squares) in comparison with exact relativistic calculations; j= 1/2: full line, $2p_{3/2}$: dashed line (Stöhlker *et al.*, 1996). All data given in the figure are normalized to the sum of both contributions. In addition, the result of the non-relativistic dipole-approximation for capture into the $j = 1/2$ levels is given (dotted line).

The data for capture into the j=1/2-levels show a considerable bending of the angular distribution into the forward direction whereas the distribution for capture into the pure p-state (j=3/2) exhibit a strong enhancement at backward angles. As can be seen from the figure the measured very pronounced forward/backward asymmetry is in excellent agreement with the result of the rigorous theoretical treatment (Ichihara *et al.*, 1994), whereas the dipole approximation fails completely in describing the experimental findings (Hino and Watanabe, 1987). The experimental results confirm in particular the predictions of the exact relativistic theory that the REC angular distributions depend crucially on the angular momentum of the final projectile state.

4.3 Ionization and excitation processes

At the relativistic energy regime covered by the ESR the K-shell ionization process for initially H- and He-like ions is of particular interest. Up to now no systematic investigations of this process have been performed at the ESR, although the low dense gas-jet target provides ideal experimental conditions for such studies. Only, during commissionning of the ring and during some atomic physics experiments a few K-shell ionization data could be gained for H-like Dy, Au, and Pb projectiles colliding with N_2 or Ar molecules/atoms (Stöhlker *et al.*, 1993a). As has been pointed out in Chapter 2, the projectile K-shell ionization cross sections follow, within a strict non-relativistic treatment, an universal

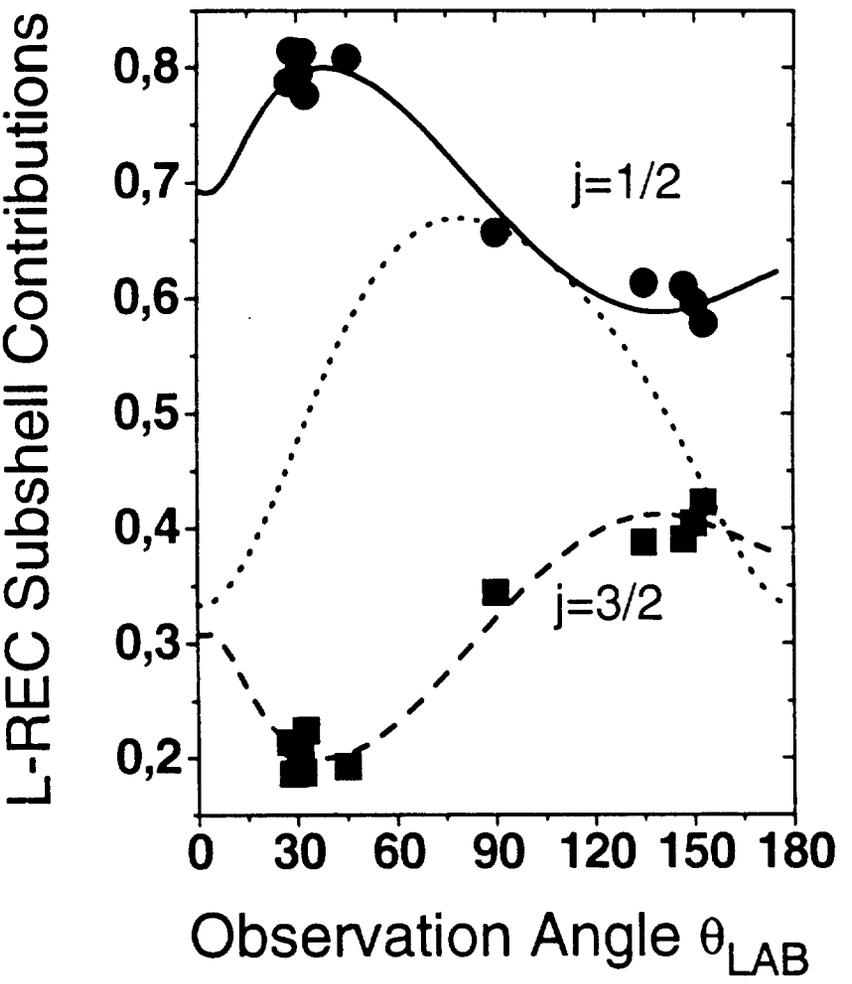
L-REC Subshell Contributions
0,8
0,7
0,6
0,5
0,4
0,3
0,2
j=1/2
j=3/2
0
30
60
90
120
150
180
Observation Angle θLAB

4.11

scaling law. By considering the correct relativistic bound and continuum wave functions this simple scaling is abolished. However, for beam energies below 300 MeV/u, the predictions of a relativistic treatment of this process deviate, depending on the projectile charge, from the ones of the non-relativistic approach by only about 20% which is in general within the systematic uncertainty of the experimental data. Within the overall experimental uncertainties of the ESR data, a general agreement with the first order perturbation theories is found. We have to emphasize that these findings seem to be in disagreement with results of solid target experiments where a systematic deviation of about 50% were observed with respect to relativistic SCA calculations (Rymuza *et al.*, 1993). This is depicted in Fig. 4.12 where the ratio between solid target data for K-shell ionization of high-Z projectiles (per K-shell electron) and the predictions of relativistic SCA calculations (Rösel *et al.*, 1982) are given as a function of the reduced velocity v/v_k. Note, that only data of such collision systems are considered where the requirements of first order perturbation theory are fulfilled. From the figure a general enhancement of the experimental data compared to theory is obvious. Therefore, further studies of this process at the ESR are urgently needed in order to clarify this point.

Fig. 4.12: The ratio between the experimental K-shell ionization cross sections for high-Z projectiles and relativistic SCA calculations (solid line) (Rymuza *et al.*, 1993).

The Coulomb excitation of a projectile electron is mediated by exactly the same reaction mechanism in ion-atom collision as projectile ionization, except that the active electron is excited into a bound and not into a continuum projectile state. The formation of excited projectile states via direct Coulomb excitation can be studied uniquely for one- and two-electron high-Z ions by the observation of the radiative decay of the excited levels to the ground state. Owing to the large L-subshell splitting in such ions the cross sec-

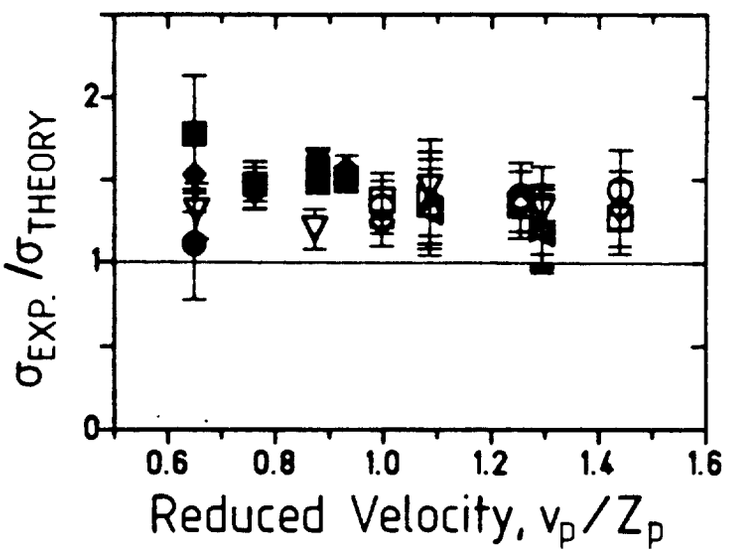
$\sigma_{EXP.}/\sigma_{THEORY}$
2
1
0
0.6
0.8
1.0
1.2
1.4
1.6
Reduced Velocity, v_p/Z_p

4.12

tion for ground state excitation into the various L-shell sublevels can be unambiguously determined. In particular, due to the very large $2s_{1/2} \rightarrow 1s_{1/2}$ M1 decay width, the E0 excitation to the $2s_{1/2}$ can directly be detected. The same holds true for the E1 excitation mode. Up to now no K-shell excitation experiments have been performed for high-Z ions except one first pilot experiment conducted for H- and He-like Bi ions by using solid targets at the SIS facility (Stöhlker *et al.*, 1992). For such investigations the ESR gas jet target provides excellent experimental conditions and experiments aiming on a precise study of the excitation process in the relativistic regime are in preparation. We have to add that within these planed experiments the detection of the characteristic Lyα/Kα photons can be performed in coincidence with a registration of the recoil momentum of the target atoms. This will provide a very first direct measurement of the impact parameter dependence for the various excitation modes for high-Z projectiles.

In collisions between highly-charged heavy-ions and low-Z targets, the process of Resonant Transfer and Excitation is – additionally to the interest in relativistic effects discussed already – of practical importance for all atomic structure and collision experiments. Considering the Compton profile of the target electrons RTE might be an important Kα production process even outside the RTE resonance energies and may also contribute significantly to the total projectile charge-exchange cross-section. This can be read from Fig. 4.6 where the measured KLL-RTE excitation functions is plotted for the case of initially He-like U^{90+} projectiles colliding with C atoms (Kandler *et al.*, 1995a). In general, the whole RTE resonance regime should be avoided by K excitation experiments as the Kα transitions are blended by the Kα hypersatellites produced by RTE. Also cross-section measurements of the non-resonant processes are of course problematic within this resonance regime. Moreover, near the resonances the total capture cross-section can increase considerably. Hence, by collisions with remnant gas molecules in the ring (mainly H_2) the lifetime for stored ions can be reduced there.

5 Atomic structure studies

5.1 The ground-state LAMB-shift

By capture and recombination processes in particular for single electron atomic reactions excited levels in highly-charged, very heavy ions can selectively be populated. Probing the subsequent radiative transitions with high spectroscopic resolution will give detailed information on the atomic structure for strong central fields. All inner-shell transitions $(L-K)$ for the heaviest species with only one and, to a great deal, also with two electrons can be considered as prompt (cf. e.g. Mokler *et al.*, 1994). Only in He-like systems the $1s_{1/2}2p_{1/2}\,^3P_0$ state may show compared to the flight velocity of the ions a delayed decay pattern (Marrus *et al.*, 1995 and 1989). These inner-shell transitions have energies in the 100 keV region (e.g. for U) and a high-resolution x-ray spectroscopy seems to be the adequate vehicle for precision structure studies. However, crystal spectrometers have in reality such small overall detection efficiencies, that until now their use was prohibitive. Solid state detectors as for example intrinsic Germanium diodes, Ge(i), have a reasonable good resolution and an almost perfect detection efficiency, only determined by their sizes. At present, results based on solid state detectors are available for the heaviest ultimately charged ions (see below).

A further severe obstacle for a fast beam precision spectroscopy is the Doppler effect. Not only that the radiation from the emitting fast projectiles has to be transformed by the Lorentz transformation into the laboratory system also the finite solid angle of the detector causes a Doppler broadening for the observed line radiation. Moreover, the divergence of the beam and the uncertainty in the knowledge of the absolute beam velocity contribute to the final uncertainty for the transition energies wanted (cf. Mokler *et al.*, 1995a). We note, that for instance at a specific energy of 300 MeV/u and for an observation angle of 0^o the projectile emission is blue shifted by a factor of 2.2; at 180^o backward observation

we have a red shift of a factor of 0.45. For this case, the unshifted line is found at about 70° in the laboratory. At an laboratory angle of about 48° the sensitivity on the beam velocity is minimal, whereas the changes in Doppler shift with observation angle is maximal there. For a 0° observation the opposite is the case. In order to overcome the variation in Doppler shift with observation angle segmented or "granular" detectors are used. Thus, large solid angles can be covered without loosing resolution by the Doppler broadening. Each segment has to be corrected individually on its correct Doppler shift before all the spectra can be added up to one high resolution CM spectrum with a good statistical significance (Stöhlker *et al.*, 1992a). Due to the active and redundant use of the Doppler effect this fast beam technique is labeled as Doppler-shift assisted ion spectroscopy (Mokler *et al.*, 1995a). This is in some way a modern version of the classical dispersive Doppler-tuned edge spectroscopy at fast ion beams (Schmieder and Marrus, 1973; Lupton *et al.*, 1994).

Excited projectile states can efficiently be produced either by radiative recombination in the electron cooler or by electron capture in the gas jet target of the *ESR*. Complimentary experiments are performed at both areas. The cooler with its bulky magnetic coils is only accessible to an almost 0° or 180° observation of the emitted radiation. In contrast, such an observation is not possible at the gas jet in its present design. However, the range from 30° to 150° on both sides of the gas target can be used for x-ray detection giving ample of angular redundancy. Naturally, at both the areas single electron events are assured by the corresponding coincidences of the x-ray emission with the down-charged ions detected behind the corresponding next down-stream dipole magnet. In Fig. 5.1. a and b the two methods and the resulting spectra are compared.

Fig. 5.1: Comparison of projectile x-ray spectroscopy at the electron cooler and the gas jet section of the *ESR*. In both cases, single electron events are assured by coincidences between x rays registered by a Ge(i) detector and the

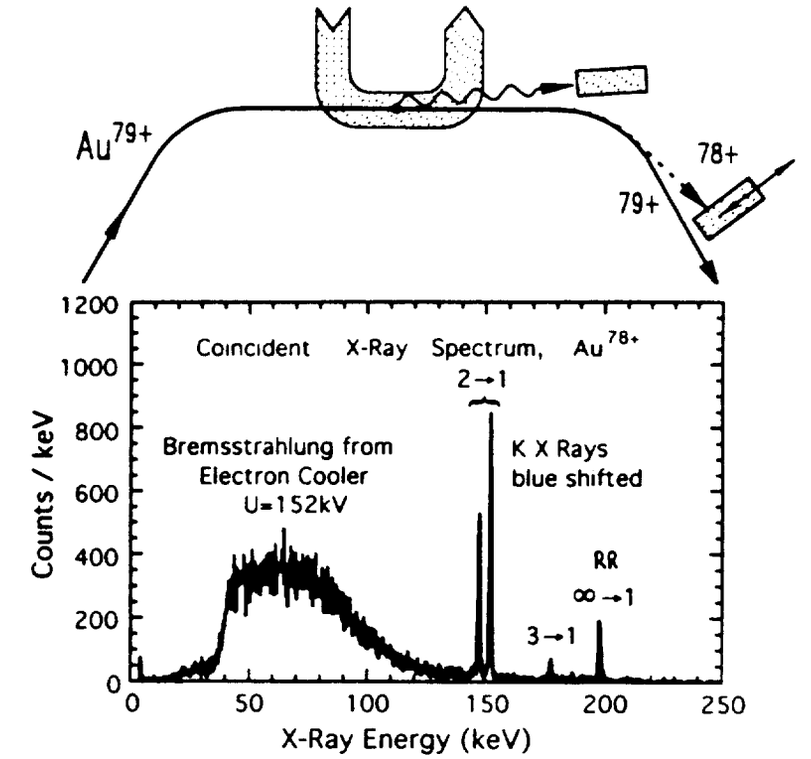
Au79+
78+
79+
Coincident X-Ray Spectrum, Au78+
2→1
Bremsstrahlung from
Electron Cooler
U=152kV
K X Rays
blue shifted
RR
∞→1
3→1
Counts / keV
X-Ray Energy (keV)

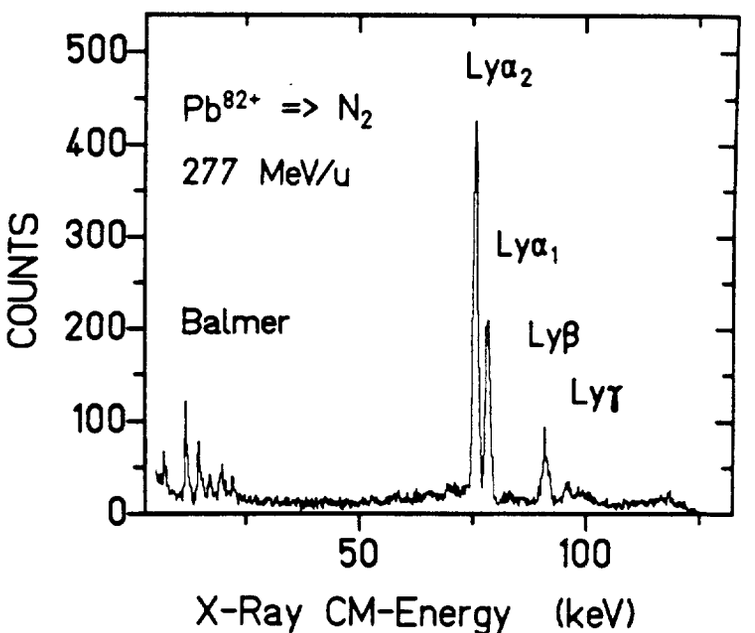
Pb82+ => N2
277 MeV/u
Lyα2
Lyα1
Lyβ
Lyγ
Balmer
COUNTS
X-Ray CM-Energy (keV)

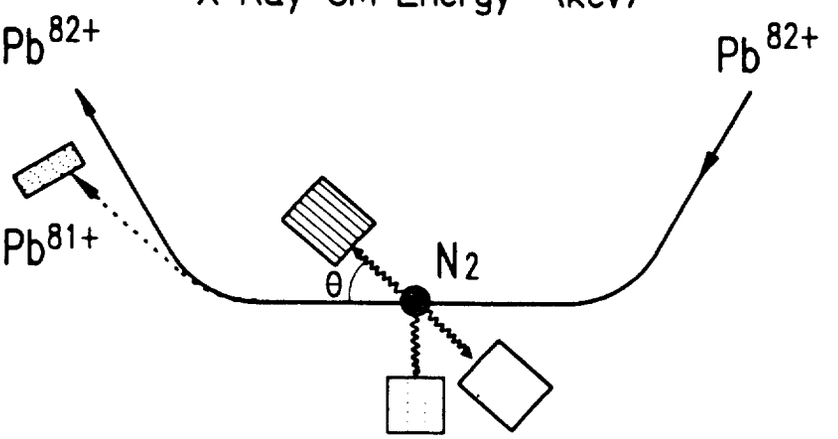
Pb82+
Pb82+
Pb81+
N2
θ

down-charged ions.

Part 'a' at the top displays the near 0° arrangement at the electron cooler and a spectrum taken for a coasting bare Au^{79+} beam at 278 Mev/u (Liesen *et al.*, 1994)

Part 'b' at the bottom elucidates the Doppler-shift assisted, multi-angle spectroscopy at the gas-jet target; bare Pb^{82+} ions from a coasting beam capture an electron from N_2 gas molecules (Mokler *et al.*, 1995a).

From Fig. 5.1 it is obvious that both the methods give complimentary information. First, the population of the projectile L-shell levels is quite different: In the cooler we have low-energy electron-ion collisions preferring more the high angular momentum states; whereas at the gas target high energy ion-atom collisions, mainly REC, favour the low angular momenta. Correspondingly, the intensity ratio of the $Lyman - \alpha$ doublet is at variance for both the cases. For the cooler target additionally the radiative recombination line to the ground state gives directly the ground state binding energy. The analogous REC line at the gas target is due to the high, relative kinetic energy of the quasifree electrons outside the range of the shown spectrum (Fig. 5.1.b). However, also the dependence of the K-REC peak on beam velocity can be used for a precise spectroscopy of the ground state binding energy (Mokler *et al.*, 1991). Finally, in the electron cooler one has to deal with an appreciable bremsstrahlungs background at lower x-ray energies caused by scattered electrons. The coincidence spectrum at the gas target is absolutely clean down to the lowest x-ray energies allowing also a spectroscopy of higher shell transitions as is demonstrated by the Balmer lines in the shown spectrum.

For the case of transitions in H-like U^{92+} we display in an enlarged scale the region for the $LYMAN$ transitions for both cases. At the top of the figure the corresponding transitions are indicated. The top spectrum (LAB energies) was taken under 0° at the cooler for a 321 MeV/u coasting bare U^{92+} beam (Beyer *et al.*, 1995). The radiative

recombination line as well as the $LYMAN-\alpha$ transitions are clearly visible at strongly Doppler shifted energies. The Lyman lines show a strong low energy tail from a cascade feeding via recombination to high-lying Rydberg states. This delayed emission involves different geometries and, hence, a different Doppler relevant detection angle. The spectrum at the bottom was taken at the gas target for a cooled U^{92+} beam decelerated in the ring to 68 MeV/u and colliding with N_2 molecules (Stöhlker, 1995; Mokler *et al.*, 1995b). The Lyman lines are symmetric; even the $LYMAN-\beta$ transitions split clearly into two lines for different j values in the feeding M shell. The $LYMAN-\alpha 2$ line is in contrast to the single transition in the $LYMAN-\alpha 1$ line composed of two transitions, the $2p_{1/2}-1s_{1/2}$ E1 radiation and the $2s_{1/2}-1s_{1/2}$ M1 transition, cf. Chapter 2.1.

Fig. 5.2: $LYMAN$ spectra for H-like U^{92+} measured at the cooler section - top spectrum (Beyer *et al.*, 1995) - and at the gas jet target - bottom spectrum (Stöhlker, 1995; Mokler *et al.*, 1995b). A coasting bare U^{92+} beam of 321 and 68 MeV/u respectively, was used. In the upper spectrum Lab. energies and in the lower one CM x-ray energies are given. For convenience the $LYMAN$ decay scheme is displayed at the very top.

Determining the exact transition energies for the various lines and subtracting the theoretical expectation values for the corresponding transitions from a solution of the Dirac equation one ends up with an experimental value for the 1s ground state $LAMB$–shift. The presently best value for the ground state $LAMB$–shift in H-like uranium is 470 ± 16 eV (Beyer *et al.*, 1995) which has to be compared with theoretical values of 463.4 ± 0.6 eV (Soff, 1993) and 464.6 ± 0.6 eV (Mohr, 1994). Within the errors there is an excellent agreement between experiment and QED expectations. On the other hand, the experimental accuracy is not yet sensitive to the estimated accuracy of theory. An evaluation of the more recent and statistically more significant data from the gas target shown at

Lyman Series for U^{1e}

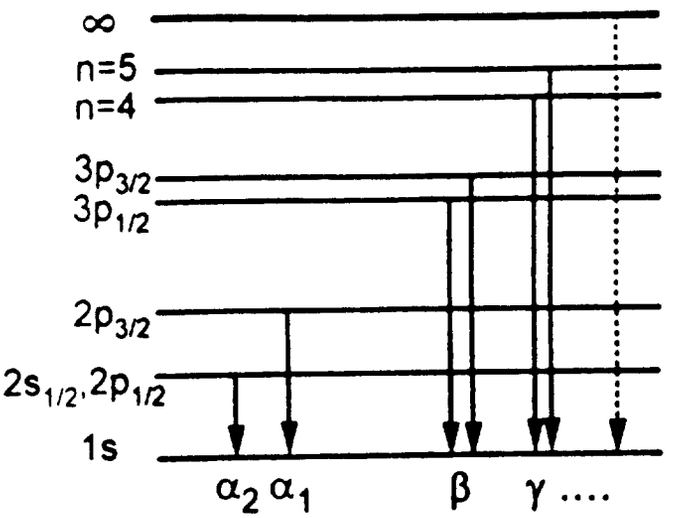

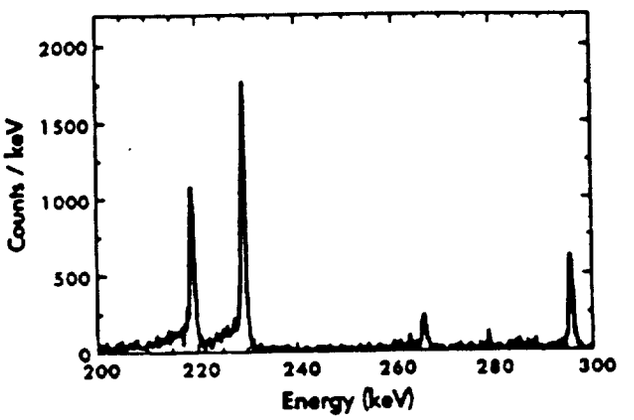

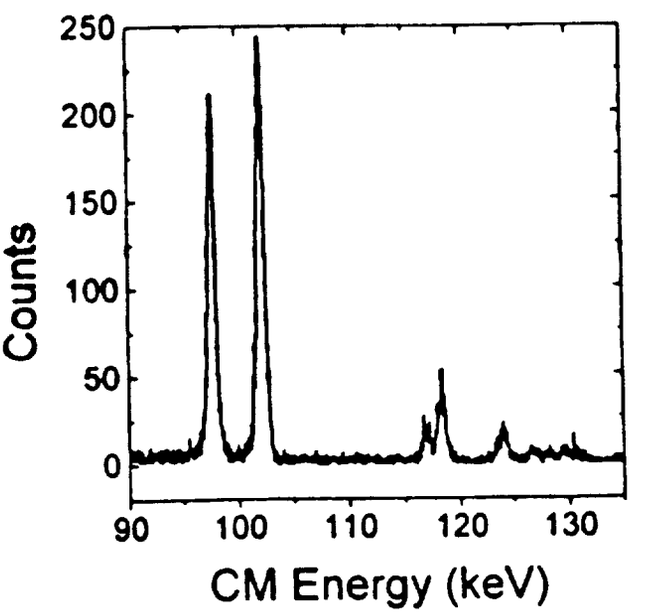

5.2

the bottom of Fig. 5.2 may improve the experimental situation slightly (Stöhlker, 1995). However, an experimental accuracy better by an order of magnitude is needed in order to compete with the theoretical uncertainties. Here, more advanced spectroscopic techniques have to be applied in future. An other way to tackle this problem is to investigate transitions into or within higher shells. There, not only the QED contributions are smaller, but also the transition energies are dramatically reduced allowing in the end possibly for a more accurate determination of the QED terms. However, the higher main quantum number wavefunctions (e.g. in the L-shell) do not probe so sensitively the strongest parts of the strong central potentials.

Independently, the recent advances in the ground state $LAMB$–shift measurements at the heaviest H-like ions are a tremendous success in this challenging field. In Fig. 5.3 these results are summarized and compared to theory. The predictions of Johnson and Soff (1985) are excellently reproduced by the recent experimental findings. In the figure, the data - reduced by the Z^4 scaling - are compared to the $F(Z\alpha)$ function discussed in Chapter 2.1 (see also Eq. 2). The full points in the figure are the new results from the synchrotron/storage ring facility SIS/ESR for Dy (Beyer *et al.*), 1993, for Au (Beyer *et al.*, 1994), for Pb (Mokler *et al.*, 1995a), for Bi (Stöhlker *et al.*, 1992), and for U (Stöhlker *et al.* 1993; Beyer *et al.*, 1995). For the other data see the references given in Mokler *et al.* (1995a). Similar agreement has also be found for ground state transitions in He-like heavy systems (cf. Mokler *et al.*, 1994). However, due to the more complex decay pattern and due to the uncertainties from the blending contributions in the different lines the situation is more complicated there and will not be discussed here. Anyhow, these measurements triggered sophisticated calculations including higher order QED terms, in particular also the electron-electron QED contributions (cf. Lindroth, 1995; Pearson *et al.*, 1995; Indelicato, 1995). There is the hope, that these effects can be tested soon by experiments.

Fig. 5.3: Comparison of the measured ground state $LAMB$–shift reduced by Z^4 for heavy, H-like ions with the predictions by Johnson and Soff (1985).

5.2 Doubly excited states

In the previous chapter we emphasized already that dielectronic recombination provides an ideal tool for atomic structure studies. In particular, it gives access to an exploration of doubly excited states. For highly-charged, very heavy ions the structure of doubly excited states is governed by several fundamental effects. Besides relativistic effects, the current-current interaction i.e. the Breit term, as well as QED contributions, and nuclear size effects have to be included into calculations. As was pointed out in Chapter 4.1, fully relativistic calculations including all these effects describe not only the total recombination rates fairly well, they also give an excellent accordance with the resonance positions within the measuring accuracies.

In Fig. 5.4 the most recent recombination spectrum measured for Li-like Au^{76+} ions is displayed (Spies *et al.*, 1995). The test measurement was performed at the ESR with an energy uncertainty of presently about 0.5 eV. With some technical modifications already scheduled for the ESR cooler the accuracy will be improved by an order of magnitude in the near future. For the present experiment Li-like Au^{76+} ions have been bred in the ESR from He-like Au^{77+} ions originally injected from the heavy ion synchrotron SIS, *cf.* Chapter 3.3.4 (Spies *et al.*, 1992). For detuning the relative energies between electron and ion beams, high voltages up to $\pm$ 5 kV have been applied to a drift tube in the cooler. A fast periodic switching from cooling to measuring position was incorporated. The recombined Be-like Au^{75+} ions have been detected by the recombination detector behind the next down-stream magnet as a function of the detuning voltage. In the figure this voltage is already converted into the center of mass energy.

Fig. 5.4: Recombination rate for Li-like Au^{76+} ions as a function of the relative

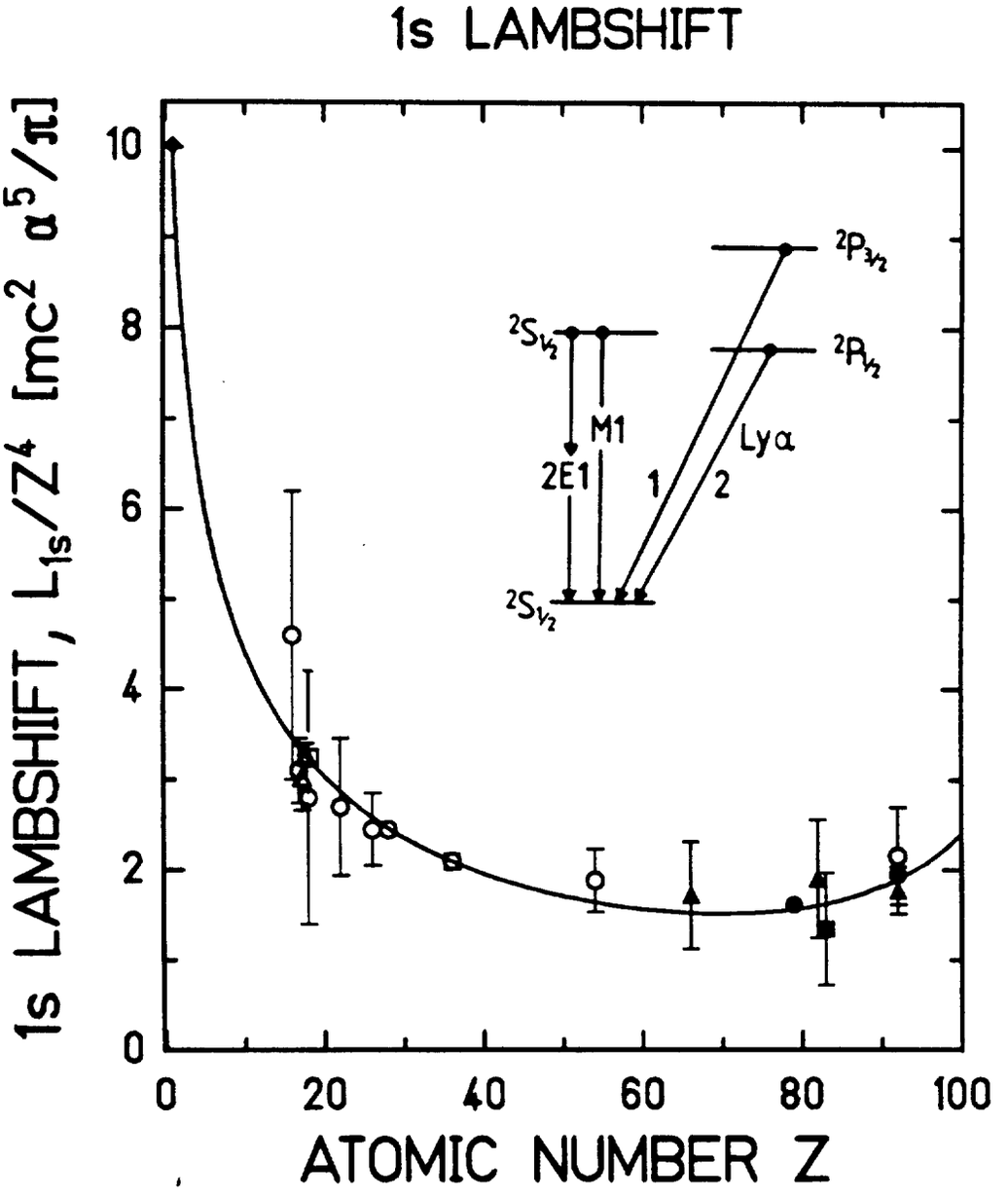
1s LAMBSHIFT
1s LAMBSHIFT, L_{1s}/Z^4 [mc^2 α^5/π]
10
8
6
4
2
0
0
20
40
60
80
100
ATOMIC NUMBER Z
$^2P_{3/2}$
$^2P_{1/2}$
$^2S_{1/2}$
M1
2E1
Lyα
1
2
$^2S_{1/2}$

energy between electron and ion beam (Spies *et al.*, 1995). The full curve is a result of sophisticated calculations on dielectronic and radiative recombination convoluted with the experimental velocity distribution of the electrons over the whole interaction region (for details see text). For clarity the energy region beyond 60 eV is shown in the insert with an enlarged scale. The experimental arrangement is sketched at the top of the figure.

The recombination spectrum in Fig. 5.4 shows on top of the rapidly decreasing radiative recombination continuum, sharp lines for the $\Delta n = 0$ dielectronic recombination resonances ($1s^2 2s_{1/2} + e \quad \rightarrow \quad 1s^2 2p_j n l_{j'}$). Excitations involving $2p_{3/2}$ electrons are the most prominent lines. Due to the large energy gaps between the atomic shells (n) at this high atomic number, we find here within our energy range only the $2p_{3/2}6l_j$ resonance group which is splitted into several lines. We like to point out that to one j value of the electron with n = 6 two angular momenta l contribute causing an additional small splitting. This is best visible for the $j = 3/2$ states. All the resonances of the $2p_{3/2}6l_j$ group cover due to the large fine structure splitting an energy range of 50 eV. This has to be compared with dielectronic recombination spectra for lighter ions as e.g. Li-like Cu^{26+} shown previously in Fig. 4.4. There, within one series no additional fine structure can be resolved at all.

The fine structure seen for the $2p_{3/2}6l_j$ resonances is well reproduced by fully relativistic calculations including Breit interaction, QED corrections and nuclear size effect (Spies *et al.*, 1992). The curve shown in Fig. 5.4 together with the data is the result of such a calculation convoluted with the effective velocity distribution of the electrons over the interaction region of the cooler including all the distortions caused by the drift tubes. For the $2p_{3/2}$ excitations a full relativistic calculation of Zimmerer (1992) was applied, for the weak resonances involving $2p_{1/2}$ excitations (see below) a semi-relativistic approach of Pindzola and Badnell (1992) was used, and the radiative recombination continuum is

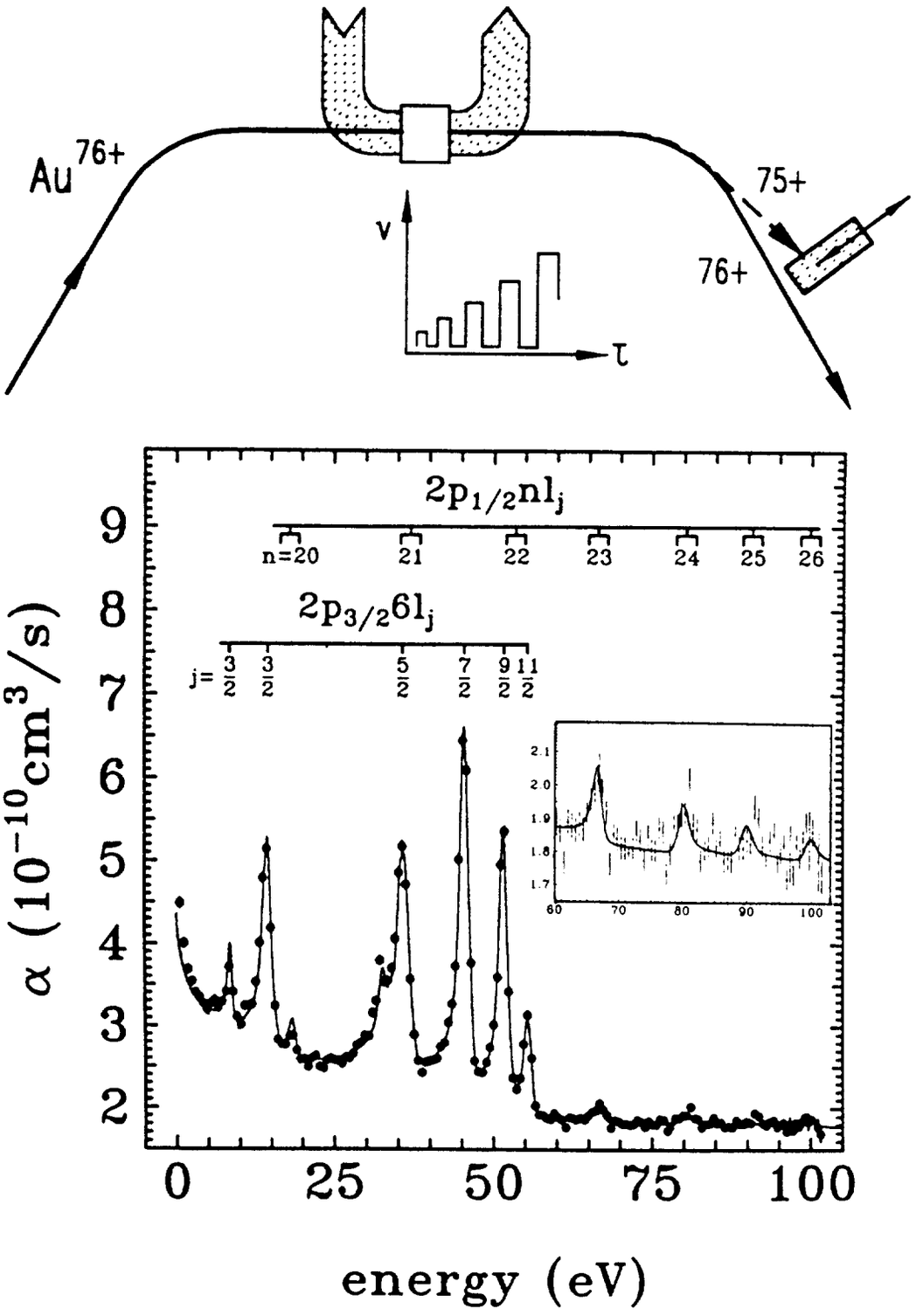
Au 76+
75+
76+
v
τ
$2p_{1/2}nl_j$
n=20
21
22
23
24
25
26
$2p_{3/2}6l_j$
j= 3/2 3/2 5/2 7/2 9/2 11/2
α (10^{-10}cm^3/s)
energy (eV)
0
25
50
75
100
2
3
4
5
6
7
8
9

5.4

based on the theory of Bethe and Salpeter (1957). An excellent agreement between the final result in an isolated resonance approximation (i.e. neglecting interferences between the various reaction channels) and the data can be stated.

Additionally to the discussed prominent resonances we see the weak resonances of the $2p_{1/2}$ excitation series with an nl_j Rydberg electron. The positions for the resonances with n = 20 to 26 are indicated in the Fig. 5.4. The resonances with n = 20 and 23 are clearly visible within the measured spectrum. For the higher n resonances we display the energy region between 60 and 100 keV separately in the insert. There, the resonances up to n = 26 are visible. Although the rates are small for the $2p_{1/2}nl_j$ resonances and the present statistics is not adequate for a precise extrapolation of energies to higher n states one can try to determine roughly the series limit. Using an effective charge (76.48) in the Rydberg formula or using correspondingly a quantum defect (0.098) formula a $2s_{1/2} \rightarrow 2p_{1/2}$ energy splitting of 219.0±3 eV and 218.4±3 eV, respectively, has been reported for the limiting case that the second electron is just in the continuum, i.e. $n \rightarrow \infty$ or Li-like Au^{76+} ions (Spies *et al.*, 1995).

A first calculation for this case gave a splitting of 217.5 eV (Zimmermann *et al.*, 1994) which is in excellent agreement with the experimental result. Here, the one-electron LAMB-shift contribution to the 2s level is in the order of 30 eV. This test experiment gave already an accuracy of 3 eV, i.e. a 10 % measurement of the LAMB-shift. As was pointed out, in future the accuracy of those experiments will be improved at least by an order of magnitude after introducing some technical modifications at the cooler. In the end, we expect that the accuracy of the DR experiments described above will be superior to those quoted for Li-like U^{89+} by Schweppe *et al.* (1991) using a Doppler tuned spectroscopy technique for the $\Delta n = 0$ transition in the VUV range.

Moreover, there is the definite hope that in future even for the heaviest ions dielectronic recombination resonances with $\Delta n = 1$ transitions involving K-shell electrons can be

measured. Assuming similar accuracies as already achieved for lighter ions or for $\Delta n = 0$ transitions, dielectronic recombination may be a very competitive tool for precision spectroscopy of the heaviest, highly charged ions.

5.3 Rydberg states

By radiative recombination also highly excited projectile levels (n,l), i.e. Rydberg states, can be populated in the cooler. According to Stobbe (1930) the population distribution (n,l) can be calculated, cf. Eq. 4 in Chapter 2. For small relative energies of the free electron compared to the emitted photon energy, the recombination rate is proportional to Z^2/n and decreases with the relative kinetic electron energy. Additionally (n,l) dependend coefficients have to be used. This spontaneous radiative recombination gives a very wide distribution for the Rydberg states. On the other hand, radiative recombination can also be induced by a corresponding photon field. This Laser-induced radiative recombination (LIR) is a resonant process, populating selectively only one Rydberg state (Wolf, 1992). The induced recombination rate depends trivially on the Laser intensity and more important on the third power of the photon wavelength. If we use the Rydberg formula for the binding energies, the induced rate is proportional to $(n/Z)^6$. Assuming a fixed Laser wavelength, that means, very high Rydberg states can particularly be populated for heavy Z projectiles. On the other hand, for the heavy ions the spontaneous rates increase also, masking increasingly stimulated transitions and the relative gain factor.

It is obvious, that the Laser induced recombination LIR is an ideal tool to probe on the one side the temperature distribution of the electrons in the cooler. On the other side, also the projectile Rydberg states can be examined with high spectroscopic precision. For a real heavy ion, Laser induced recombination was measured first at the TSR: By a dye Laser the recombination of a bare C^{6+} ion with a cooler electron into the n = 14 level of C^{5+} was stimulated; the recombined ions were detected behind the

next downstream dipole magnet, for details see Wolf *et al.* (1993). In particular, the electron density distribution around the continuum could be investigated. The Rydberg states for dressed, highly-charged ions are very sensitive on the core potential of the ions, especially on the core polarizability. This long-range interaction has recently been studied for oxygen ions with a Li-like core (Schüssler *et al.*, 1995a and 1995b).

Loosely bound electrons in high Rydberg levels with their relative long lifetimes may be field ionized by the motional electric field seen by the ion in the next down stream transversal magnetic dipole field. This is especially true for fast, i.e. for heavy ions and the stimulated recombination can not be observed due to field ionization. However, transferring the electron by an appropriately tuned second Laser pulse to a deeper bound state the recombination can be stabilized. Recently, this Laser stimulated two-step recombination process was first seen for stored bare Ar^{18+} ions in the ESR (Borneis *et al.*, 1994). More recently, this Laser induced two-step recombination technique was also used at the TSR to study the fine structure of inter-Rydberg transitions mentioned just above (Schüssler, 1995a and 1995b).

In Fig. 5.5 the principles for the two-step Laser induced recombination experiment at the ESR are outlined as an example. Bare Ar^{18+} ions were stored at an energy of about 147 MeV/u ($\beta \approx 0.5$). In the overlap region of the cooler a Nd:YAG Laser was colinearly superimposed stimulating an induced recombination into the $n_i = 84$ Rydberg level of Ar^{17+}. Here, the photon energy in the ion system is strongly red-shifted by the Doppler effect. Simultaneously, a tunable Ti:sapphire Laser was superimposed anti-parallel to the ion and electron beams direction, inducing a stimulated transition down to the $n_f = 36$ and $n_f = 37$ Rydberg state. Here, also the blue-shift of the photons was used to come down to Rydberg levels below the field ionization limit which is in the present case at about $n_{IONIZ} = 41$. The recombined Ar^{17+} ions were registered in the particle detector behind the next down-stream dipole magnet provided the spatial and time overlap of

all the four beams was adjusted correctly. The recombination rate was measured as a function of the tunable wavelength of the second Laser (Borneis *et al.*, 1994).

Fig. 5.5: Layout of the first two-step Laser induced recombination experiment performed at the ESR with initially bare Ar^{18+} ions at 147 MeV/u. In the beam overlap region of the electron cooler time-coincident co- and contra-moving Laser pulses are superimposed. Recombined Ar^{17+} ions are measured in the next down-stream particle detector as a function of the timely overlap and wavelength of the tunable contra-moving Laser pulses. For details see text and Borneis *et al.* (1994).

With this two-step Laser induced recombination technique a precise Rydberg spectroscopy in an electron beam environment is now accessible, see also Schüssler *et al.* (1995a and 1995b). In particular, using contra moving Laser beams an almost Doppler free spectroscopy of Rydberg states in fast beams might be possible. This is not only important for the physics involving Rydberg states, but it gives an unique way to calibrate precisely ion velocities in storage rings. On the other hand, this technique may also be utilized to probe the critical structure of the continuum-bound state transition region in the cooler section.

5.4 Hyperfine interactions

Laser resonance fluorescence spectroscopy is a sensitive probe for atomic structure investigations. For high-Z ions this method is in particular well suited for studying the hyperfine interaction where the angular momentum of the electron core J and the nuclear spin I couple together to the total angular momentum F. In atomic hydrogen this mechanism leads to the well known 21 cm M1 transition between the two hyperfine levels of F=1 and F=0. By applying the Laser resonance method at the ESR storage ring, the same

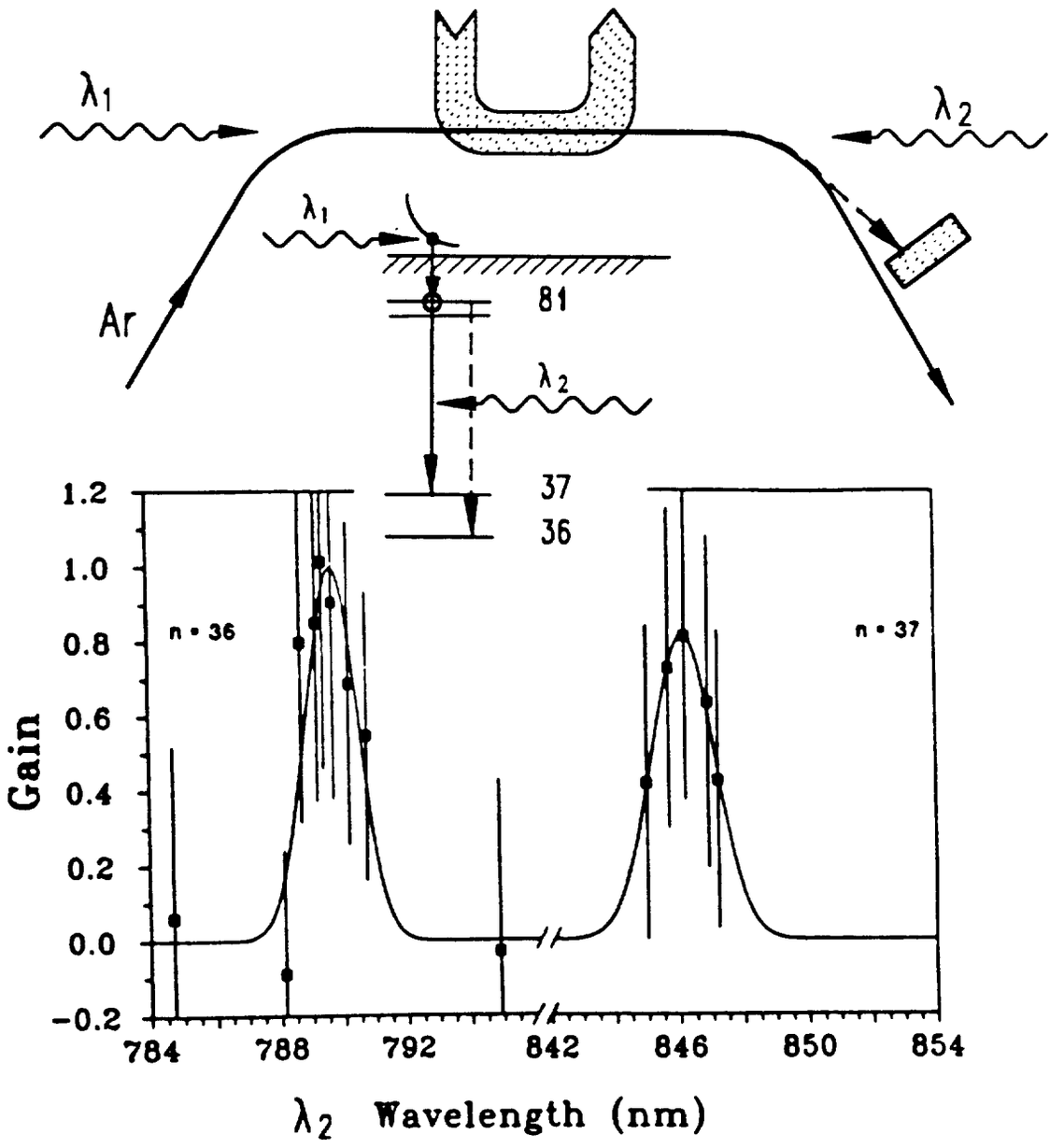
λ1
λ2
λ1
Ar
81
λ2
37
36
1.2
1.0
0.8
0.6
0.4
0.2
0.0
-0.2
Gain
n = 36
n = 37
784
788
792
842
846
850
854
λ2 Wavelength (nm)

5.5

HFS transition mode was identified for the very first time in a hydrogenic high-Z system (Klaft *et al.*, 1994) i.e. $^{209}_{83}\mathrm{Bi}^{82+}$, which has a nuclear spin of $I = 9/2$ and a magnetic nuclear dipole moment of $\mu_I = 4.1\mu_N$. The measured Laser induced fluorescence yield for the hyperfine transition ($F = 5 \rightarrow F = 4$) is given in Fig. 5.6 ass function of excitation wavelength and delay time after excitation.

Fig. 5.6: Sketch of the experimental procedure used for the identification of the M1 hyperfine ground state transition in $_{83}Bi^{82+}$ (Klaft *et al.*, 1994). In addition the measured Laser fluorescence yield is shown as a function pf excitation wavelength. The spectral width of the resonance signal is caused by the Doppler broadening due to the velocity spread of the stored ions. Also the observed fluorescence yield of the M1 transition is depicted as function of the time delay after the Laser pulse.

Since the HFS scales proportional to Z^3 the $F = 5 \rightarrow F = 4$ transition in hydrogenic bismuth is in the optical regime and the calculated splitting is approximately 243 nm whereas the lifetime of the excited $F = 5$ is calculated to be about 400 ns (Finkbeiner *et al.*, 1993; Schneider *et al.*, 1993). These theoretical predictions have to be compared with the experimental findings for the transition wavelength of 243.87(4) nm and for the lifetime of 351(15) ms. Whereas the measured lifetime is about 15% smaller than the predicted value the experimental transition energy is close to the theoretical one. Here, the theoretical estimation takes into account the distribution of the nuclear magnetisation (Bohr-Weisskopf effect), however neglects QED effects which should be in principle of considerable influence. In particular the coupling of the electron to the magnetic part of the virtual photon field - which is a tiny effect for the total Lamb shift - can be probed here for the very first time. Further experiments to this challenging topic are in preparation, e.g. for $^{207}Pb^{81+}$ where the nuclear moment arises from an unpaired neutron rather than from a proton as in the case of $^{209}\mathrm{Bi}^{82+}$ (Kühl, 1995).

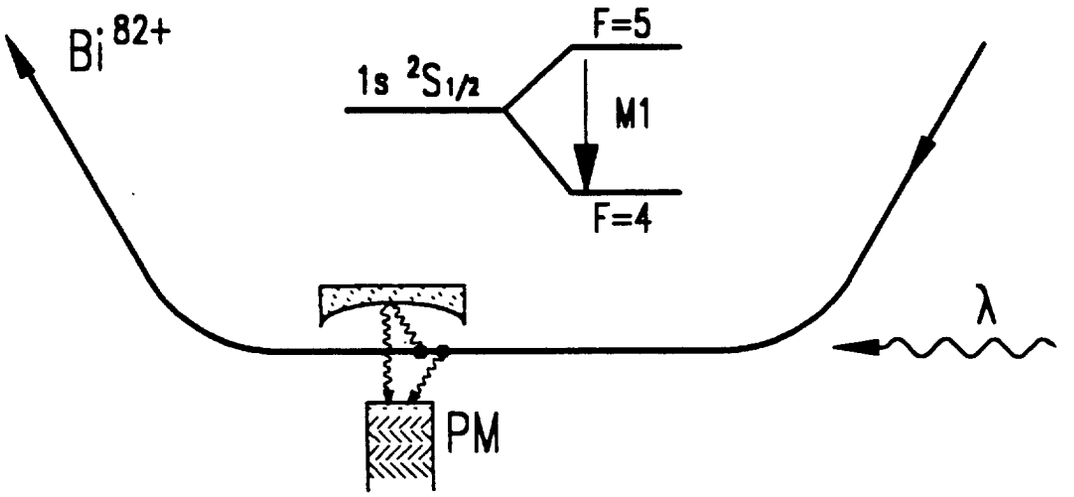
Bi 82+
F=5
1s 2S1/2
M1
F=4
λ
PM

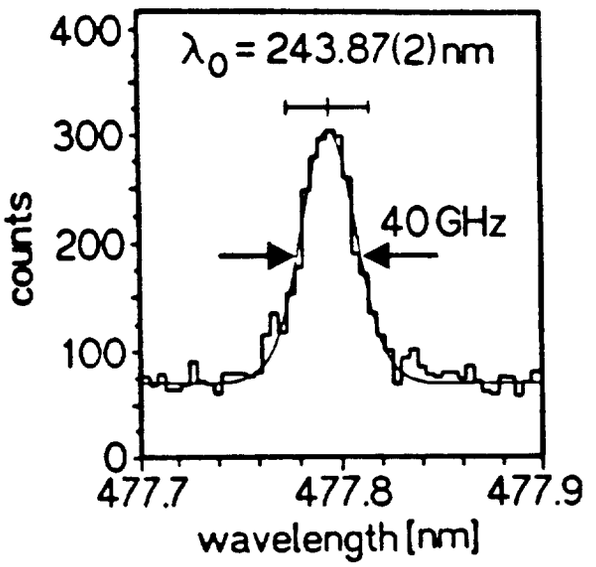
λ0 = 243.87(2) nm
40 GHz
counts
400
300
200
100
0
477.7
477.8
477.9
wavelength [nm]

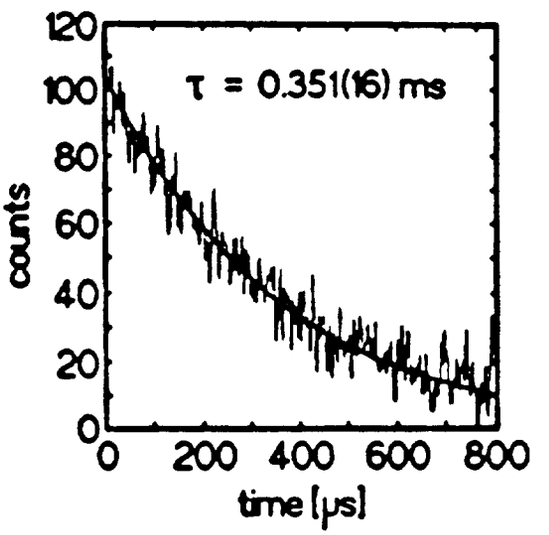
τ = 0.351(16) ms
counts
120
100
80
60
40
20
0
0
200
400
600
800
time [μs]

5.6

5.5 β-decay into bound states

Heavy ion storage rings provide presently the most direct access for the investigation of the interplay between the atomic and nuclear structure. One of the most impressive experiments performed at the ESR in this new field of research is the observation of the bound β-decay of bare $^{163}_{66}Dy^{66+}$ into hydrogenlike $^{163}_{67}Ho^{66+}$ (Jung *et al.*, 1992). This decay channel is completely forbidden for neutral dysprosium as the Q-value of the decay is not sufficient for the emission of the β-decay electron into the continuum. Therefore, neutral Dy remains stable. For completely stripped Dy, however, this decay channel is opened up as the electron can be transfered into an unoccupied bound state. The influence of the atomic structure on the decay channels of the nucleus is in particular of astrophysical relevance because during nucleo-synthesis in stellar plasmas one has to consider high ionic charge-states.

The experiment, proposed by Bosch (1987), has been performed at the ESR storage ring for up to 10^8 stored and cooled Dy^{66+} ions (Jung *et al.*, 1992). Depending on the storage or elapse time Ho^{66+} ions are built up in the ring by bound state β decay. Both the Ho^{66+} ions and the Dy^{66+} ions are moving on almost the same trajectory, due to the nearly equivalent charge to mass ratio. The holmium ions were identified after a certain elapse time by stripping off the one electron, changing so the charge from 66+ to 67+. For this purpose the gas-jet target was applied and the bare holmium ions produced in the gas-jet target ions were separated magnetically from the main circulating beam. Finally, the bare Ho^{67+} ions were detected by using a position sensitive multiwire detector behind the next downstream dipole magnet. In Fig. 5.6 the experimental procedure is sketched. At the beginning t=0 of a measuring cycle the Ho^{66+} ions are stripped in the gas-jet target yielding a strongly decreasing rate in the inner detector registering ionization events. The rate in the outer ion detector (electron capture) gives a measure for the stored Dy ions. After a certain elapse time the gas-jet target is switched on again. Once more, in the

inner detector an increase of the Ho^{67+} ion rate is monitored.

Fig. 5.7: Sketch of the experimental procedure used for the first identification of the bound state β decay (Jung *et al.*, 1992). At the top the current of the bare Dy^{66+} ions stored in the ESR during the various stages of the experiment is presented. At the bottom the corresponding rates seen by the outer (Dy^{65+}) and the inner particle detector (Ho^{67+}) are shown. These detectors are moved in after a certain accumulation period (labeled with "storage") before the Ar gas-jet is switched on.

Alternatively to this method, the Schottky Diagnostics was used for the identification of the Ho^{67+} ions. Here, (without using particle detectors) the amount of particles with a different revolution frequency as the main stored beam was measured. The corresponding Ho^{67+} ion signal strength increases with time, see Fig. 3.10. By using both methods the bound β-decay mode could be identified to the very first time with a resulting halflife of $T_{1/2} = 47^{+5}_{-4}$ d, which is in excellent accordance with theoretical predictions (Jung *et al.*, 1992).

Very recently, in a second experiment to this topic conducted at the ESR storage ring, the bound β-decay of bare $^{187}Re^{75+}$ to $^{187}Os^{75}$ could also be identified experimentally (Bosch and Nolden, 1995). For $^{187}Re^{75+}$ the precise knowledge of the bound β decay probability is of particular interest because the effective lifetime of ^{187}Re serves as one of the clocks for the age of our galaxis. A decay time of about 30 years was preliminary deduced.

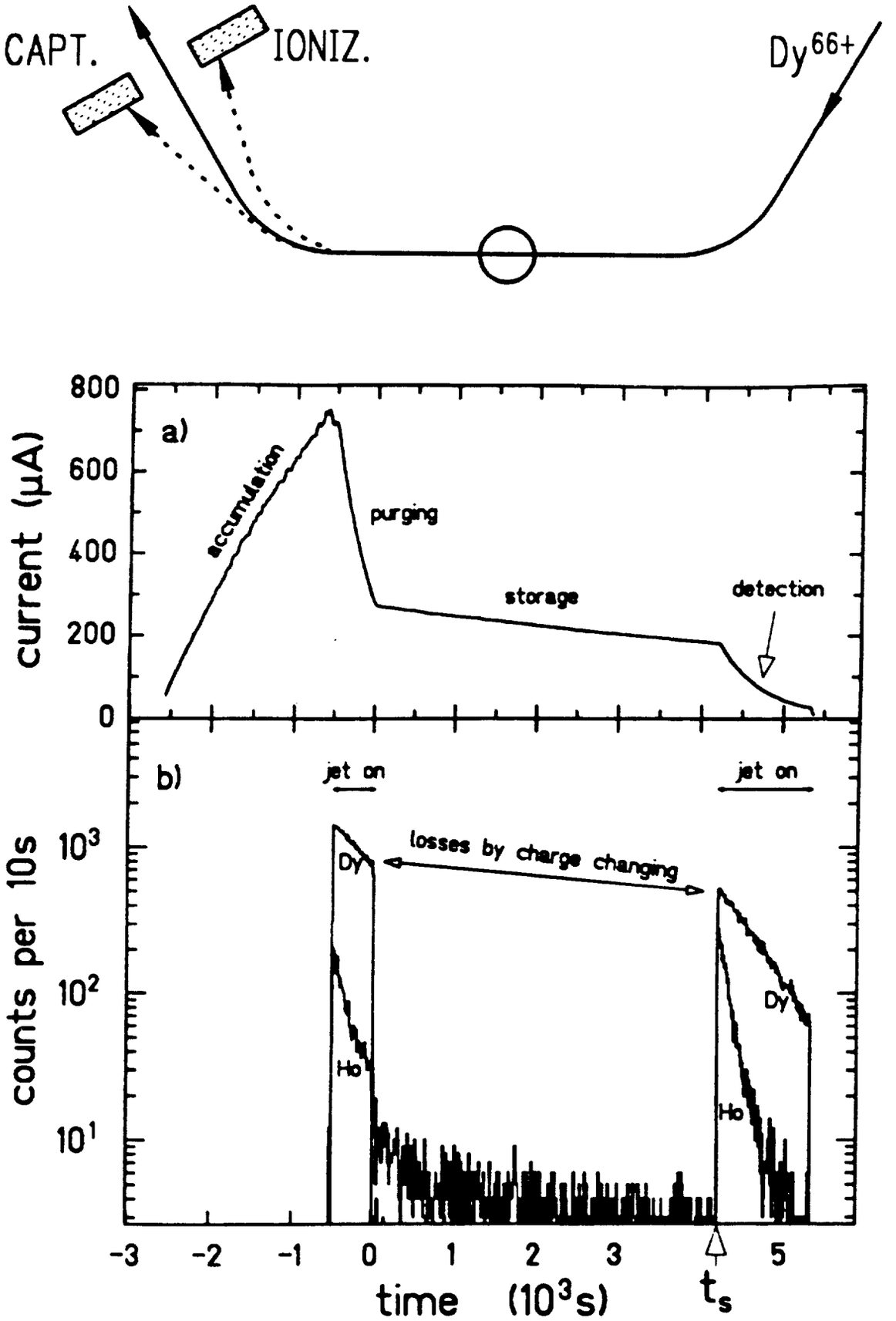
CAPT.
IONIZ.
Dy66+
a)
accumulation
purging
storage
detection
current (μA)
800
600
400
200
0
b)
jet on
jet on
losses by charge changing
Dy
Ho
Dy
Ho
counts per 10s
10³
10²
10¹
-3
-2
-1
0
1
2
3
5
time (10³s)
ts

5.7

6 Future Developments

In 1988 the first storage and cooler ring for heavy ions, the TSR, came into operation; the storage ring for the heaviest possible ions such as bare U^{92+}, the ESR, was commissioned in 1990. The present review tries to summarize the enormous progress achieved with these novel and powerful tools for the basic physics of highly charged, heavy ions within only about half a decade. Fundamental insight, both, into the detailed structure of heavy atomic few-electron systems and into the subtelties of the collision mechanisms could be gained. With the structure investigations, the strong central fields of heavy nuclei could be probed on a new level of accuracy. The QED structure contributions are now confirmed up to the highest Z systems testing already higher order $Z\alpha$ terms. The accuracy approaches presently the threshold of testing sensitively the higher-order QED terms for instance in He-like ions, see also the work performed at EBIT (Marrs *et al.*, 1995). For the one-electron ground state LAMB-shift new spectroscopic systems are currently developped. There is the hope, that with high resolution detector devices such as cryodetectors or crystal spectrometers the accuracy of the present most accurate theories can be tested in a region not accessible by light ions or myonic atoms. Depending on the population mechanism of higher shells a spectroscopy of Balmer transitions is of particular interest. Due to the comperatively large fine structure splitting most of the levels can be determined without any blendings. Intra L-shell transitions are governed by correlation, relativistic and QED effects, therefore providing a very special tool to probe these influences with a high accuracy. Here, also VUV spectroscopy – maybe by using Doppler tuned techniques – will possibly yield to the most accurate structure investigations for very heavy, few-electron ions. In high-Z He-like systems, around Z=90, almost degenerated s and p levels in the L shell may mix, possibly leading to atomic parity violation (Soff, 1991).

Beyond photon spectroscopy, also dielectronic recombination gives an equivalent access to fundamental questions of the structure of highly-charged very heavy atoms. In

particular $\Delta n = 1$, i.e. KLL resonances will give detailed answers to QED contributions. With a cooler independent second electron target these fundamental questions can be precisely studied in the near future. Here, also the reaction dynamics governed by relativistic effects, particularly by magnetic interactions, will give novel insight into the important correlation contributions governing also the Auger effect at high Z atoms.

Very subtle magnetic interactions lead to ground state hyperfine splitting. The QED coupling to the magnetic part of the virtual photon field can be probed uniquely here. Up to now, the uncertainties in the knowledge of the nuclear magnetisation distribution (Bohr Weisskopf effect) limits the accuracy for the QED part. In this case, as in general for all heavy ions, the nuclear part has to be known precisely in order to determine accurately the atomic structure effects.

A particular interplay between atomic and nuclear structure is the bound state β-decay, measured at the ESR already for two heavy species (Ho and Dy). These results will fix the important time scale for the age of the universe. On the other hand, tuning the storage rings as high resolution mass spectrometers, the whole zoo of nuclear masses can be coupled precisely together via nuclear reactions, and their products stored in the rings. This may provide also a new basis for the understanding of the composition of our matter.

A crucial issue for heavy ion storage rings with the indispensible electron cooling devices is the radiative recombination. On the one hand, colder and colder electron beams are provided, leading to high luminosity heavy ion beams with very low emittances (Danared *et al.*, 1994). For instance DR, resonance structures can be measured with higher accuracies. On the other hand, the plasma physics in the cooler is of interest in itself. There, highly charged ions are in a temperature bath of extremely cold electrons. However, due to the recombination loss, due to the ionic Coulomb potential, and due to the magnetic guidance field the normal thermodynamics may get complicated. Moreover,

RR seems to be an ideal tool to probe the energy and temperature distribution of the electrons around the highly-charged ions.

Equivalent to RR, we have radiative electron capture, REC. This process tests the interaction of a quasi-free electron with the photon field of the Coulomb potential. In principle, the photoelectric effect has been studied at the ESR in the relativistic regime not accessible even at the third generation of synchrotron radiation facilities. Due to the high-Z values of the ions and due to the relativistic velocities, higher-multipole transitions, in particular M1 transitions contribute considerably to REC and, hence, to the photo effect. Here, quite different emission patterns have been found. Normally forbidden 0^o and 180^o emission is allowed for K-REC at high transition energies. These effects have to be studied in more detail in the near future. Similar unrevealed relativistic effects can be expected for excitation and ionization processes, especially at high energies.

Non-radiative capture will be of particular interest at low projectile velocities. There, one and multiple electron capture into excited states dominates. A quite new aspect gives the multielectron capture populating predominately high-excited states: in the end highly inverted systems may be created. Correlated decay may give information on the true emission volume (Hanbury-Brown and Twiss, 1954; see also Cindro *et al.*, 1993). For the measurements not only decelerated ions are needed, one may benefit there also from extracting them to external experimental areas. First experimental tests with extracted low energy beams (e.g. 50 MeV/u U^{91+}) have already been performed at the ESR.

Extracted beams give additionally the possibility to study classical atomic reactions at low collision energies – such as quasimolecular collisions –, however, now with well defined initial charge state conditions. In particular, by $Pb^{81+} \rightarrow$Pb(gas) collisions superheavy atoms can be probed testing transiently the highest possible atomic fields. Interferences in the quasimolecular radiation can measure the transient structure of these superheavy quasiatoms (Schuch *et al.*, 1988), near the diving into the negative continuum (Reinhardt

and Greiner, 1977). Also, collision studies using the recoil momentum technique will be used at external and at in-ring experiments (Ullrich *et al.*, 1995).

There is also the challenging field of forbidden transitions. Lifetimes can be studied, in particular for not too heavy ions revealing the crucial overlap of wavefunctions. For very heavy systems, e.g. the 2E1 decay of $1s2s\,^1S_0$ level in He-like ions reflects the complete structure of all the relevant bound and continuum states. All this information can be extracted from the continuum two-photon spectrum. These experiments will also benefit from decelerated extracted beams.

This brief summary on future possibilities of the physics with highly charged, very heavy ions is in no way complete. However, it demonstrates the unique power and the great potential of storage ring facilities in this challenging field of the fundamental physics of highly charged heavy ions. A florishing future and a new understanding of the basics in this field is expected.

Acknowledgements

Both the authors are deeply indepted in the support of their families during writing this review. It is a pleasure to devote this article to our wifes each. The good collaboration with our colleagues at the rings in particular in Darmstadt as well as in Aarhus, Heidelberg, and Stockholm is highly acknowledged. We appreciate the data from their work appearing in the figures. One of the authors PHM benefited greatly from a stay at the University of Aarhus within a Humboldt professorship to Denmark in 1995.

REFERENCES

Andersen L.H., Hvelplund P., Knudsen H., Kvistgaard P. (1989). *Phys. Rev. Lett.* **62**, 2656

Andersen L.H., Bolko J. (1990a). *Phys. Rev.* **A42**, 1184

Andersen L.H., Bolko J., Kvistgaard P. (1990b). *Phys. Rev.* **A41**, 1293

Andersen T., Andersen L.H., Balling P., Haugen H.K., Hvelplund P., Smith W.W., Taulbjerg K. (1993). *Phys. Rev.* **A47**, 890

Andersen L.H., Hvelplund P., Lorents D.C., Mathur D., Shen H. (1995a). in *Biennal Report 1993/94* (Inst. of Physics and Astronomy, Univ. Aarhus), 49

Andersen L.H., Mathur D., Schmidt H.T., Vejby-Christensen L. (1995b). *Phys. Rev. Lett.* **74**, 892

Anholt R. (1979). *Phys. Rev.* **A19**, 1004

Bell M., Chaney J., Herr H., Krienen F., Möller-Petersen P., Petrucci G. (1981). *Nucl. Instr. Meth.* **190**, 237

Bethe H.A., Salpeter E.E. (1957). *Quantum Mechanics of One- and Two-Electron Atoms*, in: Handbuch der Physik (ed. Flügge S.; Springer)

Beyer H.F., Bollen G., Bosch F., Egelhof P., Franzke B., Hasse R.W., Kluge H.J., Kozhuharov C., Kühl T., Liesen D., Mann R., Mokler P.H., Müller A., Müller R.W., Münzenberg G., Poth H., Schweikard L., Schuch R., Werth G. (1990). *internal report* **GSI 90-20**

Beyer H.F., Finlayson K.D., Liesen D., Indelicato P., Chantler C.T., Deslattes R.D., Schweppe J., Bosch F., Jung M., Klepper O., Koenig W., Moshammer R., Beckert K., Eickhoff H., Franzke B., Gruber A., Nolden F., Spaedtke P., Steck M., (1993). *J. Phys.* **B26**, 1557

Beyer H.F., Liesen D., Bosch F., Finlayson K.D., Jung M., Klepper O., Moshammer R., Beckert K., Eickhoff H., Franzke B., Nolden F., Spaedkte P., Steck M. (1994). *Phys. Lett.*

A184, 435

Beyer H.F., Menzel G., Liesen D., Gallus A., Bosch F., Deslattes R., Indelicato P., Stöhlker Th., Klepper O., Moshammer R., Nolden F., Eickhoff H., Franzke B., Steck M. (1995). *Z. Phys.* **D35**, 169

Bohr A., Weisskopf V.F. (1950). *Phys. Rev.* **77**, 94

Borneis S., Bosch F., Engel T., Jung M., Klaft I., Klepper O. , Kühl T., Marx D., Moshammer R., Neumann R., Schröder S., Seelig P., Völker L. (1994). *Phys. Rev. Lett.* **72**, 209

Bosch F. (1987). Nucl. Instr. Meth. **B23**, 190

Bosch F. (1989). *Nucl. Instr. Meth.* **B52**, 945

Bosch F. (1993). *"The Physics of Electronic and Atomic Collisions"* AIP Conf. Proc. 295; (eds.: Andersen T., Fastrup B., Folkmann F., Knudsen H., Andersen N.) 3

Bosch F. and Nolden F. (1995). *internal report*: Nachrichten **GSI 05-95**, 3

Burgess A. (1964). *Astrophys. J.* **139**, 776

Chen M.H. (1990). *Phys. Rev.* **A41**, 4102

Cindro N., Karolija M., Shapira D. (1993). *Prog. Part. Nucl. Phys.* **30**, 65

Danared H., Andler G., Bagge L., Herrlander C.J., Hilke J., Jeansson J., Källberg A., Nilsson A., Paal A., Rensfelt K.-G., Rosengard U., Starker J., af Ugglas M. (1994). *Phys. Rev. Lett* **72**, 3775

Drake G.W. (1988). *Can. J. Phys.* **66**, 586

Eickhoff H., Beckert K., Franczak B., Franzke B., Nolden F., Poth H., Schaaf U., Schulte H., Spädtke P., Steck M. (1991). in *Cooler Rings and Their Application* (eds.: Katayama T., Noda A.; World Scientific), 11

Eichler J. (1985). *Phys. Rev.* **A312**, 112

Eichler J. (1990). *Phys. Rep.* **193**, 165.

Eichler J., Ichihara A., Shirai T. (1995). *Phys. Rev.* **A51**, 3027.

Finkbeiner M., Fricke B., Kühl T. (1993). *Phys. Lett.* **A176**, 113

Fontes C.J., Sampson D.H., Zhang H.L. (1995). *Phys. Rev.* **A51**, R12

Franzke B. (1987). *Nucl. Instr. Meth.* **B24/25**, 18

Franzke B. (1988). *Physica Scripta* **T22**, 41

Franzke B. (1995). private communication

Graham W.G., Berkner, Bernstein E.M., Clark M.W., Feinberg B., McMahan M.A., Morgan T.J., Rathbun W., Schlachter A.S., Tanis J.A. (1990). *Phys. Rev. Lett.* **65**, 2773

Grieser R., Kühl T., Huber G. (1995). *Am. J. Phys.* **63**, 665

Gruber A., Bourgeois W., Franzke B., Kritzer A., Treffert C. (1989). *Nucl. Instr. Meth.* **A282**, 87

Hangst J.S., Kristensen M., Nielsen J.S., Poulsen O., Schiffer J.P., Shi P. (1991). *Phys. Rev. Lett.* **67**, 1238

Hanbury-Brown R., Twiss R.Q. (1954). *Phil. Mag.* **45**, 663

Herlander C.J. (1991). in *Cooler Rings and their Application* (eds.: Katayama T., Noda A.; World Scientific), 15

Hino K.I., and Watanabe T. (1987). *Phys. Rev.* **A36**, 581

Ichihara A., Shirai T., and Eichler J. (1994). *Phys. Rev.* **A49**, 1875

Indelicato P. (1990). In *"X-Ray and Inner Shell Processes"* (X-90, AIP Conf.Proc. 215; New York, 1990) 591

Indelicato P. (1995). *Phys. Rev.* **A51**, 1132

Irnich H., Geissel H., Nolden F., Beckert K., Bosch F., Eickhoff H., Franzke B., Fujita Y., Hausmann M., Jung H.C., Kraus G., Klepper O., Kozhuharov C., Magel A., Münzenberg G., Nickel F., Radon T., Reich H., Schlitt B., Schwab W., Sümmerer K., Suzuki K., Steck M., Wollnik H. (1995). *Phys. Rev. Lett., submitted*

Jaeschke E., Bisoffi G., Blum M., Friedrich A., Geyer C., Grieser M., Holzer B., Heyng H.W., Habs D., Jung M., Krämer D., Noda A., Ott W., Pollok R.E., Repnow R., Schmitt

F., Steck M. (1990). *Part. Acc.* **32**, 97

Johnson W.R., Soff G. (1985). *At. Data Nucl. Data Tables* **33**, 405

Jung M., Bosch F., Beckert K., Eickhoff H., Folger H., Franzke B., Kienle P., Klepper O., Koenig W., Kozhuharov C., Mann R., Moshammer R., Nolden F., Schaaf U., Soff G., Spädtke P., Steck M., Stöhlker Th., Sümmerer K. (1992). *Phys. Rev. Lett.* **69**, 2164

Kandler T., Mokler P.H., Stöhlker Th., Geissel H., Irnich H., Kozhuharov Ch., Kriessbach A., Kucharski M., Münzenberg G., Nickel F., Rymuza P., Scheidenberger C. Stachura Z., Suzuki T., Warczak A., Dauvergene D., Dunford R.W. (1995a). *Phys. Lett.* **204**, 274

Kandler T., Mokler P.H., Stöhlker Th. (1995b). *Nucl. Instr. Meth.* **B...**, in press

Kandler T., Mokler P.H., Geissel H., Irnich H., Kozhuharov C., Kriessbach A., Kucharski M., Münzenberg G., Nickel F., Rymuza P., Scheidenberger C., Stachura Z., Stöhlker Th., Suzuki T., Warczak A., Dauvergne D., Dunford R.W. (1995c) *Nucl. Instr. Meth.* **B98**, 320

Kienle P. (1985). *internal report* **GSI 85-16**

Kilgus G., Berger J., Grieser M., Habs D., Hochadel B., Jaeschke E., Krämer D., Neumann R., Neureither G., Ott W., Schwalm D., Steck M., Stokstad R., Szmola E., Wolf A., Schuch R., Müller A., Wagner M. (1990). *Phys. Rev. Lett.* **64**, 737

Kilgus G., Habs D., Schwalm D., Wolf A., Badnell N.R., Müller A. (1992). *Phys. Rev.* **A46**, 5730

Kilgus G., Habs D., Schwalm D., Wolf A., Schuch R., Badnell N.R. (1993). *Phys. Rev.* **A47**, 4859

Klaft I., Borneis S., Engel T., Fricke B., Grieser R., Huber G., Kühl T., Marx D., Neumann R., Schröder S., Seelig P., Völker L. (1994). *Phys. Rev. Lett.* **73**, 2425

Kleber M., Jakubassa D.H. (1974). *Nucl. Phys.* **A252**, 152

Klepper O., Bosch F., Daues H.W., Eickhoff H., Franczak B., Franzke B., Geissel H., Gustafsson O., Jung M., Koenig W., Kozhuharov C., Magel A., Münzenberg G., Stelzer

H., Szerypo J., Wagner M. (1992) *Nucl Instr. Meth.* **B70**, 427

Kluge H.-J. (1995). *Nucl. Instr. Meth.* **B98**, 500

Knapp D.A., Marrs R.E., Elliott S.R., Magee E.W., Zasadzinski R. (1993). *Nucl. Instr. Meth.* **A334**, 305

Kühl T. (1995). private communication

Labzowsky L.N., Klimchitskaya G.L., Dmitriev Y.Y. (1993). *Relativistic Effects in the Spectra of Atomic Systems* (IOP publ.)

Lamb W.E., Retherford R.C. (1947). Phys. Rev. **72**, 241

Larsson M. (1995). *Rep. Prog. Phys.* , in print

Levine M.A., Marrs R.E., Bardsley J.N., Beiersdorfer P., Bennett C.L., Chen M.H., Cowan T., Dietrich D., Henderson J.R., Knapp D.A., Osterheld A., Penetrante B.M., Schneider D., Scofield J.H. (1989). *Nucl. Instr. Meth.* **B43**, 431

Liesen D., Beyer H.F., Finlayson K.D., Bosch F., Jung M., Klepper O., Moshammer R., Beckert K., Eickhoff H., Franzke B., Nolden F., Spädtke P., Steck M., Menzel G., Deslattes R.D. (1994). *Z. Phys.* **D30**, 307

Lindgren I., Persson H., Salomonson S., Labzowsky (1995a). *Phys. Rev.* **A51**, 1167

Lindgren I., Persson H., Salomonson S., Sunnergren P. (1995b). *Physica Scripta* **T59**, 179

Lindroth E. (1995). *Nucl. Instr. Meth.* **B98**, 1

Lotz W. (1968). *Z. Phys.* **216**, 241

Lupton J.H., Dietrich D.D., Hailey C.J., Stewart R.E., Ziok K.P. (1994). *Phys. Rev.* **A50**, 2150

Madison D.H., Merzbacher E. (1975). in *Atomic Inner-Shell Processes*, (ed. Crasemann B.)

Marrs R.E., Elliott S.R., Knapp D.A. (1994a). *Phys. Rev. Lett.* **72**, 4082

Marrs R.E., Beiersdorfer P., Schneider D. (1994b). *Physics Today* **Oct. 94**, 27

Marrs R.E, Elliott S.E., Stöhlker Th. (1995). *Phys. Rev.* **A52**, 3577

Marrus R., Birkett B., Simionovici A., Indelicato P., Beyer H.F., Bosch F., Gallus A., Liesen D., Menzel G. (1995). in *GSI Scientific Report 1994*, **GSI 94-1**, 136

J. Phys. **14**, 181

Marrus R., Siminiovici A., Indelicato P., Dietrich D., Charles P., Briand J.P., Finlayson K., Bosch F., Liesen D., Parente F. (1989). *Phys. Rev. Lett.* **63**, 502

Meyerhof W.E., Anholt R., Eichler J., Gould H., Munger Ch., Alonso J., Thieberger P., Wegner H.E. (1985a). *Phys. Rev.* **A32**, 3291

Meyerhof W.E., Anholt R., Eichler J., Gould H., Munger C., Alonso J., Thieberger P., and Wegner H.E. (1985b). *Phys. Rev.* **A49** 1975

Meyerhof W.E. (1994). private communication

Möhl D. (1988). *Physica Scripta* **T22**, 21

Möller S.P. (1990). in *1 Eur. Part. Accel. Conf.* (ed. Tazzari S.; World Scientific), 328

Möller S.P. (1994). *Proc. IV Eur. Part. Accel. Conf.* (eds.: Suller V., Petit-Jean-Genaz Ch.; World Scientific) 173

Mohr P.J. (1994). *Nucl. Instr. Meth.* **B87**, 232

Mokler P.H., Liesen D. (1978). in *Progress in Atomic Spectroscopy, Part C* (eds. Beyer H.J., Kleinpoppen H.; Plenum), 321

Mokler P.H., Reusch S. (1988). *Z. Phys.* **D8**, 393

Mokler P.H., Reusch S., Stöhlker Th. (1989). *Nucl. Instr. Meth.* **A278**, 93

Mokler P.H., Stöhlker Th., Kozhuharov C., Stachura Z., Warczak A. (1991). *Z. Phys.* **D21**, 197

Mokler P.H., Stöhlker Th., Kozhuharov C., Moshammer R., Rymuza P., Bosch F., Kandler T. (1994). *Physica Scripta* **T51**, 28

Mokler P.H., Stöhlker Th., Kozhuharov C., Moshammer R., Rymuza P., Stachura Z., Warczak A. (1995a). *J. Phys.* **B28**, 617

Mokler P.H., Stöhlker Th., Dunford R.W., Gallus A., Kandler T., Menzel G., Prinz H.T., Rymuza P., Stachura Z., Swiat P., Warczak A. (1995b). *Z. Phys.* **D35**, 77

Müller A. (1992). in *Recombination of Atomic Ions* (eds.: Graham W.G., Fritsch W., Hahn Y., Tanis J.A.; Plenum) NATO ASI **B296**, 155

Müller A. (1994). *Nucl. Instr. Meth.* **B87**, 34

Persson H., Salomonson S., Sunnergren P., Lindgren I., (1996). *Phys. Rev. Lett.***76**, 204

Pindzola M.S., Badnell N.R. (1992). Communication in Spies *et al.*, 1992

Pollock R.E. (1991). *Annu. Rev. Part. Sci.* **41**, 357

Poth H. (1990a). *Phys. Rep.* **196**, 135

Poth H. (1990b). *Nature* **345**, 399

Reinhardt J., Greiner W. (1977). *Rep. Progr. Phys.* **40**, 219

Rice R., Basbas G., McDaniel D (1977). *At. Data and Nucl. Data Tables* **20**, 503

Rösel F., Trautmann D., Baur G. (1982). *Nucl. Instr. Meth.* **B 192**, 43

Rymuza P., Stöhlker Th., Cocke C.L., Geissel H., Kozhuharov C., Mokler P.H., Moshammer R., Nickel F., Scheidenberger C., Stachura Z., Ullrich J., and Warczak A. (1993). *J. Phys.* **B26**, 169

Schennach S., Müller A., Wagner M., Haselbauer J., Uwira O., Spies W., Jennewein E., Becker R., Kleinod M., Pröbstel U., Angert N., Klabunde J., Mokler P.H., Spädtke P., Wolf B. (1991). *Z. Phys.* **D21**, S 205

Schennach S., Müller A., Uwira O., Haselbauer J., Spies W., Frank A., Wagner M., Becker R., Kleinod M., Jennewein E., Angert N., Mokler P.H., Badnell N.R., Pindzola M.S. (1994). *Z. Phys.* **D30**, 291

Schmidt H.T., Forck P., Grieser M., Habs D., Kenntner J., Miersch G., Repnow R., Schramm U., Schüssler T., Schwalm D., Wolf A. (1994). *Phys. Rev. Lett.* **72**, 1616

Schmieder R.W., Marrus R. (1973). *Nucl. Inst. Meth.* **110**, 459

Schneider D., Church D., Weinberg G., McDonald J., Steiger J., Beck B., Knapp D.

(1994). *EBIT annual report 1993*; UCRL-ID-118274, 72

Schneider S.M., Schaffner J., Soff G., Greiner W. (1993). *J. Phys.* **B26**, L581

Schröder S., Klein R., Boos N., Gerhard M., Grieser R., Huber G., Karafillidis A., Krieg M., Schmidt N., Kühl T., Neumann R., Balykin V., Grieser M., Habs D. Jaeschke E., Krämer D., Kristensen M., Music M., Petrich W., Schwalm D., Sigray P., Steck M., Wanner B., Wolf A. (1990). *Phys. Rev. Lett.* **64**, 2901

Schuch R., Meron M., Johnson B.M., Jones K.W., Hoffmann R., Schmidt-Böcking H., Tserruya I. (1988). *Phys. Rev.* **A37**, 3313

Schuch R. (1993). in *Review of Fundamental Processes and Applications of Atoms and Ions* (ed.: Lin C.D.; World Scientific), 169

Schüssler T., Schramm U., Grieser M., Habs D., Rüter T., Schwalm D., Wolf A. (1995b). *Nucl. Instr. Meth.* **B98**, 146

Schüssler T., Schramm U., Rüter T., Broude C., Grieser M., Habs D., Schwalm D., Wolf A. (1995a). *Phys. Rev. Lett.* **75**, 802

Schweppe J., Belkacem A., Blumenfeld L., Claytor N., Feinberg B., Gould H., Kostroun V.E., Levy L., Misawa S., Mowat J.R., Prior M.H. (1991) *Phys. Rev. Lett.* **66**, 1434

Soff G. (1991). *Z. Phys.* **D21**, S7

Soff G. (1993). unpublished

Soff G. (1995). private communication

Spädtke P., Angert N., Beckert K., Bourgeois W., Emig H., Franzke B., Langenbeck B., Leible K.D., Nolden F., Odenweller T., Poth H., Schaaf U., Schulte H., Steck M., Wolf B.H. (1991). in *Cooler Rings and Their Aplication* (eds.: Katayama T., Noda A.; World Scientific), 75

Spies W., Müller A., Linkemann J., Frank A., Wagner M., Kozhuharov C., Franzke B., Beckert K., Bosch F., Eickhoff H., Jung M., Klepper O., Koenig W., Mokler P.H., Moshammer R., Nolden F., Schaaf U., Spädtke P., Steck M., Zimmerer P., Grün N.,

Scheid W., Pindzola M.S., Badnell N.R. (1992). *Phys. Rev. Lett.* **69**, 2768

Spies W., Uwira O., Müller A., Linkemann J., Empacher L., Frank A., Kozhuharov C., Mokler P.H., Bosch F., Klepper O., Franzke B., Steck M. (1995). *Nucl. Instr. Meth.* **98**, 158.

Stevefelt, Boulmer J., Delpech J.F. (1975). *Phys. Rev.* **A12**, 1246.

Ann. Phys. **7**, 661

Stöhlker Th., Geissel H., Folger H., Kozhuharov C., Mokler P.H., Münzenberg G., Schardt D., Schwab Th., Steiner M., Stelzer H., Sümmerer K. (1991). *Nucl. Instr. Meth.* **B61**, 408

Stöhlker Th., Mokler P.H., Geissel H., Moshammer R., Rymuza P., Bernstein E.M., Cocke C.L., Kozhuhorov C., Münzenberg G., Nickel F., Scheidenberger C., Stachura Z., Ullrich J., Warczak A. (1992). *Phys. Lett.* **A168**, 285

Stöhlker Th., Mokler P.H., Beckert K., Bosch F., Eickhoff H., Franzke B., Jung M., Kandler T., Klepper O., Kozhuharov C., Moshammer R., Nolden F., Reich H., Rymuza P., Spädtke P., and Steck M. (1993). *Phys. Rev. Lett.* **71**, 2184

Stöhlker Th., Mokler P.H., Kandler T., Kozhuharov C., Moshammer R., Rymuza P., Stachura Z., Warczak A., Beckert K., Bosch F., Eickhoff H., Franzke B., Jung M., Klepper O., Nolden F., Reich H., Spädtke P., Steck M. (1993a). *Abstracts of Contributed Papers, XVIII International Conference on the Physics of Electronic and Atomic Collisions* (eds.: Andersen T., Fastrup B., Folkmann F., and Knudsen H.; Aarhus Universitet), 615

Stöhlker Th., Geissel H. Irnich H., Kandler T., Kozhuharov C. Mokler P.H., Münzenberg G., Nickel F., Scheidenberger C., Suzuki T., Kucharski M., Warczak A., Rymuza P., Stachura Z., Kriessbach A., Dauvergene D., Dunford B., Eichler J., Ichihara A., and Shirai T. (1994). *Phys. Rev. Lett.* **73**, 3520

Stöhlker Th., Kozhuharov C., Mokler P.H., Warczak A., Bosch F., Geissel H., Eichler J., Ichihara A., Shirai T., Stachura Z., Rymuza P. (1995). *Phys. Rev.* **A51**, 2098

Stöhlker Th. (1995). *internal report: Nachrichten* **GSI 05-95**, 4

Stöhlker Th. (1996). *"The Physics of Electronic and Atomic Collisions"* AIP Conf. Proc. 360; (eds. Dube L.J., Mitchell J.B., McConkey J.W., Brion C.E.) 525

Thompson R.C. (1990). *Meas. Sci. Technol.* **1**, 93

Ullrich J., Dörmer R., Mergel V., Jagutzki O., Spielberger L., Schmidt-Böcking H. (1994). *Com. Atom. Mol. Phys.* **30**, 285

Uwira O., Müller A., Spies W., Linkemann J., Frank A., Cramer T., Empacher L., Becker R., Kleinod M., Mokler P.H., Kenntner J., Wolf A., ScGramm U., Schüssler T., Schwalm D., Habs D. (1995). *Hyperfine Interaction ...*, in print

Van der Meer S. (1972). *internal report* CERN-ISR-PO/72-31

Weitz M., Schmidt-Kahr F., Hänsch T.W. (1992). *Phys. Rev. Lett.* **68**, 1120

Wolf A. (1988). *Physica Scripta* **T22**, 55

Wolf A. (1992). in *Recombination of Atomic Ions*, Nato ASI (eds.: Graham W.G., Fritsch W., Hahn Y., Tanis J.A.; Plenum) **B 296**, 209

Wolf A., Habs D., Lampert A., Neumann R., Schramm U., Schüssler T., Schwalm D. (1993). in *Atomic Physics 13* (eds.: Walther H., Hänsch T.W., Neibert B.; AIP), 228

Zimmerer P., Grün N., Scheid W. (1990). *Phys. Lett.* **A 148**, 457

Zimmerer P. (1992). *PhD Thesis, University of Giessen*

Zimmerer P., Grün N., Scheid W. (1991). *J. Phys.* **B24**, 2633

Zimmermann M., Grün N., Scheid W. (1994). in *GSI Scientific Report 1993* **GSI-1994-1**, 167.